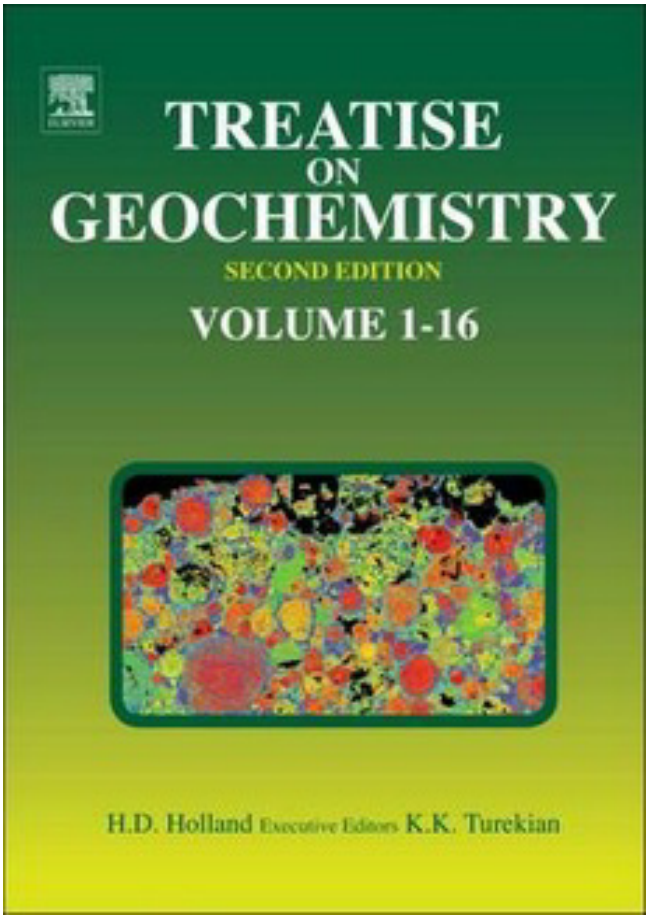

Aller R.C. (2014) Sedimentary Diagenesis, Depositional Environments, and Benthic Fluxes. In: Holland H.D. and Turekian K.K. (eds.) Treatise on Geochemistry, Second Edition, vol. 8, pp. 293-334. Oxford: Elsevier.

8.11 Sedimentary Diagenesis, Depositional Environments, and Benthic Fluxes

RC Aller, Stony Brook University, Stony Brook, NY, USA

8.11.1 Introduction

8.11.1.1 Early Diagenesis and the Global Sedimentary Cycle

The global sedimentary cycle and attendant biogeochemical processes are major controls on the composition of the Earth's surface over a wide spectrum of timescales (Drever et al., 1988; Kump et al., 2000; see **Chapter 9.15**). One part of this grand cycle is the deposition and buildup of lithogenic and biogenic debris at the seafloor and the dynamic physical and chemical interactions of these deposits with overlying water and the atmosphere. Seabed geochemical interactions are driven by components of sedimentary mixtures that are thermodynamically unstable and undergo a wide range of reactions, including hydrolysis, dissolution, oxidation–reduction, precipitation, and recrystallization. Many such reactions are rapid, biologically mediated, and occur in the upper few microns to meters of deposits where both dissolved and particulate reactants and products can readily exchange with adjacent regions.

Treatise on Geochemistry, Second Edition, (2014), vol. 8, pp. 293-334

The chemical and physical changes that accompany these reactions and occur during the initial stages of sediment accretion at low temperature (usually <50 °C) define early diagenesis. The factors and mechanisms internal to deposits that govern diagenesis are referred to as diagenetic processes, and the associated mass transport of solutes, fluids, and particulate material across the upper surface of deposits are termed benthic or sediment–water fluxes (Burdige, 2006; Schulz, 2006).

Because sedimentary deposits behave as open systems, early diagenetic reactions and associated mass refluxing can have major impacts on ocean water composition and ecosystem processes. These impacts are particularly obvious in shallow waters (<50 m) where benthic release of regenerated nutrients (e.g., N, P, and Si) interacts closely with the biologically productive photic zone and can supply 25–80% of planktonic nutrient requirements (Heip et al., 1995; Jahnke, 2004; Middelburg and Soetaert, 2004). However, more subtle yet significant effects on a range of elemental cycles (e.g., N, P, Si, K, Li, F, and Fe) in the ocean and atmosphere can also be demonstrated and are still being quantified (Jahnke, 1996; Michalopoulos and Aller, 2004; Middelburg and Soetaert, 2004; Middelburg et al., 1996; Sayles, 1979; Severmann et al., 2010; see also **Chapter 10.12**). Diagenetic processes can significantly alter sediment composition and modify initial inputs of constituents that would otherwise be directly useful for paleoenvironmental reconstruction, for example, selective dissolution of skeletal fossils, but these same processes can leave an alternative record of environmental conditions in the form of authigenic mineral suites and derived compositional relationships (e.g., S and Fe; Goldhaber, 2003; Lyons et al., 2009; Raiswell and Canfield, 1998). The recognition and accurate reading of this record depends on a detailed understanding of diagenesis in varied depositional conditions.

Biogenic debris in particular is often inherently unstable at Earth surface conditions and, once separated from sites of formation and active maintenance by energy flow, undergoes progressive net reactions. Organic matter, carbonates ($CaCO_3$ and $Ca_xMg_{x-1}CO_3$), and opaline silica (SiO_2) are the dominant general classes of biogenic solids involved in early diagenetic reactions, authigenic mineral product formation, and biogeochemical cycling in the seabed (Emerson and Hedges, 2003; Martin and Sayles, 2003; see **Chapters 9.4** and **10.12**). Examples of the overall patterns of change of such reactants and the corresponding buildup of products with depth in deposits during diagenesis are illustrated schematically in **Figure 1**. The behaviors of each of these biogenic components and reactive lithogenic fractions, such as Fe, Mn, and Al oxides, are closely coupled, directly or indirectly, during burial. Organic matter decomposition and remineralization plays a central role in early diagenesis because of its impact on the master reaction variables pH and pe (Eh – redox potential), its direct role in the CO_2 cycle, its role in generating authigenic minerals, its coupling to the recycling of nutrient elements to overlying water and the atmosphere, and its fueling of secondary production in the benthic ecosystem. On longer timescales, the quantity of organic matter (or an equivalent reduced material, such as authigenic pyrite) that escapes diagenetic oxidation and is sequestered in sedimentary rocks is directly tied to atmospheric oxygen levels and to societal energy resources (Berner, 1982, 2004; Holland, 1984). Thus, understanding the early diagenetic controls on organic matter remineralization and preservation, and developing predictive models to describe them, are central goals in diagenetic research.

8.11.1.2 General Classes of Conceptual Diagenetic Models

Five general classes of conceptual models are commonly utilized separately or in combination for the investigation of diagenetic processes and as a basis for interpretation and prediction of compositional patterns and mass fluxes (Berner, 1980; Boudreau, 1997; Burdige, 2006; Emerson and Hedges, 2003; Middelburg and Soetaert, 2004; Van Cappellen et al., 1993): (1) thermodynamic models to evaluate solution speciation, solution saturation states, reaction probability, and mineral composition and stabilities in the context of known energy relations; (2) stoichiometric models to define or infer reactions and reaction balances and to examine relationships between reactant and product abundances; (3) transport models to evaluate mass fluxes, compositional relations, and system time dependence; (4) kinetic models to examine system time dependence, extent of reactions, and mechanistic relationships between reactants and products; and (5) ecological models that combine theories of microbial substrate competition, benthic community structure, and ecological interactions with thermodynamic, transport, and kinetic models of sedimentary biogeochemical cycling. As illustrated in the succeeding text, combinations of these models, for example, transport–kinetic reaction–equilibrium modeling, play major roles in the recognition, quantification, and interpretation of diagenetic processes, the quantification of mass fluxes, and the prediction of diagenetic responses under steady and unsteady conditions. Proper application of any of these models requires a thorough understanding of the depositional environment and ecosystem context in which diagenesis occurs.

8.11.1.3 Diagenetic Regimes and Depositional Environments

The expression of particular sets of early diagenetic reactions in deposits and their interactions with overlying water depend strongly on the depositional environment and the corresponding boundary conditions and internal transport–reaction regime. Depending on the environmental setting and history, deposits may be composed of coarse- or fine-grained particles and be more or less permeable to advective flow of fluid; they may be relatively permanent and accrete steadily upward; they may be transient accumulations that exchange dynamically and frequently with adjacent regions; they may be inhabited by macrobenthic communities that rework particles and bioirrigate the seabed; or they may lie in the photic zone and be affected by plant rhizospheres or algal mats. These different depositional conditions result in a spectrum of possible diagenetic transport–reaction regimes, the broadest representation of which occurs in estuarine, continental shelf, and margin environments where most sediment, ~80–90% (Berner, 1982; Einsele, 2000; Milliman and Farnsworth, 2011), is processed and accumulates (**Figure 2**). Each regime can produce very different balances between specific boundary conditions, internal reactions, benthic fluxes, burial efficiencies, and authigenic minerals.

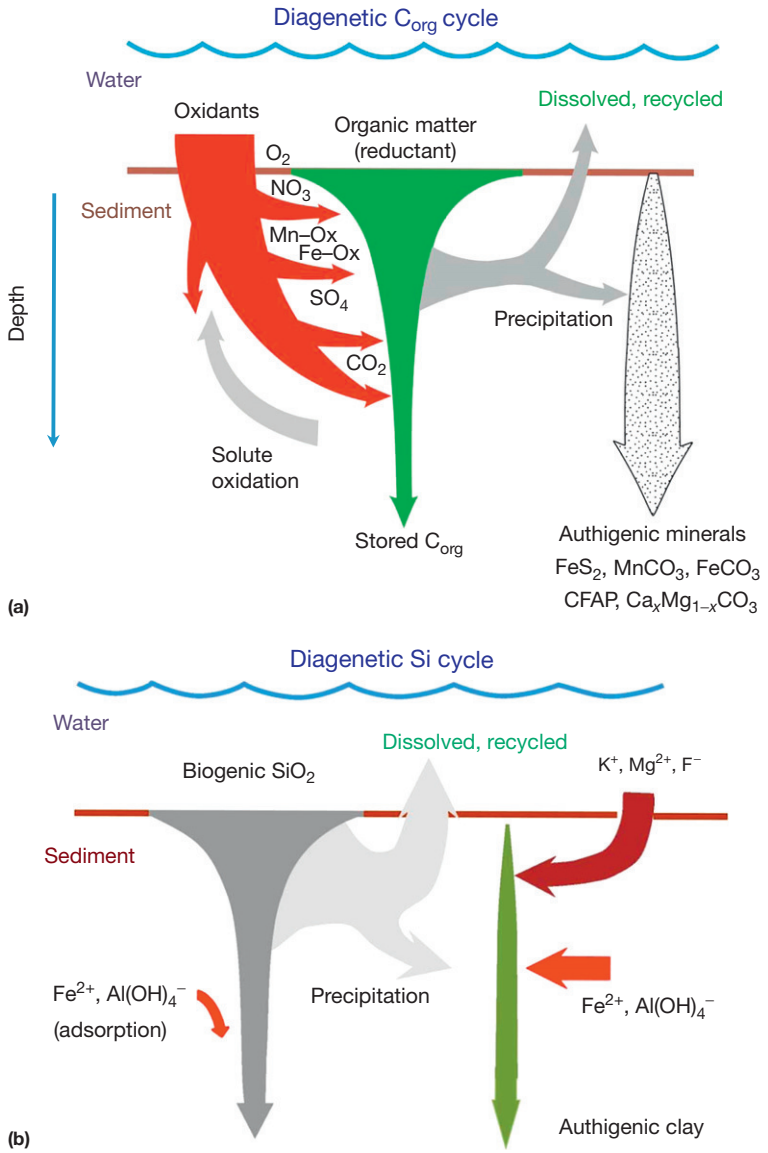

Figure 1 (a) Schematic depiction in vertical cross section of major diagenetic processes exemplified by the remineralization of organic matter in marine deposits. After deposition, reactive organic matter reductant is decomposed and oxidized. The rate of decrease of organic substrate with time and depth is a function of both its inherent reactivity and burial conditions, as is the quantity of residual carbon eventually preserved. A set of naturally occurring dissolved and particulate oxidants (O_2, NO_3^-, Mn oxides, Fe oxides, SO_4^{2-}, and CO_2) is utilized successively by the benthic community in these reactions, producing suites of corresponding dissolved products (e.g., HCO_3^-, HPO_4^{2-}, and HS^-) and reduced authigenic minerals. These reaction products build up with depth or are transported into overlying water and adjacent regions depending on a range of boundary and internal properties determined by the depositional environment and ecosystem (after Aller, 2004). (b) Schematic representation of diagenetic reactive Si cycle. Biogenic opaline SiO_2 delivered to sediments undergoes progressive alteration and dissolution. A portion is recycled as dissolved $Si(OH)_4$ into overlying water, a portion is buried, and a portion is subject to conversion into authigenic clays. The formation of clay consumes a wide range of solutes, including $Al(OH)_4^-$, K^+, Li^+, $Fe^{2+,3+}$, Mg^{2+}, and F^-.

Water column and lateral sediment transport drive material exchange between these local diagenetic environments and the corresponding sedimentary facies over various timescales, ranging from minutes to thousands of years. An accurate conceptualization of elemental cycling in sedimentary deposits, sediment–water interactions, and global-scale models requires a proper description of transport–reaction relationships in these individual diagenetic regimes and also requires an evaluation of their relative role and coupling in different depositional systems. A subset of diagenetic regimes dominates most subaqueous environments globally, several members of which are emphasized and described individually here (Figure 2(a)–2(d)).

The conceptual model of transport and reaction at the heart of most early diagenetic theory was developed approximately 50 years ago, initially for use in deepwater muds of the California margin and borderlands (Berner, 1964). Deposits are modeled as laterally homogeneous bodies, diffusively and advectively open to exchange of solutes and particles with an

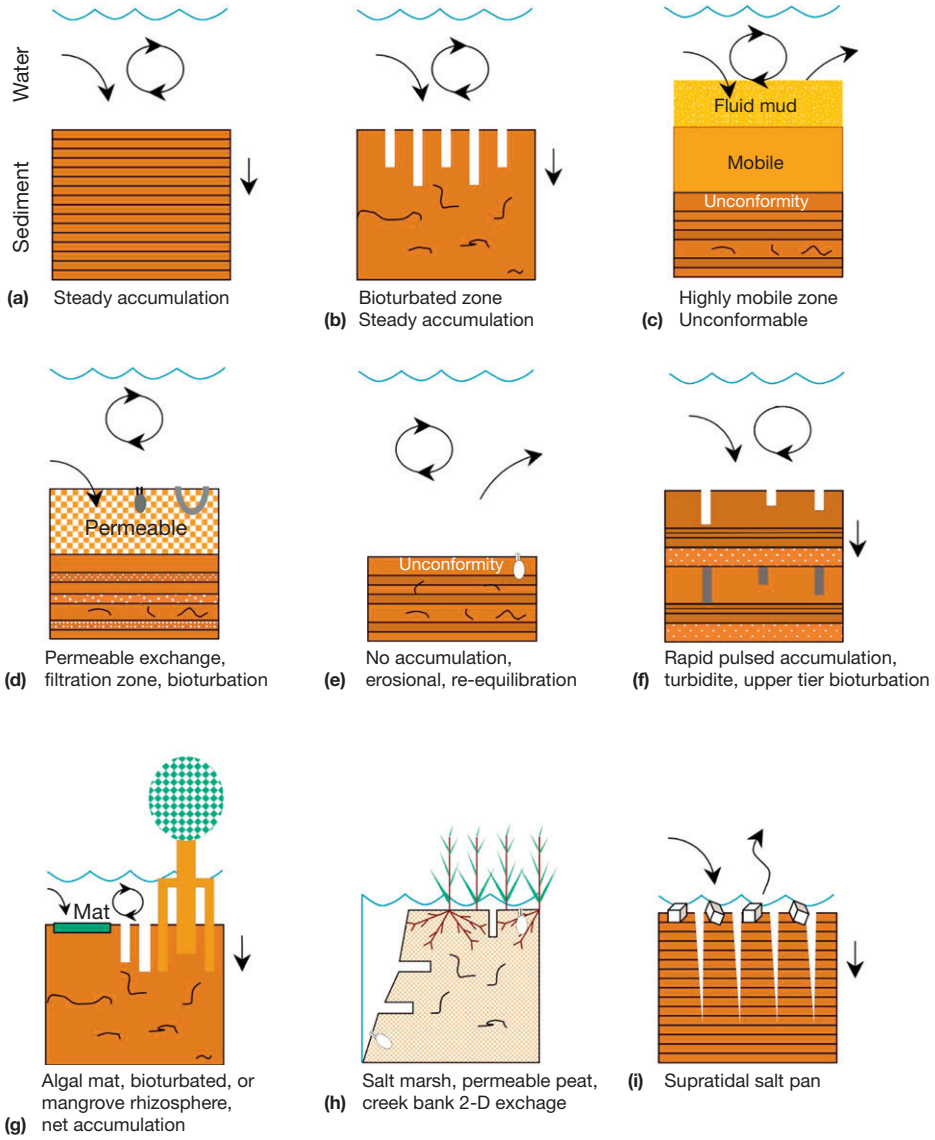

Figure 2 A suite of steady and unsteady diagenetic regimes is typically present in marine environments, the widest spectrum of which is expressed in continental margin and coastal deposits. The individual regimes differ in boundary conditions, sediment mass properties, and interior transport–reaction processes. Major examples, shown schematically, include (a) Steady accumulation regime assumed in most diagenetic models (e.g., Berner, 1980; Boudreau, 1997; Burdige, 2006). (b) Bioturbated surface region within an otherwise steadily accumulating deposit. (c) Highly mobile and periodically reworked sediment layer unconformably overlying older, relict deposit. Fluid mud, often tidally mobile, may be present. (d) Permeable sands and physical/biofiltration zones dominated by advective flow, such as in beach face, river bed, bar, or open shelf edge areas (Huettel et al., 1996; Jahnke, 2004; Middelburg and Soetaert, 2004). (e) Unsteady, exhumed deep deposits exposing previously reduced material (relict) directly to oxygenated water (e.g., mobile layer removed; Blair and Aller, 1996). Macrofaunal colonization and biofiltration can occur. (f) Major pulsed turbidite sedimentation and stable bioturbation alternation sequence (e.g., Anschutz et al., 2002; Thomson et al., 1998). (g) Rhizosphere, benthic primary production and bioturbation dominated surface zone (e.g., mangrove fringe; Alongi, 1991). (h) Permeable salt marsh peat and rhizosphere system, two-dimensional advective exchange (creek bank) (Bollinger and Moore, 1993; Howarth, 1993). (i) Supratidal salt pans and halophyte region (e.g., Alsharhan and Kendall, 2003; Kinsman, 1969; Swart et al., 1989) (after Aller, 2004).

overlying water reservoir, and accreting upward in the vertical dimension at a regular rate equivalent to net sedimentation (**Figure 2(a)**; **Section 8.11.3.2**). Advection is primarily determined by sediment accumulation and, particularly in the surface-most region, compaction. These assumptions, which view sediments as a type of one-dimensional plug flow reactor at steady state, have proven extraordinarily robust and remain the principal basis for the quantitative elucidation and interpretation of a range of fundamental diagenetic relationships in modern environments and for inferences from ancient deposits in the geologic record (Berner, 1980; Canfield, 1994; Emerson and Hedges, 2003; Hedges et al., 1999; Martin and Sayles, 2003; Middelburg et al., 1997; Tromp et al., 1995). They are particularly appropriate assumptions for fine-grained deposits in relatively quiescent, low O_2 environments with minimal or no bottom fauna. Over the years, basic model

formulations derived from these concepts have become progressively more complicated, numerically based, and used for global-scale extrapolations of coupled diagenetic patterns and reaction balances (Archer et al., 2002; Boudreau, 1997; Soetaert et al., 1996a; Van Cappellen and Gaillard, 1996).

Under oxygenated waters, physically stable sediments are generally inhabited by a diverse benthic fauna (e.g., polychaetes, crustaceans, and mollusks) that rework and irrigate deposits during feeding, burrowing, respiratory ventilation, and construction activities. These activities, in total termed bioturbation, are focused into the upper ~10–50 cm of deposits but may extend several meters into the seabed. Bioturbation creates complex, time-dependent, three-dimensional transport–reaction patterns, resulting in coupling between reactions and solute exchange that would not otherwise occur in a one-dimensional system, and which are subject to all the complex ecological interactions and dynamics that occur within benthic communities (**Figure 2(b)**). Particle transport in the bioturbated zone is not determined exclusively by net sedimentation but rather by modes of particle mixing that can be variously approximated by diffusion, advection, or nonlocal exchange mechanisms depending on the time and space scales characterizing a sediment property and the temporal–spatial resolution of sampling (Aller, 1982b; Boudreau, 1986; Meysman et al., 2008). Similarly, approaches to incorporating these biogenic effects into models of solute transport have used modifications of the primary one-dimensional conceptualization with empirically adjusted rates of biodiffusion, bioadvection, and nonlocal source–sink functions to account for altered solute transport processes. An alternative conceptual approach to the adjustment of transport parameters has been to abandon the one-dimensional formulation (**Figure 2(a)**) and define a simplified three-dimensional analogue (a type of conformal mapping) that duplicates the primary properties and scaling of the complex, biogenic transport–reaction geometry (Aller, 1980b, 2001; Meysman et al., 2006). This latter class of model, and more complex exact forms of geometric descriptions of burrow systems permeating deposits (e.g., Koretsky et al., 2002), allows the examination of processes such as redox reaction coupling as a function of biogenic three-dimensional transport geometry and benthic community structure (dictated by animal size, abundance, and distributions). The effect of macrofaunal digestion of sedimentary debris is seldom explicitly incorporated into diagenetic models, although its impact on dissolution–precipitation (e.g., $CaCO_3$; redox-sensitive metals) and organic matter remineralization processes is potentially considerable (Jansen and Ahrens, 2004; Mayer et al., 1997; Woulds et al., 2012).

During movement of lithogenic debris from continental sources into deepwater depocenters, sediments typically transit or are stored in energetic shallow water environments that are well oxygenated, including estuarine channels and deltaic topset regions at <50 m depth. In these environments, surface deposits are commonly subject to periodic or stochastic reworking by energetic tides, waves, and currents and episodically reoxidized. In fine-grained deposits, a local two-zone diagenetic transport–reaction regime can result, consisting of a surface mobile layer unconformably overlying more consolidated, often relict, deposits (**Figure 2(c)**). Fluid mud formation may occur as a third distinct water–sediment transition zone, further enhancing sediment mobility, reoxidation reactions, and sediment–water exchange (Allen et al., 1980; Kineke et al., 1996). These environments are virtually devoid of large macroinfauna and are dominated by abundant and metabolically diverse bacteria (Aller and Aller, 2004; Aller et al., 2010). The spatial and temporal scaling of mobile sediment layers varies substantially. Vertical reworking must involve at least several centimeters of a deposit in order to differentiate this case from the simple resuspension of a thin layer (micrometer to millimeter) of particles at the sediment–water interface, which occurs frequently in most sedimentary environments. Overall, a frequently disturbed mobile layer as a unit has properties of an unsteady batch reactor, rather than the more commonly assumed advective or plug flow reactor (**Figure 2(a)**). In sharp contrast to these latter diagenetic models where net sedimentation rate is a critical master variable, net accumulation has only a minor role in determining seabed batch reactor properties. The critical master variables for the seabed batch reactor are frequency of disturbance, efficiency of reoxidation–exchange (related to duration of exposure), and magnitude (depth). These reflux variables are determined by sedimentary dynamics rather than net sedimentation and result in periodic or episodic resetting of reaction conditions as discussed in the succeeding text. Because deltaic systems, where such conditions are common, are the major depocenters for sediment on Earth, batch reactor diagenesis has a significant impact on global elemental cycling (Aller and Blair, 2006; Michalopoulos and Aller, 2004).

Whereas fine-grained deposits have low permeability with respect to advective flow of fluids, coarse-grained deposits, particularly well-sorted sands, have high permeabilities and overlying water readily flows through them in response to pressure gradients generated by waves and the interactions of boundary currents with bedforms (Huettel and Webster, 2001). Sands are common in energetic coastal regions, such as shoreface deposits, mobile tidal flats, and river mouth bars, and can also dominate the outer portion of continental shelves as relict deposits from lower sea stands (60% of shelf area; Hayes, 1967; Walsh, 1988). Suspended particles in overlying water, a large portion of which are typically small organic-rich planktonic debris, are filtered out as overlying water flows through sands (Huettel et al., 1996, 2007). Such physical filtration supplies reactive material independently from net sedimentation, similar in result to the role of entrainment in the case of mobile muds. In addition, sands are often inhabited by well-developed suspension feeding communities or large deposit feeders, which further enhance incorporation of reactive particles by biodeposition and extensively rework and bioirrigate the seabed (Heip et al., 1995; Middelburg and Soetaert, 2004). Thus, although many of the same reactions occur in both muds and sands, coarse-grained deposits can be exceedingly complex with respect to transport–reaction conditions and interact extensively with overlying water in ways distinctly different from stable mud deposits having low permeability (Huettel et al., 1998). The flow-through nature of sands, the low surface areas of particles per unit volume, and the mineralogies commonly found in sands (e.g., quartz and low reactive Fe oxides and hydroxides) result in a low efficiency of storage of diagenetic reactants and authigenic products (Hedges and Keil, 1995; Mayer, 1994a,b). These properties

result in a minimal sedimentary record of the high benthic fluxes and intense reactivity that typically characterize surficial sands (e.g., low C_{org}). In this respect, sand deposits are again similar to mobile muds: both types of diagenetic regimes have a major role as seabed reactors that are not necessarily evident in residual burial fluxes of diagenetic products.

8.11.2 Diagenetic Oxidation–Reduction Reactions

8.11.2.1 Biogeochemical Redox Reaction Sequence

General reactions of organic matter will be considered initially not only because of their critical role in diagenetic processes but also because organic matter behavior and associated redox reaction patterns can be used readily to illustrate the range of factors that determine the varied possible outcomes of diagenesis as a function of the depositional environment. One of the fundamental concepts guiding the interpretation of early diagenetic processes associated with organic matter remineralization is that, given an initial set of natural oxidants in sedimentary deposits, biogeochemical oxidation–reduction (redox) reactions follow a regular progression with time, in many cases equivalent to depth (Claypool and Kaplan, 1974; Froelich et al., 1979; Stumm and Morgan, 1996). The primary naturally occurring oxidants are O_2, NO_3^-, Mn oxides, Fe oxides, SO_4^{2-}, and CO_2. These oxidants can react with organic and inorganic reductants, potentially yielding different quantities of free energy for the growth of heterotrophic and chemoautotrophic bacteria that commonly mediate the reactions (Table 1 and Figure 1). These differential energies of reaction together with the ecological theory of competitive exclusion result in the principle that oxidants are used preferentially and sequentially by heterotrophic bacteria to oxidize organic C substrate as a function of free energy yield, optimizing growth. As discussed in more detail subsequently, the further combination of this principle with the idea that in many cases deposits accrete steadily, predicts a biogeochemical reaction stratigraphy where the presence and scales of reaction zones are determined by the relative fluxes of oxidants and reductants, diffusive transport, and advection rates of material away from the sediment–water interface (Froelich et al., 1979).

Although net redox reaction relationships and dominant metabolic reaction sequence are well represented by the simple set of major oxidants and organic C reductant, as a rule, multiple nested redox reactions and intermediate reactants and products can and do occur within individual zones. For example, a complex network of oxidation–reduction reactions and intermediates (SO_3^-, $S_2O_3^{2-}$, polythionates, and polysulfides) characterizes S cycling associated with the net overall reduction of SO_4^{2-} (Canfield et al., 2005; Goldhaber, 2003; Jorgensen, 2006). Another more recently recognized example is Mn^{3+}, which is an intermediate product during reduction and oxidation cycling of Mn, and can represent as much as 80% of total dissolved Mn in pore water (Madison et al., 2011). This powerful dissolved oxidant can diffuse into anoxic sediments along concentration gradients when total dissolved Mn otherwise appears constant and which traditionally would be interpreted as composed entirely of Mn^{2+}.

It is critical to recognize that the oxidant sequence reflects not only the metabolic optimization of C_{org} remineralization and free energy yields but also the relative thermodynamic stabilities and compatibilities of specific oxidized and reduced species associated with each major half reaction, that is, their order within the electromotive reaction series (Table 1). As a result of natural transport processes within deposits, a wide range of oxidants and reductants, either in solution or as particles, are continually brought into unstable associations or can react, most often through biologically mediated pathways which are chemoautotrophic (Table 2). If reduced species in solution or solids are transported into a region where a higher-order oxidant is present, they can be oxidized, or vice versa. For example, HS^- is energetically unstable in the presence of FeOOH and may be oxidized spontaneously to S or SO_4^{2-}. Similarly, the transport or release of Fe^{2+} into a region containing MnO_2 will result in the oxidation of Fe^{2+} and reduction of MnO_2. The generation of dissolved intermediates that are diffusively mobile, for example, NO_3^-, Mn^{3+}, or chelated Fe^{3+}, and that can migrate into adjacent redox zones greatly complicates redox interactions during general reaction progressions in sediments. Globally, the anaerobic (SO_4^{2-}) and aerobic oxidation of migrating CH_4 represents one of the most important expressions of the interaction between mobile

Table 1 The standard free energy of reaction, ΔG_r^0, for the dominant environmental redox reactions

Reaction	*ΔG_r^0 (kJ mol^{-1}) (half reaction)*	*ΔG_r^0 (kJ mol^{-1}) (whole reaction CH_2O)*
Oxidation		
CH_2O[a]$_{(aq)} + H_2O \rightarrow CO_{2(g)} + 4H^+ + 4e^-$	−27.4	
$^2/_3CH_3OH_{(aq)} + {}^2/_3H_2O \rightarrow {}^2/_3CO_{2(g)} + 4H^+ + 4e^-$	12.1	
$\frac{1}{2}\,CH_{4(aq)} + H_2O \rightarrow \frac{1}{2}CO_2 + 4H^+ + 4e^-$	57.2	
Reduction		
$4e^- + 4H^+ + O_{2(aq)} \rightarrow 2H_2O$	−491.0	−518.4
$4e^- + 4.8H^+ + 0.8NO_3^-{}_{(aq)} \rightarrow 0.4N_{2(g)} + 2.4H_2O$	−480.2	−507.6
$4e^- + 8H^+ + 2MnO_{2(s)} \rightarrow 2Mn^{2+}{}_{(aq)} + 4H_2O$	−474.5	−501.9
$4e^- + 12H^+ + 2FeOOH_{(s)} \rightarrow 4Fe^{2+}{}_{(aq)} + 8H_2O$	−258.5	−285.9
$4e^- + 5H^+ + \frac{1}{2}SO_4^{2-}{}_{(aq)} \rightarrow \frac{1}{2}H_2S_{(aq)} + 2H_2O$	−116.0	−143.4
$4e^- + 4H^+ + \frac{1}{2}CO_{2(g)} \rightarrow \frac{1}{2}CH_{4(aq)} + H_2O$	−57.2	−84.6

Standard free energies of formation from (Stumm and Morgan, 1996).

[a]CH_2O represents average organic matter with carbohydrate oxidation state (0) ($\Delta G_f^0 = -129$ kJ mol^{-1}). More oxidant is required per mole CO_2 produced as C_{org} oxidation state decreases (e.g., alcohols and lipids) (Adapted from Emerson and Hedges, 2003).

dissolved reductants and oxidants both within and at the surface of sedimentary deposits (Burdige, 2006; Jorgensen and Kasten, 2006; Reeburgh, 2007).

The occurrence of any of the diagenetic reactions, such as those in Table 1 or 2, depends on the accessibility of reactants one to another. Thus, most diagenetic reactions involving solutions and solids are dominated by surface associated reactants rather than bulk solid compositions. Reactants in the interior of mineral structures, while measureable analytically in bulk analyses, are relatively inaccessible during early diagenesis. For example, Fe^{3+} in the interior of specific mineral particles may react only very slowly with HS^- present in pore solution (10^4–10^5 years; Canfield et al., 1992; Goldhaber and Kaplan, 1974). Likewise, C_{org} may be incorporated into mineral structures or closely packed aggregates, inhibiting remineralization (Curry et al., 2007; Hedges and Keil, 1995; Mayer, 1994a,b). Diagenetic reactivity is therefore defined in large part by physical distribution and availability as well as native chemical composition and thermodynamic stability.

8.11.2.1.1 Coupled stoichiometric relations

In addition to the stoichiometric requirements of oxidation–reduction balances, minor and trace constituents of organic matter are often remineralized and released to solution in proportion to their abundance in metabolized substrate sources. As illustrated in Table 3, overall stoichiometric relations can be written for C/N/P during the remineralization of organic matter. Other non-C_{org} constituents, such as I, also show stoichiometric release, but at far lower concentrations than N and P (e.g., 0.4–0.6 mmol I $mol^{-1} C^{-1}$) (Ullman and Aller, 1985). These stoichiometric relations may vary at different stages of decomposition; for example, P and N can be preferentially released relative to C, during the initial stages of reaction, reflecting greater lability of P- and N-rich organic matter fractions, but tend in many cases toward the bulk composition of reactive organic matter when time averaged (Burdige, 2006). The usual representation of reduced products in these overall reactions reflects thermodynamic stabilities dictated by redox conditions, for example, while NH_4^+ might be released initially during the ammonification of proteins, NO_3^- is the stable form of dissolved N in the presence of O_2 and is rapidly generated during biological nitrification (Table 2). Stoichiometric relationships expressed during diagenesis, for example, in pore water compositions, often represent the net of multiple reactions, including uptake or precipitation, and may or may not simply reflect a single dominant process, such as heterotrophic remineralization of C_{org} or unidirectional dissolution of a mineral.

Table 2 Example aerobic and anaerobic metabolite oxidation reactions that can occur in marine sediments

Reactions coupled to O_2 reduction	*Reactions coupled to NO_3^- reduction*
$NH_4^+ + 2O_2 \rightarrow NO_3^- + 2H^+ + H_2O$	
$Mn^{2+} + {}^1/_4O_2 + {}^3/_2H_2O \rightarrow MnOOH + 2H^+$	$NH_4^+ + NO_2^- \rightarrow N_2 + 2H_2O$ (anammox)
$Mn^{2+} + ½\ O_2 + H_2O \rightarrow MnO_2 + 2H^+$	${}^5/_3NH_4^+ + NO_3^- \rightarrow {}^4/_3N_2 + 3H_2O + {}^2/_3H^+$ (anammox)
$Fe^{2+} + {}^1/_4O_2 + {}^5/_2H_2O \rightarrow Fe(OH)_3 + 2H^+$	$NO_3^- + {}^5/_8FeS + H^+ \rightarrow {}^1/_2N_2 + {}^5/_8SO_4^{2-} + {}^5/_8Fe^{2+} + ½\ H_2O$
$FeS + {}^9/_4O_2 + 5/2H_2O \rightarrow Fe(OH)_3 + SO_4^{2-} + 2H^+$	$NO_3^- + 5Fe^{2+} + 12H_2O \rightarrow 5Fe(OH)_{3+} ½\ N_2 + 4\ H^+$
$FeS_2 + {}^{14}/_4O_2 + 7/2H_2O \rightarrow Fe(OH)_3 + 2SO_4^{2-} + 4H^+$	${}^5/_2Mn^{2+} + NO_3^- + 2H_2O \rightarrow {}^5/_2MnO_2 + {}^1/_2N_2 + 4H^+$
$½\ CH_4 + O_2 \rightarrow ½\ CO_2 + H_2O$	
Reactions coupled to Mn oxide reduction	*Reactions coupled to Fe oxide reduction*
$4MnO_2 + NH_4^+ + 6H^+ \rightarrow 4Mn^{2+} + NO_3^- + 5H_2O$	$2Fe(OH)_3 + HS^- + 5H^+ \rightarrow 2Fe^{2+} + S^0 + 6H_2O$
${}^3/_2MnO_2 + NH_4^+ + 2H^+ \rightarrow {}^3/_2Mn^{2+} + ½\ N_2 + 3H_2O$	$4FeOOH + ½\ HS^- + 8H^+ \rightarrow 4Fe^{2+} + ½\ SO_4^{2-} + 6H_2O$
$2H^+ + MnO_2 + {}^1/_4FeS \rightarrow Mn^{2+} + {}^1/_4SO_4^{2-} + {}^1/_4Fe^{2+} + H_2O$	$8FeOOH + FeS + 16H^+ \rightarrow 9Fe^{2+} + SO_4^{2-} + 12H_2O$
$3H^+ + MnO_2 + HS^- \rightarrow Mn^{2+} + S^0 + 2\ H_2O$	$4Fe(OH)_3 + ½\ CH_4 + 8H^+ \rightarrow 4Fe^{2+} + ½\ CO_2 + 11H_2O$
$MnO_2 + 2Fe^{2+} + 4H_2O \rightarrow Mn^{2+} + 2Fe(OH)_3 + 2H^+$	
Reactions coupled to SO_4^{2-} reduction	
$CH_4 + SO_4^{2-} \rightarrow HCO_3^- + HS^- + H_2O$	

All reactions shown in **Table 2** are spontaneous for typical concentrations found in specific zones in marine sediments. Example free energy calculations are given in Burdige (2012).

Table 3 Overall stoichiometric (C/N/P) organic matter oxidation reactions. Model Redfield ratios for *x*, *y*, and *z* are typically taken as 106, 16, and 1

Metabolic redox process	*Overall reaction*
Aerobic respiration	$(CH_2O)_x(NH_3)_y(H_3PO_4)_z + (x+2y)O_2 \rightarrow xCO_2 + (x+y)H_2O + yHNO_3 + zH_3PO_4$
Nitrate reduction	$5(CH_2O)_x(NH_3)_y(H_3PO_4)_z + 4xNO_3^- \rightarrow xCO_2 + 3xH_2O + 4xHCO_3^- + 2xN_2 + 5yNH_3 + 5zH_3PO_4$
Manganese reduction	$(CH_2O)_x(NH_3)_y(H_3PO_4)_z + 2xMnO_2(s) + 3xCO_2 + xH_2O \rightarrow 2xMn^{2+} + 4xHCO_3^- + yNH_3 + zH_3PO_4$
Iron reduction	$(CH_2O)_x(NH_3)_y(H_3PO_4)_z + 4xFe(OH)_3 + 7xCO_2 \rightarrow 4xFe^{2+} + 8xHCO_3^- + 3xH_2O + yNH_3 + zH_3PO_4$
Sulfate reduction	$2(CH_2O)_x(NH_3)_y(H_3PO_4)_z + xSO_4^{2-} \rightarrow xH_2S + 2xHCO_3^- + 2yNH_3 + 2zH_3PO_4$
Methane production	$(CH_2O)_x(NH_3)_y(H_3PO_4)_z \rightarrow {}^x/_2CH_4 + {}^x/_2CO_2 + yNH_3 + zH_3PO_4$

Source: Modified from Aller, 1980a; Tromp et al., 1995. Note: NH_3, H_3PO_4, and H_2S commonly speciate to NH_4^+, HPO_4^{2-}, and HS^-, affecting carbonate speciation, carbonate alkalinity balances, and potential for additional reactions.

8.11.2.1.2 Pore water solutes as reaction indicators

As is evident from the preceding examples, many of the early diagenetic reactions taking place in sediments involve both dissolved and particulate reactants and products. Because of the relative mass relations of solutions and solids and respective sensitivities of analysis, solute compositions can be extremely sensitive indicators of reactions. The change in concentration in solution, ΔC (mass cm^{-3} pore water), corresponding to a change in solid mass concentration, $\Delta\hat{C}$ (mass g^{-1}), is given by

$$\Delta C = \Delta\hat{C}\rho_s\left(\frac{1-\varphi}{\varphi}\right) \quad [1]$$

where φ = saturated porosity (ratio of pore solution volume to total sediment volume) and ρ_s = particle density (g cm^{-3} solid particle volume).

For a typical porosity and particle density in surface sediment of ~0.8 and 2.6 g cm^{-3}, a readily detectable change in solution concentration of 1 mM (mM = millimole $Liter^{-1}$ pore water) for dissolved HCO_3^- corresponds to a mass loss of organic C (C_{org}) or inorganic C (C_{inorg}) of ~0.0024% weight solids, which would be undetectable by standard analytical methods. Thus, pore water compositions can reflect minute changes in solids and solution–solid interactions, and their analysis and distributions are often emphasized in the examination of early diagenetic processes. In addition, solution compositions usually dictate mineral stabilities, reactivities, and dissolution–reprecipitation processes, and, as illustrated subsequently, mass transport and redistribution within deposits usually take place dominantly through fluids.

8.11.2.2 Reaction Rates and Kinetics

The rates of diagenetic reactions determine in part the potential for a particular energetically favorable reaction or set of reactions to be expressed in deposits. Reactions with extremely slow or rapid rates are of little consequence for sediment composition during early diagenesis. The former may be important at great depth, and the latter restricted to a vanishingly thin zone at the sediment surface where reaction products are not retained or effectively define a boundary condition. Reaction kinetics and specific relationships between reactants also determine the response of reactions to particular sedimentary transport regimes, as outlined in the succeeding text. In the case of redox reactions associated with organic matter decomposition, a commonly assumed general kinetic form relating organic matter reductant and oxidants is (Boudreau, 1997; Burdige, 2006; Paul and van Veen, 1978; Van Cappellen and Gaillard, 1996)

$$\frac{d\hat{C}_r}{dt} = -k_i\hat{C}_r\frac{(Ox_i)}{(K_{Ox,i}+(Ox_i))}In_{ij} \quad [2]$$

where $\hat{C}_r$ is the concentration of reactive organic carbon (often designated as $\hat{G}$), t is the time, k_i is the reaction rate coefficient for oxidant i, $K_{ox,i}$ is the reaction half-saturation constant for oxidant i, and In_{ij} represents the metabolic inhibition of oxidant i by all other oxidants j. The stoichiometries of reactions relate $\hat{C}_r$ and oxidants as a function of time (Tables 1 and 3). When multiple oxidants are present, the inhibition function allows for continuous transition between successive, energetically favorable oxidants as concentrations are depleted. An inhibition function can also be written to represent the negative effect of metabolite buildup (e.g., H_2S and NH_4^+) on microbial communities (Bailey and Ollis, 1986; Humphrey, 1972; Van Cappellen et al., 1993). These functions may have a form such as

$$In_{ij} = \frac{1}{1+\frac{C_j}{K_j}} \quad [3]$$

where K_j is an inhibition constant for solute C_j on solute C_i.

The hyperbolic kinetics of eqn [2] can be substantially simplified in practice to more practically useful forms appropriate to particular reactants, conditions, and regions of deposits. Within a distinct zone or a deposit dominated by a given redox reaction, the inhibition function (eqn [3]) can be discarded. A reactant concentration may also be in excess relative to the half-saturation constant, $K_{m,i}$, allowing further simplification to a zeroth order dependence in that reactant. For example, in the case of SO_4^{2-} reduction, $K_{m,SO_4^{2-}}$ for SO_4^{2-}-reducing bacteria is in the range of ~0.1–0.3 mM (Habicht et al., 2002; Pallud and Van Cappellen, 2006). Because seawater SO_4^{2-} is ~28 mM, the rate of SO_4^{2-} reduction is effectively zeroth order in SO_4^{2-} concentration (i.e., $[SO_4^{2-}]/(K_{m,SO_4^{2-}}+[SO_4^{2-}]) \sim 1$), and its reduction rate is thus dependent largely on the reactivity and quantity of organic matter reductant over extensive regions of marine deposits (Berner, 1964; Boudreau and Westrich, 1984; Goldhaber, 2003). Similarly, if oxidant concentrations are much lower than $K_{m,NO^{3-}}$, such as often characterizes zones of NO_3^- reduction (denitrification) in surface sediments, then NO_3^- reaction kinetics are effectively first order with respect to NO_3^- concentration, and its reduction rate otherwise determined by the availability and reactivity of organic matter (e.g., Billen, 1982). As illustrated subsequently, when concentration distributions within deposits are at steady state, it is not necessary to know detailed kinetic relationships in order to estimate the magnitude of net reaction rates.

Organic carbon (C_{org}) reactivity is determined by inherent properties of particular compound groups (molecular structure), physical–chemical associations (organic–mineral complexes), and conditional environmental factors, including oxygen availability, redox oscillation, and metabolite buildup. Oxygen availability (exposure time) plays a particularly important role for the decomposition of relatively refractory components (Emerson and Hedges, 2003; Hedges et al., 1999; Hulthe et al., 1998; Kristensen and Holmer, 2001). Despite the potential for complex controls, phenomenologically, the apparent reactivity, k, of bulk sedimentary organic matter varies regularly as $1/t$, where t represents time since the initial synthesis of an organic component ($10^{-3} < t < 10^6$ yr) (Middelburg, 1989; Middelburg et al., 1993). The value of k changes during decomposition progressively with time, ranging over more than 8 orders of magnitude: from $\sim 10^2$–10^3 per year for recently formed algal biomass to 10^{-7} per year for deeply buried, residual deposits millions of years old (Figure 3; Middelburg et al., 1993).

Because sediments typically reflect mixtures of material from varied sources with different ages, for example, reworked ancient rock debris and recently formed or actively forming

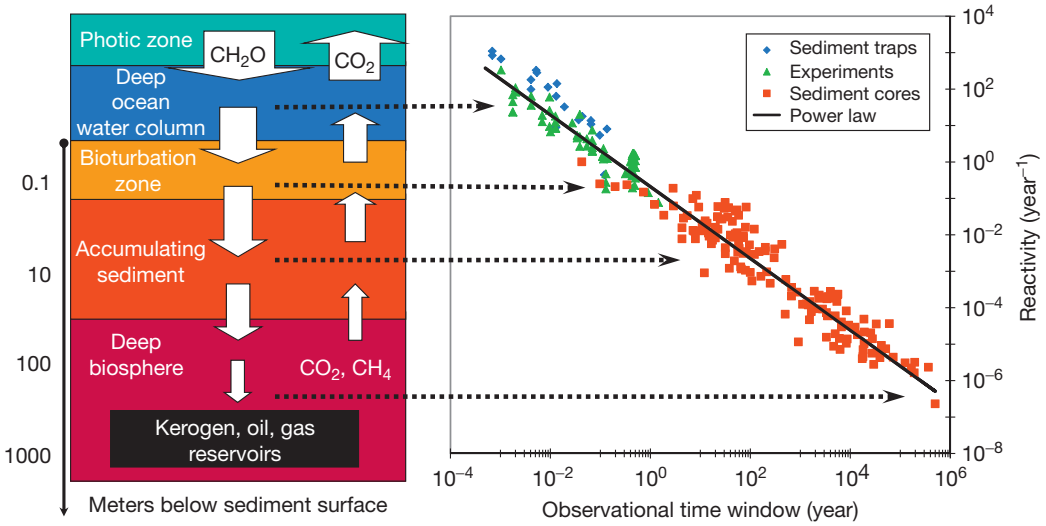

Figure 3 The reactivity of sedimentary organic matter, and thus the intensity of coupled diagenetic processes (**Figure 1(a)**), decreases with time after initial biogenic synthesis and with progressive stages of decomposition. Estimates of reactivity derived from both experimental measurements and diagenetic modeling, based largely on regime (a) of **Figure 2**, follow the power law relation $k = 0.21t^{-0.985}$ per year, where k is a first-order kinetic coefficient and t is time (Middelburg et al., 1993). Although organic matter of different bulk reactivities are mixed during sedimentary recycling, general ranges of average reactivity characterize specific environmental zones and sediment burial depths. Modified from Middelburg JJ and Meysman FJR (2007) Burial at sea. *Science* 316: 1294–1295; Middelburg JJ, Vlug T, and Vandernat F (1993) Organic-matter mineralization in marine systems. *Global Planetary Change* 8: 47–58.

biomass, surface deposits usually contain a wide spectrum of organic materials having different ages and reactivities (Blair and Aller, 2012). Thus, the reactivity of bulk sedimentary organic matter is most accurately conceptualized and quantified as a weighted average of reactivities corresponding to a continuum of compositions and degradation states of sediment components rather than a single k (Boudreau and Ruddick, 1991). For reasonable assumptions regarding the nature of the reactivity distribution function, the reactive continuum model predicts the observed $1/t$ dependence of the apparent k observed for bulk sedimentary organic matter (Tarutis, 1993).

The continuum of organic matter reactivities in surface sediments is often approximated by a set of discrete reactivities that characterize averaged subsets, usually taken as three subpools (k_1, k_2, and k_3 ($k_3 = 0$)), of the bulk organic matter present (Hales, 2003; Martin and Sayles, 2003; Westrich and Berner, 1984). Heterotrophic synthesis and secondary production of organic matter accompanies all biologically mediated degradation, continuously modifying unidirectional changes in reactivity with time (e.g., eqn [2]), but these synthetic processes are seldom included in quantitative models of net decomposition kinetics (Paul and van Veen, 1978). The wide spectrum of organic debris and differential reactivities in sediments are demonstrated directly by the differences between ^{14}C activities of bulk sedimentary C and the CO_2 (HCO_3^-) released into pore water during early diagenesis, the latter showing far higher ^{14}C activities than bulk sediment and reflecting preferential biological utilization of distinctly younger substrates (Blair and Aller, 2012; Emerson et al., 1987; Martin et al., 2000).

8.11.2.3 Sedimentary Redox Reaction Patterns

The expression of the thermodynamic redox reaction sequence in sedimentary deposits is dependent on the relative and absolute abundance of specific reactants, on reaction rates, and on transport conditions dictated by the local diagenetic regime. If all natural oxidants are available in a depositional environment, sufficient reactive organic matter reductant is supplied, and sediment accretes regularly upward with time, a distinct reaction stratigraphy is typically observed with depth (**Figure 4(a)**). If specific oxidants are absent or minimal, for example, minor quantities of Fe oxides in shallow water carbonate deposits or minor SO_4^{2-} at low salinities, the corresponding reaction zone is absent or minimized. Specific terminologies are used to describe the redox conditions and net reaction zones. The most commonly used terms to describe the dominant redox conditions and corresponding reaction zones are oxic (O_2 present) and anoxic (O_2 absent), the demarcation being defined operationally as regions where microbial populations can or cannot function effectively as aerobes (the analytical detection of O_2 can be below biologically viable levels). The anoxic zone is often further subdivided into suboxic (inclusive of NO_3^-, MnO_2, and FeOOH reduction), sulfidic (SO_4^{2-} reduction), and methanic (CO_2 reduction) (Berner, 1981; Froelich et al., 1979). Some investigators prefer the use of the term postoxic rather than suboxic (Berner, 1981) or abandoning a group term such as suboxic altogether and defining only individual reactant or product zones, for example, nitrogenous ($NO_3^- \leftrightarrow N_2$), manganous ($MnO_2 \leftrightarrow Mn^{2+}$), and ferruginous ($FeOOH \leftrightarrow Fe^{2+}$) (Canfield and Thamdrup, 2009; Emerson and Hedges, 2003). Because the compositional expressions of the redox reactions associated with NO_3^-, MnO_2, and FeOOH reduction can be (1) individually distinctive, or (2) present but subdued (e.g., Fe^{2+} product undetectable in solution but adsorbed to solid and nitrification–denitrification occurring but not expressed by obvious net NO_3^- production or analytically detectable N_2), or (3) overlapping and very difficult to resolve spatially in reductant-rich or unsteady shallow water

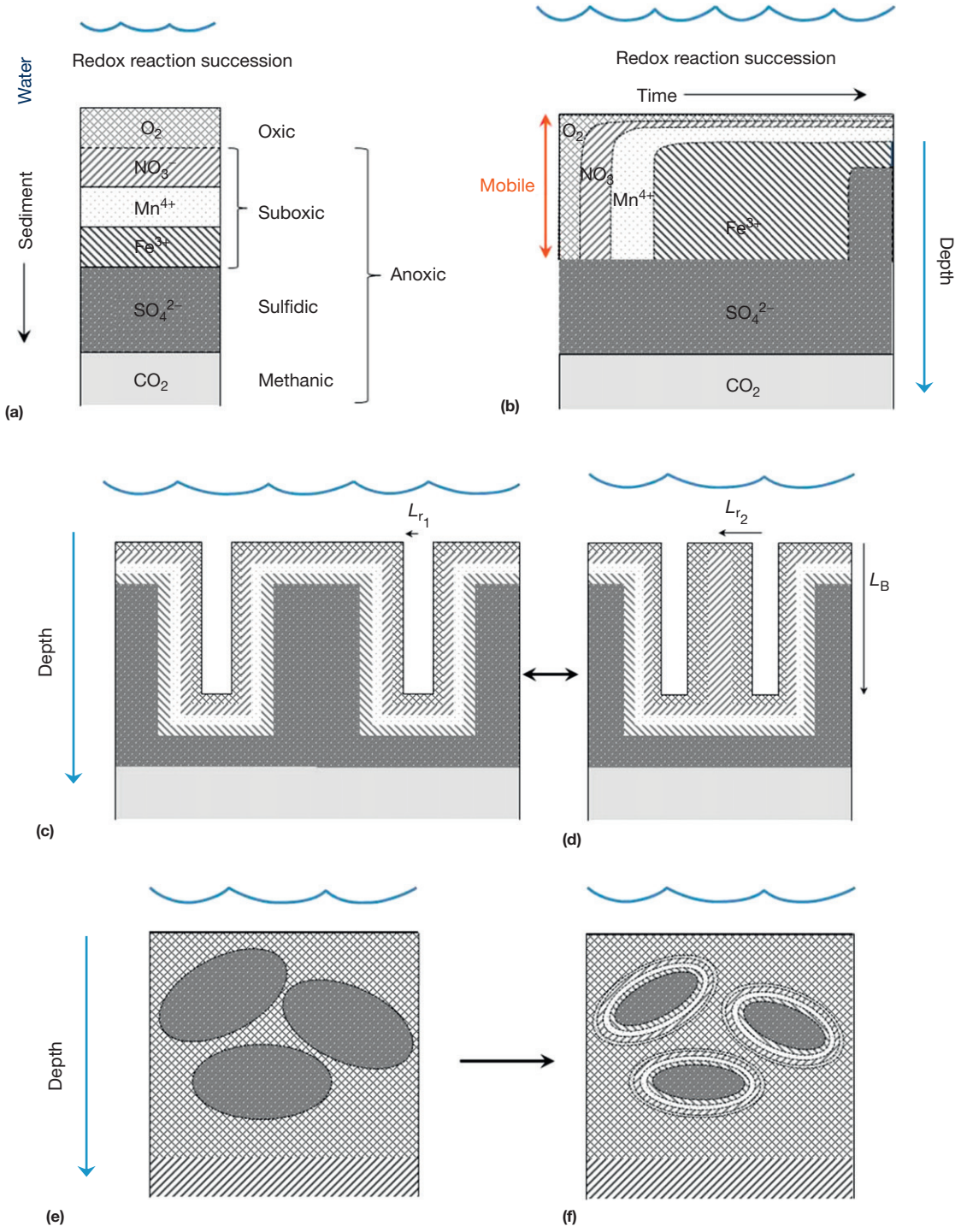

Figure 4 (a) Classic general redox reaction zonation with depth and time in steadily accreting sedimentary deposits (as per **Figure 2(a)**). Relative zonal depth scaling depends on absolute and relative fluxes of oxidants and reductants. Terminology applied to individual zones is indicated (Adapted from Aller, 1982b; Berner, 1980). (b) Unsteady redox succession and diagenetic ingrowth sequence in the surface mobile zone following a reoxidation–exchange event (as per **Figure 2(c)**). Duration of individual redox stages is largely a function of oxidant and reactive reductant abundance (entrainment) following disturbance. Suboxic conditions often dominate the mobile zone for extended periods (after Aller, 2004). (c) Characteristic redox reaction scaling associated with oxygenated cylindrical biogenic burrow structures. (d) Redox reaction patterns are a function of burrow packing patterns and characteristic structure scales L_{r1} (burrow radius), L_{r2} (burrow spacing), and L_B (burrow length). (e) Ellipsoidal (spherical) redox microenvironments associated with fecal pellet or aggregate formation may be initially anoxic and embedded in an otherwise oxic background. (f) Unsteady redox reaction distributions, such as (e) transition through multiple stages with time and progressive oxidation (reactions as in **Table 2**).

and hemipelagic deposits, the term suboxic is retained here to describe the set of redox conditions that are anoxic, nonsulfidic, and nonmethanic and in which any or all of the oxidants NO_3^- and Fe–Mn oxides are subject to preferential reduction, and the reactions of which dominate diagenetic properties.

Redox reaction zones need not be expressed in a strictly vertical sequence within deposits. Major sedimentary examples are mobile muds that are commonly found in energetic topset regions of clinoform deltas or in most river channels, the surface zones of which behave as episodically mixed batch reactors (Figure 2(c)). In these cases, the reaction sequence takes place with time after physical reworking and reoxidation of a distinct layer of sediment, which overlies a stable layer unconformably from both a depositional and diagenetic perspective (Figure 4(b)). The redox reaction sequence within the reworked layer can occur multiple times depending on the frequency of reworking. Macrofaunal bioturbation is absent in these systems and reworked sediment behaves as a microbial reactor (Aller et al., 2010). The length of time during which particular reaction conditions dominate depends on the relative abundance of oxidants and reductants. For example, the relatively abundant highly reactive FeOOH ($\sim$300–400 μmol g^{-1}) often present in tropical deltaic deposits, whose sources are well-weathered terrain, promotes lengthy periods (0.5–1 year) of Fe reduction following reworking, exposure, and reoxidation events (Aller, 2004; Aller et al., 2004b). When the frequency of disturbance and oxidant regeneration match the length of time a particular oxidant is dominant, sediment can be effectively poised in a single dominant suboxic redox state (e.g., Fe reduction) despite abundant reactive reductant. If reworking ceases for an extended period and residual reductant is sufficiently abundant, the deposit eventually transitions to the vertically expressed sequence characteristic of steady sedimentation and the surface boundary condition (e.g., Figure 4(a)).

In less energetic sedimentary environments, the macrofaunal burrows that typically permeate the bioturbated zone are periodically irrigated with oxygenated overlying water (Kristensen and Kostka, 2005). These irrigated biogenic structures generate a complex pattern of redox reactions centered around oxic microenvironments embedded in an otherwise anoxic deposit. Many burrows or tubes are cylindrical or approximations thereof and a cylindrical distribution of redox zones tends to form around them. The radial scaling of these zones depends on the relative abundance of reactants in the deposits within which burrows or tubes are formed and irrigated (Figure 4(c)). Additionally, the reaction zonation has scaling characteristic of the fauna that create structures and is typically superimposed on the overall vertical redox stratigraphy. Reaction scaling and coupling between reaction zones (e.g., reactions per Table 2) is further dependent on population densities and microenvironment packing distributions. Redox zones can meld in various configurations as burrow structures become closer or farther apart within a deposit (Figure 4(d)). Thus, it is possible in a bioturbated deposit to have multiple reaction patterns and net balances of reactions, for example, nitrification–denitrification or SO_4^{2-} reduction, dominating laterally within different patches of faunal sizes and abundances in both space and time.

Spherical, ellipsoidal, or irregular reaction geometries are also commonly present in deposits, particularly at scales typical of biogenic fecal material or sediment aggregates and flocs (mm) (Figure 4(e)). Such microenvironments may be sites of enhanced reaction rates because of elevated reductant content and be embedded as transient but continuously renewed features in a more oxidizing redox zone (Figure 4(f); Jahnke, 1985; Jorgensen, 1977). The presence and scaling of such microenvironments can be directly demonstrated using planar optical imaging sensors, which resolve small-scale hotspots of remineralization, for example, O_2 distributions or exoenzyme activity (Cao et al., 2011; Glud, 2008); various forms of equilibration probes, which reveal equivalent reaction heterogeneity (Stockdale et al., 2009); and in preserved patterns of authigenic minerals where aggregates are centers of accumulated reaction products (e.g., Cole, 1985; Hein and Griggs, 1972; Hein et al., 1979).

8.11.2.3.1 Redox oscillation

Although much of the theory of redox reactions and diagenetic processes centers on concepts of stable oxic and anoxic conditions and respective diagenetic behavior, it should be obvious from previous examples that redox patterns in surface deposits can be highly variable and dynamic over a wide range of spatial and temporal scales, particularly in geometrically structured bioturbated deposits (e.g., Aller, 1994a; Forster and Graf, 1992; Kristensen and Kostka, 2005) but also in highly dynamic fluidized mud environments (e.g., Aller, 2004). A volume of sediment may be subject to multiple successive redox conditions which oscillate between oxic and anoxic, allowing for a repetitive spectrum and variable dwell times of redox reactions and reaction intermediates. This oscillating condition can itself be considered a biogeochemical state or end-member (Aller, 1994a; Volkenborn et al., 2010, 2012). The development of optical imaging sensors (planar optodes; Glud et al., 1996) has allowed the direct visual documentation of such oscillations in two spatial dimensions and time and the quantification of the probability distributions of different redox conditions (Figure 5; Volkenborn et al., 2010, 2012). In addition to the introduction of O_2 into sediments by bioirrigation and physical ventilation of permeable sediments, the direct injection into overlying water of plumes of anoxic or low-O_2 water from burrows or more diffuse advective flow-through anoxic sediments results in small-scale redox oscillations and excursions in the bottom water boundary layer (Figure 5(c); Huettel et al., 1998; Volkenborn et al., 2010). Oxygen-driven redox oscillations also interact closely with and modify coupled sedimentary redox processes, such as denitrification (Gilbert et al., 2013) and the degradation pathways of specific compounds, such as lipids (Sun et al., 2002). Understanding these fluctuating reaction patterns, reaction probabilities, dwell times within individual redox states, and repetition patterns is a critical part of understanding processes that control microbial diversity and activity, the ultimate preservation of organic matter, and the burial of authigenic minerals.

8.11.2.3.2 Microenvironmental heterogeneity

The microenvironmental heterogeneity generated by physical disturbance or by biogenic structures within sediment can dramatically affect compositional patterns and diagenetic reaction distributions. Biogenic heterogeneity is time-dependent and characterized by multiple scales and geometries dictated by the life habits, feeding types, sizes and abundances of macrofauna, the interactive response of microbes to transport structure, and variously coupled reactions. For example, two-dimensional

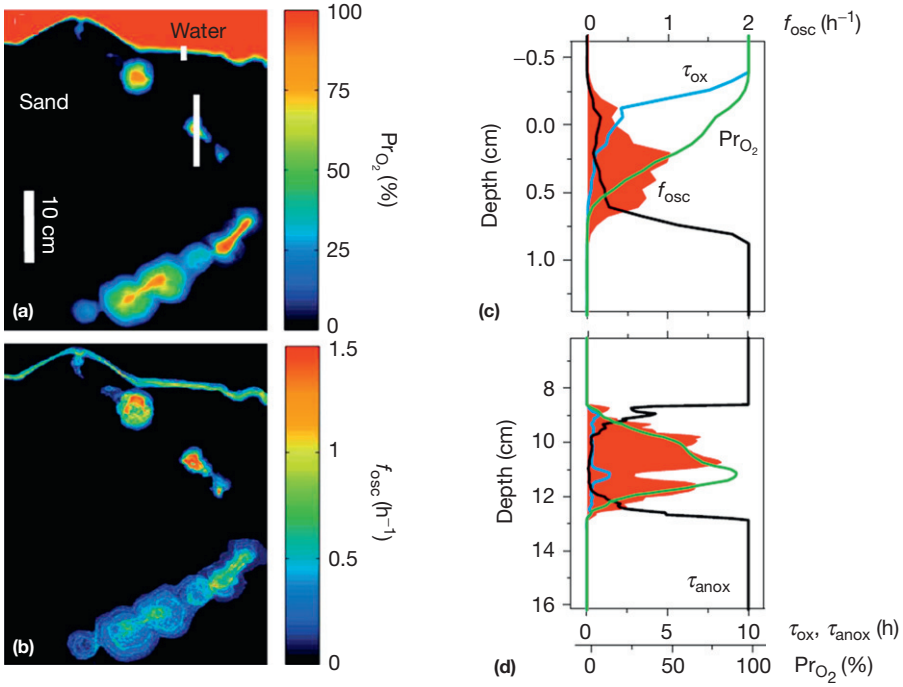

Figure 5 Redox reaction patterns in surface sediments are typically unsteady and oscillation of redox conditions is the rule. Ventilation of biogenic structures generates a wide spectrum of frequencies of oxygenation. Planar optode sensors allow 2-D visualization and quantification of O_2 exposure and residence time within deposits (Glud et al., 1996). (a) Example of 2-D O_2 distributions associated with thalassinidean ghost shrimp burrows (*Neotrypaea*) in sandy sediment (permeable) showing the probability of oxygenation (Pr-O_2) in overlying water and at sites around a single burrow structure within a deposit (Volkenborn et al., 2012). (b) 2-D image of frequency patterns of oxic–anoxic oscillations (f_{osc}) associated with ventilation patterns in different burrow regions. (c) Patterns of redox conditions across the sediment–water interface (along the upper vertical white line in (a)). The duration of oxic and anoxic conditions is given by timescales τ_{ox} and τ_{anox}, respectively. f_{osc} is plotted in solid fill (red). (d) Example patterns of subsurface redox conditions generated by burrow irrigation (along lower vertical white line in (a)). The zones of these oscillations shift with animal location and activity. Modified from Volkenborn N, Polerecky L, Wethey DS, DeWitt TH, and Woodin SA (2012) Hydraulic activities by ghost shrimp *Neotrypaea californiensis* induce oxic-anoxic oscillations in sediments. *Marine Ecology Progress Series* 455: 141–156.

optical imaging sensors for pH, an integrative master reaction variable, reveal the complex spatial and temporal patterns of sedimentary protonic reactions (e.g., oxidation–reduction and carbonate dissolution) in response to the formation, irrigation, and maintenance of burrows (**Figure 6**; Fan et al., 2011; Stahl et al., 2006; Zhu et al., 2006). Complex reaction rate patterns are rapidly generated by benthic community activities in deposits (e.g., SO_4^{2-} reduction; Bertics and Ziebis, 2010). Under these heterogeneous structural conditions, it is possible to have not only a spectrum of redox reactions but also opposing reactions, such as the dissolution and precipitation of $CaCO_3$ in close proximity (millimeter to centimeter scales) within the same vertical depth interval. These specific microenvironmental, four-dimensional redox reaction patterns in both space and time are also factors controlling net isotopic fractionations during coupled redox reactions, such as nitrification–denitrification (e.g., Brandes and Devol, 1995).

8.11.3 Diagenetic Transport Processes

8.11.3.1 Diffusive Transport

The consumption or production of solutes and particulate components within sediments, or unsteady changes in boundary conditions at the surface of deposits, generates gradients in concentrations (activities). These concentration gradients drive mass flow from regions of high to low chemical potential through the process of diffusion. The diffusive flux, J_D, which results from chemical potential gradients of a solute, can be reasonably approximated along one dimension in sediments by a form of Fick's first law:

$$J_D = -\varphi D_s \left(\frac{\partial C}{\partial z}\right) \quad [4]$$

where D_s=whole sediment diffusion coefficient (area/time), C=concentration (mass/volume solution), and z=space coordinate (length).

In porous media, such as sediments, the molecular diffusion coefficient in free solution, D, is modified by a pore geometry correction factor, usually represented as the square of the tortuosity, θ, to define $D_s = D/\theta^2$. The value of θ^2 is ≥ 1 and is determined in practice from empirical relationships with φ, such as $\theta^2 \sim 1/\varphi^2$ for muds, or $\theta^2 \sim 1 - \mathrm{Ln}(\varphi^2)$, or by analogy with electrical resistivity, $\theta^2 = \varphi F$, where F = formation resistivity factor when pore solutions are relatively good conductors (Andrews and Bennett, 1981; Boudreau, 1997). In multicomponent solutions, D_s is a tensor; however, for most early diagenetic applications for minor solutes in high ionic strength seawater, off-diagonal terms are ignored (Boudreau, 1997; Van Cappellen and Gaillard, 1996).

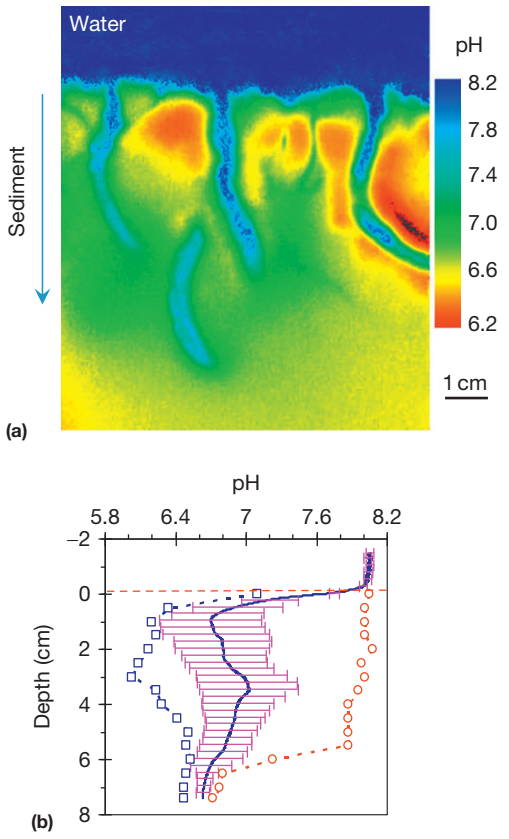

Figure 6 Biogenic structure generates complex, time-dependent reaction distributions and compositional patterns in surficial deposits as illustrated by both O_2 (**Figure 5**) and integrative reaction properties, such as pH. (a) Vertical section, 2-D pH distribution in marine mud visualized using a planar optode imaging system (Zhu et al., 2006). In this case, burrows are formed by the common polychaete *Nereis diversicolor*. (b) The 1-D vertical profile equivalent of pH in image (a) illustrating mean pH that might be measured by traditional methods (e.g., electrodes) as a function of depth, and the standard deviation, maximum, and minimum pH present within a depth interval. A wide range of reaction conditions can actually be present at any given depth in bioturbated sediments (after Zhu et al., 2006). Reproduced from Zhu QZ, Aller RC, and Fan YZ (2006) Two-dimensional pH distributions and dynamics in bioturbated marine sediments. *Geochimica et Cosmochimica Acta* 70: 4933–4949.

A major use of eqn [4] is in the estimation and prediction of diffusive solute fluxes into and out of sediment from measurements of pore water concentration gradients in the vertical dimension at the sediment–water interface. A second major application is as the basis for diffusive mass balance in the formulation of Fick's second law and general diagenetic transport–reaction models.

8.11.3.2 Advective Transport

Advection of pore fluids and solids occurs as sediment accretes upward or pressure gradients are otherwise imposed. The simplest case in this regard is a steady, unidirectional sedimentation rate and no compaction in one dimension (Berner, 1964). These approximations are often remarkably good over specific depth intervals in a deposit, particularly below the zones of bioturbation, physical remobilization, or impressed flow (e.g., **Figure 2(a)**, **2(c)**, and **2(d)**). The vertical advective flux of a solute, J_A, in this simplified case is given by

$$J_A = \varphi\omega C \qquad [5]$$

where ω = sediment accumulation rate (length/time).

In the absence of compaction or impressed flow, fluids and solids advect at the same rate (φ = constant). When compaction takes place, fluids and solids are differentially transported at depth-dependent rates as porosity decreases, often with a functional dependence of the form $\varphi(z) = \varphi_0 \exp(-\beta z) + \varphi_\infty$, where φ_0 and φ_∞ are constants over finite depth intervals. When sediments are permeable, however, such as well-sorted sands, pore fluids can respond to imposed pressure gradients and advect pore water independently of solids at a rate, v, completely decoupled from sediment accumulation or compaction (Huettel and Webster, 2001). The advection of fluids through porous deposits also results in dispersion, a process not normally incorporated into diagenetic models because of the traditional emphasis on low-permeability mud systems (Bear, 1972).

8.11.4 Diagenetic Transport–Reaction Models

8.11.4.1 General Mass Balance Relations and Reference Frames

Diagenetic transport–reaction models are utilized for a range of purposes, including the quantification of mass fluxes from compositional patterns, relating fluxes and reaction patterns to specific diagenetic regimes, predictive modeling given specific boundary and reaction conditions, and for inverse modeling, for example, inferring governing reaction rates, transport rates, or boundary conditions from compositional distributions (Berner, 1980; Boudreau, 1997; Burdige, 2006; Schulz, 2006; Van Cappellen et al., 1993). The mass balances dictated by a given set of transport–reaction processes in sediments are combined in model equations for solutes and particles of the general form

$$\frac{\partial \varphi C}{\partial t} = -\nabla J + \sum \varphi R \qquad [6a]\ \text{solute}$$

$$\frac{\partial (1-\varphi)\hat{C}}{\partial t} = -\nabla \hat{J} + \sum (1-\varphi)\hat{R} \qquad [6b]\ \text{solid}$$

where $C, \hat{C}$ = concentration of solute or particle property respectively, t = time, $J, \hat{J}$ = flux of solute or particle solid property (e.g., $J = J_D + J_A$), $R, \hat{R}$ = reactions affecting solute or particle solid property, ∇ = gradient operator in respective coordinate system, and Σ = summation operator over all reactions affecting species i.

These equations are readily written but in practice require numerous assumptions and approximations to allow evaluation, application, and reasonable interpretation. It is necessary to thoroughly consider the diagenetic regime and time–space scales within which a model is formulated, and it is in this context that application of mathematical concepts must be tempered by an understanding of environmental processes and a focus on the primary goal of a model. In the simplest traditional diagenetic application, model goals are centered on quantifying average properties as a function of vertical depth in a deposit and on the overall mass fluxes associated with

diagenetic alteration (e.g., Berner, 1964; Burdige, 2006; Schulz, 2006). The scale of lateral variation is assumed to be isotropic and small relative to vertical variation. In this case, model equations are evaluated within a one-dimensional coordinate system, the origin of which is fixed at the sediment–water interface with positive axis directed into the deposit. Taking a spatial coordinate, z, the general equations then become

$$\frac{\partial \varphi C(z,t)}{\partial t} = -\frac{\partial}{\partial z} J(z,t) + \sum \varphi R(z,t) \qquad \text{[7a] solute}$$

$$\frac{\partial (1-\varphi)\hat{C}(z,t)}{\partial t} = -\frac{\partial}{\partial z} \hat{J}(z,t) + \sum (1-\varphi)\hat{R}(z,t) \qquad \text{[7b] solid}$$

In complex diffusion–reaction geometries such as characterize the bioturbated zone of sediments, it may be appropriate to consider alternative coordinate systems. For example, application of the mass balances of eqn [7a] in a three-dimensional cylindrical coordinate system centered on individual macrofaunal burrow microenvironments can accurately reproduce averaged pore water distributions, simulate three-dimensional variability, and predict flux relations in bioirrigated deposits (Aller, 1980b, 2001). The characteristic scaling of the model microenvironments is determined by benthic community population density, burrowing depth, and the size distribution of individuals within a deposit (**Figure 4(c)** and **4(d)**).

8.11.4.2 Simplification of Diagenetic Models

For a minor solute, C_i, in seawater, it is normal to assume that diffusive transport coupling between solutes is minimal (allowing for a single D_i) and to ignore compaction and impressed flow (low permeability) over a modeled interval, giving from eqns [4]–[7]:

$$\frac{\partial C_i(z,t)}{\partial t} = -\frac{\partial}{\partial z}\left(-D_i \frac{\partial C_i}{\partial x} + \omega C_i\right) + \sum R(z,t) \qquad \text{[8a] solute}$$

Similarly, for a particle-associated solid component:

$$\frac{\partial \hat{C}(z,t)}{\partial t} = -\frac{\partial}{\partial z}\left(-D_B \frac{\partial \hat{C}_i}{\partial z} + \omega \hat{C}_i\right) + \sum \hat{R}(z,t) \qquad \text{[8b] solid}$$

In this case, particle transport resulting from the bioturbation activities of benthic communities is represented by a particle mixing coefficient, D_B, analogous, when temporally and spatially averaged, to a diffusion process (Boudreau, 1986; Meysman et al., 2008). The assumption of constant porosity in this context avoids the problem of determining whether particle mixing fluxes occur with respect to solid mass or whole sediment volume, that is, where the factor $(1-\varphi)$ should be placed in the diffusive formulation (inter- and intraphase mixing; Boudreau, 1997). D_B can be strongly depth-dependent but is often taken as constant over a finite interval of interest. D_B also varies as a function of depositional environment, for example, with food supply to bottom fauna, and in general decreases with bathymetric depth in the ocean (Boudreau, 1994; Lecroart et al., 2010; Tromp et al., 1995) (**Figure 7(b)**). Alternative representations of particle mixing may be necessary depending on the time and space scales considered (e.g., details of sampling scheme). For example, specific particle exchange functions, which describe the movement of particles between regions within the deposit, can be defined and represent a class of transport model termed 'nonlocal' (as opposed to the 'local' transport steps characteristic of diffusion). These nonlocal models for both particles and solutes have a source–sink form, mathematically similar to a first-order reaction term, and depending on application may require considerable information on the exact scaling and style of mixing and fluid transport phenomena within deposits (Boudreau and Imboden, 1987; Emerson et al., 1984; Martin and Banta, 1992; Meysman et al., 2003).

8.11.4.2.1 Characteristic scaling and steady state

It is often possible to further simplify and eliminate diagenetic model terms based on their relative contributions to fluid or solid property distributions over particular temporal and spatial scales. For example, a basis for simplification can be made by considering the relative values of characteristic timescales, τ_{dif}, τ_{ad}, and τ_{rx}, for diffusion, advection, and reaction processes, respectively, that correspond to a length scale of interest, L:

$$\tau_{dif} = \frac{L^2}{D};\ \tau_{ad} = \frac{L}{\omega};\ \tau_{rx_1} = \frac{1}{k} \qquad [9]$$

In this illustrative case, τ_{rx1} is taken for a first-order kinetic reaction having reaction constant k. The ratio τ_{dif}/τ_{ad} is the Peclet number, Pe, which provides guidance as to the relative dominance of diffusive or advective transport terms over particular scale lengths. In regions near the sediment–water interface, for example, with $L = 10$ cm a vertical length scale and a typical range of sediment accumulation rates of $\omega = 0.0001$–1 cm per year and solute diffusion $D_s = 100$–400 cm^2 per year, Pe is $\ll 1$, demonstrating that the sediment accumulation advective term is usually slow relative to diffusion and can be dropped for most purposes in models of pore water solutes focused on that zone. The ratios τ_{dif}/τ_{rx1} or τ_{ad}/τ_{rx1} are forms of Damköhler numbers (Da) and provide a means of determining the relative importance of transport modes or reaction in controlling the distribution of a reactive substance over the scale L. For example, if over a layer of thickness L a particle-associated radiotracer is mixed diffusively at a rate D_B and used to define a $\hat{\tau}_{dif}$ and the corresponding first-order radioactive decay constant, λ, used to define the reaction timescale $\hat{\tau}_{rx_1}$, then the layer is homogeneously mixed with respect to the tracer when $\frac{\hat{\tau}_{dif}}{\hat{\tau}_{rx_1}} \ll 1$. Conversely, if $\frac{\hat{\tau}_{dif}}{\hat{\tau}_{rx_1}} \gg 1$, the tracer decays before reaching depth L, and for mathematical purposes, the lower boundary can be assumed to approach $z \to \infty$, that is, with respect to processes controlling the tracer, the zone can be modeled as a semi-infinite body.

A primary assumption of most practical applications of diagenetic models is that boundary conditions and internal transport–reaction balances are steady state. Steady state is often a very reasonable assumption because sampling scales and the particular use and context of a model are such that it is valid, although for other time and space scales it might not be (Lasaga and Holland, 1976; see subsequent **Section 8.11.5.5**). The steady-state assumption eliminates the time-dependent terms in [8a] and [8b] $\left(\frac{\partial C_i(z,t)}{\partial} = 0; \frac{\partial \hat{C}(z,t)}{\partial t} = 0\right)$ and permits immediate estimates of either net reaction rates or transport directly from measured concentration distributions. Although it is not possible to infer reaction kinetics or functional

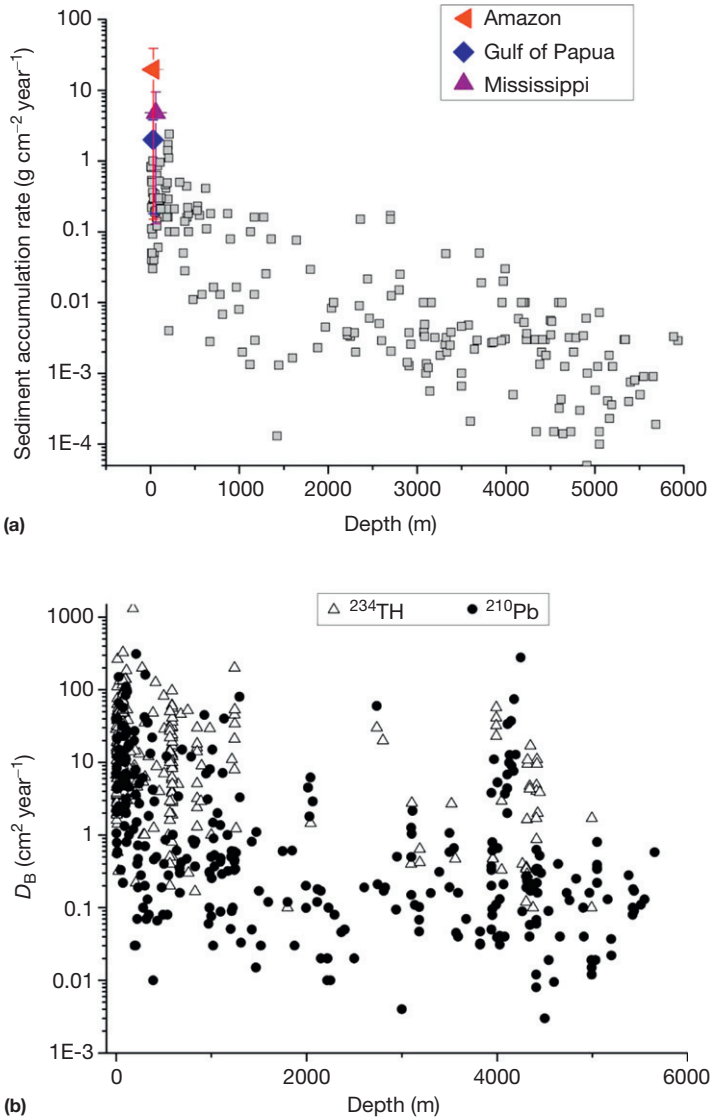

Figure 7 Particle transport processes are major controls on reactant delivery and diagenetic reaction patterns. (a) Net sediment accumulation (particle advection) varies by ~6 orders of magnitude as a function of bathymetric depth in the ocean (square data symbols from synthesis of Soetaert et al. (1996a)). Accumulation can be highly variable at any given depth and, in the case of deltaic systems, can range over at least 3 orders of magnitude within a <50 m depth interval (unweighted mid-range and accumulation range data from the Amazon, Gulf of Papua, and Mississippi deltas after Brunskill et al., 2003; Corbett et al., 2006; Dukat and Kuehl, 1995; Kuehl et al., 1986; Walsh et al., 2004). (b) Particle mixing coefficients determined using ^{234}Th ($t_{½}$ = 24 days; open triangles) and ^{210}Pb ($t_{½}$ = 22 years; solid circles) within deposits are a function of bathymetric depth in the ocean (Data summary from Lecroart et al., 2010). Rates vary by ~6 orders of magnitude and decrease overall with bathymetric depth; however, they are extremely variable at any given depth. The increasing discrepancy between ^{234}Th- and ^{210}Pb-derived rates with increasing bathymetric depth reflects deviations from the assumptions of diffusive mixing models when mixing events are infrequent (Boudreau, 1986; Lecroart et al., 2010; Meysman et al., 2008).

dependences in this way, if the transport conditions are known (e.g., diffusion coefficient and sedimentation rate), net reaction magnitudes, and thus integrated fluxes, are readily obtained by simply differentiating an optimized functional fit to the measured $C(z)$ or $\hat{C}(z)$ distributions (e.g., Berg et al., 1998; Goldhaber et al., 1977). Similarly, if reactions are known (e.g., first-order radioactive decay), transport rates, such as sediment accumulation or biogenic nonlocal transport, can be estimated, and in fact, the vast majority of sediment accumulation rates are derived from such inverse models (e.g., Berner, 1980; Burdige, 2006; Meile et al., 2001).

8.11.5 Patterns in Boundary Conditions and Reaction Balances

8.11.5.1 Spatial Patterns in Sediment Accumulation and Biogenic Transport

In addition to the modes of internal transport processes dictated by diagenetic regimes and principles governing overall reaction sequences, the boundary conditions on sedimentary deposits, including sediment input patterns, reactive organic matter input, temperature, salinity, and oxygen content of overlying water, can vary substantially depending on location

and facies within depositional systems, such as within an estuary, across a deltaic clinoform, or within a major ocean basin. There are general spatial patterns for many of these factors that track water depth (Middelburg et al., 1997; Tromp et al., 1995). For example, average sediment accumulation rates and biological mixing rates decrease generally with bathymetric depth in ocean basins (**Figure 7**). These average patterns and correlations with them are very useful in global models but tend to obscure major deviations that can be important as controls on local diagenetic and biogeochemical cycling, particularly within the dynamic continental shelf and margin regions where most sediment is processed and accumulates. Significant variations can occur at any given depth due to regional oceanographic conditions, such as increased productivity and delivery of reactive organic matter from overlying water due to seasonal upwelling or overturn, permanent or seasonal low O_2 in overlying water, or turbidity currents and pulse inputs due to particular local combinations of ocean basin physiography, circulation patterns, tectonic activity, storms, and river sources. In major deltaic systems, for example, it is not unusual for sediment accumulation to vary by 3–4 orders of magnitude over a restricted depth range of 5–100 m (**Figure 7(a)**; Brunskill et al., 2003; Corbett et al., 2006; Dukat and Kuehl, 1995; Kuehl et al., 1986; Walsh et al., 2004).

8.11.5.2 Spatial Patterns in Reactive C_{org} Delivery and Magnitudes of Benthic Fluxes

The benthic flux of O_2 reflects the availability of reactive organic matter, the concentration and supply of O_2 in the overlying water, transport processes, such as bioturbation within the sediment, and benthic community respiration (Cai and Reimers, 1995; Glud, 2008; Jahnke, 1996). The delivery of reactive organic matter to the seabed, and thus the intensity of diagenetic redox reactions, is often closely coupled with net sediment accumulation, although as noted previously, such direct coupling is minimized in permeable sand and mobile mud deposits along continental margins. One expression of this general correlation is the flux of O_2 into the seafloor as a function of bathymetric depth. Oxygen fluxes vary from ~20–100 mmol O_2 m^{-2} per day at shelf depths of ~10–100 m to ~0.1–2 mmol O_2 m^{-2} per day at abyssal depths (**Figure 8**) (Glud, 2008). When O_2 boundary conditions are also taken into account, the magnitude of the deep-sea O_2 flux shows a regular hyperbolic relation with reactive C_{org} and O_2 in the overlying water (Cai and Reimers, 1995). In shallow waters where sediments interact strongly with overlying water and the photic zone, benthic O_2 fluxes may correspond to the remineralization of 25–80% of primary production (Heip et al., 1995; Jahnke, 2004; Middelburg and

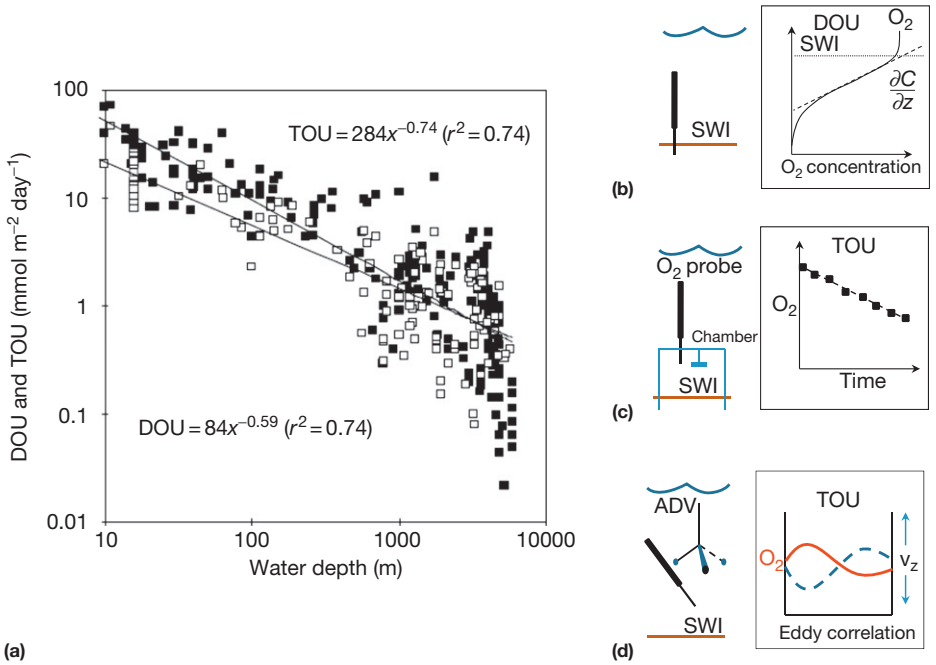

Figure 8 (a) When deposits underlie oxygenated water, O_2 fluxes into the seabed vary generally as a function of organic matter substrate delivery and thus bathymetric depth (after Glud, 2008). The diffusive O_2 flux (DOU) estimated using eqn [2] (see text) is generally lower than the total flux of O_2 (TOU) measured using either benthic incubation chambers or eddy correlation techniques, reflecting the effect of 3-D transport effects of bioturbation (bioirrigation). (b) Schematic representation of microelectrode measurement technique and model fits to profiles to derive DOU (eqn [4] in text) (Reimers et al., 1992). (c) Schematic representation of benthic chamber incubation technique and model fits to enclosed overlying water to derive TOU (Tengberg et al., 2005). (d) Schematic representation of eddy correlation system and model frequency fits to overlying water turbulent O_2 variations to derive TOU. Reproduced from Berg P, Glud RN, Hume A, et al. (2009) Eddy correlation measurements of oxygen uptake in deep ocean sediments. *Limnology and Oceanography-Methods* 7: 576–584; Glud RN (2008) Oxygen dynamics of marine sediments. *Marine Biology Research* 4: 243–289.

Soetaert, 2004). When little or no storage of reactive C_{org} or reduced diagenetic products, such as FeS_2, occurs (e.g., Figure 1(a)) and after accounting for specific redox reaction stoichiometries (Tables 1–3), the O_2 flux into deposits at steady state corresponds closely to the total flux of reactive organic matter that is remineralized (Glud, 2008). Unsteady boundary and depositional conditions, such as mobile mud batch reactor behavior (Figure 2(c)), however, can result in substantial mismatches between instantaneous sediment–water solute fluxes of O_2 and depth-integrated C_{org} remineralization rates (Aller et al., 1996).

Methods of flux measurement often differ in the estimated magnitude of benthic solute fluxes, reflecting the interactions of the diagenetic transport regime with redox reaction distributions within deposits and various assumptions of the measurement techniques. For example, a diffusive O_2 flux into a deposit can be estimated simply using eqn [4] and the vertical profile of O_2 penetration at the upper sediment–water interface. This estimate assumes 1-D transport control and provides a minimum possible estimate of O_2 flux. When labile organic matter penetrates relatively deeply into deposits (e.g., scale L ~10 cm), O_2 fluxes and other solute fluxes associated with remineralization can be strongly influenced by bioturbation over the same scale, particularly by bioirrigation, and the patterns of O_2 uptake at depth around burrows are not reflected by concentration gradients at the uppermost sediment–water interface. Thus, the difference between estimates of O_2 flux using 1-D diffusive transport models based on an interfacial gradient, and those made from direct measurements of total O_2 flux into deposits, can be used not only to constrain the magnitude of the O_2 flux but also to reveal diagenetic transport processes (e.g., bioirrigation) and respiration by macrobenthos (Figure 8). Because the intensity of macrofaunal bioturbation often decreases with bathymetric depth and because labile organic matter tends to be focused into the surface few millimeters of deposits at the low sediment accumulation rates typical of deeper regions, the differences between 1-D estimates of O_2 flux and other methods designed to measure total flux usually become minimal in the deep sea (Figures 7 and 8) (Glud, 2008).

The most common technique used to measure total solute fluxes, as opposed to 1-D model-derived fluxes, is to isolate a portion of the seabed and the immediately overlying water in an in situ chamber or retrieved core and to follow the initial rates of change of O_2 and other solutes in the enclosed overlying water (Berelson et al., 1994a; Jahnke, 2004; Pamatmat, 1971; Smith et al., 2002; Tengberg et al., 2004, 2005). Although incubation of sediment using benthic chambers in principle provides a more accurate estimate of solute fluxes than a 1-D transport model, isolation of the seabed from the natural hydrodynamic conditions may produce artifacts. Application of eddy correlation boundary layer techniques to measure benthic fluxes is a recently developed approach that integrates total O_2 and other solute fluxes over a large area of seafloor without enclosures and minimal perturbation of the hydrodynamic regime (Berg et al., 2007, 2009; Reimers et al., 2012). Eddy correlation also provides a means by which to estimate spatially integrated benthic fluxes in highly permeable sediments, seagrass meadows, across highly complex topographies, and over hard grounds where other techniques result in poor approximations to fluxes or fail entirely (Berg and Huettel, 2008; Glud et al., 2010). Agreement between in situ chambers, microelectrode profiling, and eddy correlation is excellent in stable mud environments where the assumptions of both techniques are optimal (Berg et al., 2007, 2009); however, complex hydrodynamic conditions and spatial heterogeneity may compromise straightforward comparisons (Reimers et al., 2012).

8.11.5.3 Global Patterns in the Scaling of Redox Reactions

The occurrence and vertical scaling of individual redox reaction zones is a direct function of the relative rates of reactant supply at the sediment–water boundary and diagenetic transport conditions (Froelich et al., 1979). For example, if the overlying water is well oxygenated, the supply of organic reductant is low, and the sediment accumulation rate is small, the oxic zone expands and subsequent redox reaction zones may be absent. This reductant-limited case is typical of abyssal regions of the deep sea underlying oligotrophic surface waters (Figure 9). Similarly, when the reductant is abundant and in excess, oxidants may be limiting and oxic and suboxic regions contract vertically, as in hemipelagic sediments underlying productive upwelling waters or shallow water estuarine deposits (Emerson et al., 1985). The global expression of these zones in distributions of pore water solute, reactive metal oxide, and labile organic matter reflects these patterns of expansion and contraction of dominant redox reactions and the local diffusion–advection transport conditions (Figures 9 and 10). These global patterns are generally reproduced by diagenetic models under circumstances of relatively steady accretion, low permeability, and quiescent conditions typical of deeper water mud regions (e.g., Figure 2(a) and 2(b); Archer et al., 2002; Soetaert et al., 1996a; Tromp et al., 1995).

Whereas benthic O_2 fluxes are generally measures of overall mineralization, flux patterns of other constituents can reflect particular redox reaction balances and remineralization pathways within deposits. For example, total N_2 fluxes are a measure of denitrification and anammox activity (Tables 1 and 2; anammox = anaerobic ammonium oxidation). In Arctic basin deposits, N_2 fluxes decrease with bathymetric depth as does the contribution to fluxes from macrobenthic bioturbation (Chang and Devol, 2009). Net fluxes of solutes across the sediment–water interface do not always reveal reaction pathways followed within deposits, as illustrated by the diagenetic cycles of Fe and Mn. Reoxidation of Mn^{2+} by O_2 and NO_3^-, and of Fe^{2+} by O_2, NO_3^-, and Mn^{2+}, at the sediment–water interface can obscure intense suboxic recycling internally in deposits if only net fluxes of Mn^{2+} and Fe^{2+} are used as an indicator of diagenetic reactions (Aller, 1994b; Luther et al., 1999; Severmann et al., 2010; Sundby, 2006; Thamdrup et al., 1994).

8.11.5.4 Sedimentary Record of Diagenetic Reaction Dominance and Balances

Characteristic authigenic mineral suites or elemental (isotopic) patterns can result from particular reaction balances and diagenetic regimes, leaving a record of depositional environment and diagenetic conditions. Interpretation of specific preserved compositions entails specific assumptions regarding diagenetic regime and the nature of source sediments. Most commonly,

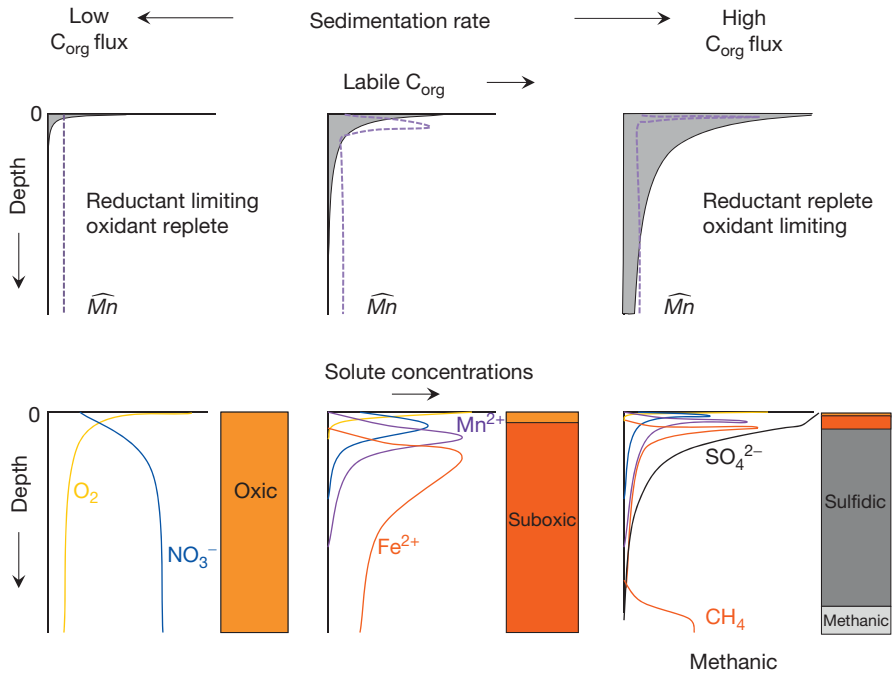

Figure 9 The changing delivery of reactive organic matter that typically accompanies sediment accumulation (**Figure 7(a)**) results in characteristic relative scaling patterns of redox reactions in sediment underlying oxygenated water as function of bathymetric depth. Oxic processes expand under reductant-limited conditions, whereas anoxic processes dominate under reductant-replete conditions (e.g., Emerson, 1985; Emerson and Hedges, 2003). Idealized solid phase reactive C_{org} and $\widehat{Mn}$ profiles, and characteristic pore water solute profiles are shown as a function of reductant delivery (~bathymetric depth) along with the corresponding representative schematic sediment color patterns.

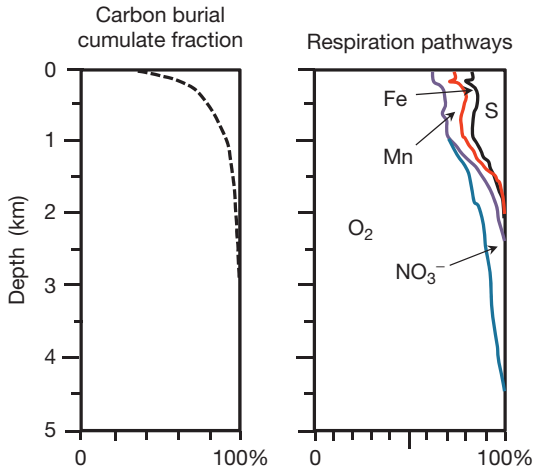

Figure 10 Steady-state diagenetic models can capture and reproduce the primary spatial patterns in reaction balances, dominant pathways, and magnitudes of remineralization in diagenetic regimes, such as **Figure 2(a)** (see also **Figure 22** for example of detailed diagenetic model profiles). (**a**) Model simulations illustrating that on a global scale most diagenetic C_{org} remineralization takes place along continental margins at bathymetric depths <1 km. (**b**) Diagenetic model simulations illustrating the bathymetric depth-dependent patterns in primary oxidants governing diagenetic remineralization. The roles of SO_4^{2-} reduction and metabolite reoxidation, which commonly exceed 50% of C_{org} remineralization and O_2 uptake (Jorgensen and Kasten, 2006), tend to be underestimated in the shallower regions (Global model calculations from Archer et al., 2002); see also (Soetaert et al., 1996a; Tromp et al., 1995).

a steadily accreting deposit is assumed for purposes of reconstruction (**Figure 2(a)**). Solid phase diagenetic reaction products include authigenic oxides, phosphates, carbonates, aluminosilicates, and sulfides (e.g., Burdige, 2006; Goldhaber, 2003; Morse, 2003; Suess, 1979; see also **Chapters 9.12** and **10.12**). Formation of aluminosilicates is favored under suboxic or anoxic nonsulfidic conditions in terrigenous deposits (promoted by enhanced mobility of Fe^{2+} and Al^{3+} and availability of reactive Si) and specific carbonates, such as siderite form under suboxic and anoxic nonsulfidic and sulfidic conditions, promoted by elevated alkalinity and Fe^{2+} and Mn^{2+} concentrations, as discussed briefly in the succeeding text (**Section 8.11.8.3**).

Diagenetically derived C/S, Fe/S, and Fe/Al relationships can be particularly useful as indicators of the relative importance of sulfate reduction in deposits and can also allow inference of water column oxygenation conditions (Berner and Raiswell, 1984; Goldhaber, 2003; Lyons and Severmann, 2006; Raiswell and Canfield, 1998; Raiswell et al., 1988). Elevated Fe/Al (>0.4 wt wt^{-1}) may reflect remobilization and lateral transport of Fe and its focusing and sequestration into euxinic facies (Lyons and Severmann, 2006). C/S and Fe/S relations derive in large part from the overall reactions governing SO_4^{2-} and Fe reduction, such as

$$2CH_2O + SO_4^{2-} + Fe(OH)_3 + CO_2 \rightarrow \frac{1}{2}FeS_2 + 3HCO_3^- + \frac{1}{2}Fe^{2+} \quad [10]$$

There are multiple possible pathways by which pyrite (FeS_2) may actually form (Goldhaber, 2003; Rickard and Luther, 2007), and eqn [10] is written to illustrate simply the

close coupling between the availability of reactants C_{org}, SO_4^{2-}, and Fe oxides that governs the *potential* quantity of diagenetic pyrite. For example, the average C/S ratio in normal marine shelf deposits is ~2.8 (wt wt^{-1}; 7.5 mol mol^{-1}), reflecting the availability of SO_4^{2-} (implying high salinity) and sufficient reactive organic reductant to allow a proportional diagenetic expression of SO_4^{2-} reduction by storage of residual precipitated sulfide (Berner, 1984). Much lower C/S or poorly correlated C/S values can indicate anoxic overlying water and much higher ratios (e.g., C/S > 10–30 wt wt^{-1}) imply low salinity, SO_4^{2-} limitation (Berner and Raiswell, 1984). However, high C/S values (low S) similar to those found in freshwater lakes can also characterize marine mobile mud, batch reactor diagenetic regimes in subaqueous tropical deltaic deposits, where suboxic conditions and extensive reoxidation by physical reworking is the rule (Figure 11). These latter examples illustrate the critical roles of both boundary and transport conditions in governing the expression of diagenetic reactions in deposits.

Fe/S relations are usually expressed as the degree of pyritization (DOP) index, which is defined as the ratio of pyrite Fe/(total residual reactive Fe + pyrite Fe) (note: the wt or mol ratios of Fe forms are identical in this case) (Berner, 1984; Goldhaber, 2003; Raiswell and Canfield, 1998). Depending on exactly how reactive Fe is defined, a substantial fraction of diagenetically reduced, reactive Fe is typically present as FeS_2 (pyrite) in steadily accreting marine deposits, and the proportion of reactive Fe tied up as pyrite can approach 90% in the absence of bioturbation, the latter condition implying anoxic overlying water. Extensive bioturbation and reoxidation lowers DOP to <0.4 (Raiswell et al., 1988). Because nonpyrite Fe may or may not be diagenetically reduced (i.e., present as either Fe(III) or Fe(II)), an additional useful index of Fe/S relations and also suboxic diagenetic reactivity is the Py–Fe(II) index, defined as pyrite Fe/(total Fe(II) + pyrite Fe) (Aller and Blair, 1996). Both DOP and Py–Fe(II) are extremely low in tropical mobile muds (DOP < 0.05; Py–Fe(II) < 0.2), indicating that suboxic diagenetic pathways and reoxidation processes dominate net diagenetic behavior (Figure 11(a)). These Fe/S and C/S relationships illustrate that similar outcomes for a particular property can derive from very different diagenetic conditions and highlight the need to independently confirm the diagenetic regime in which deposits were generated when interpreting compositional indicators.

8.11.5.5 Temporal Patterns in Boundary Conditions and the Scaling of Reactions

Regular periodic seasonal or episodic variations in temperature, salinity, overlying water oxygenation, and organic matter delivery at the seabed can characterize shallow water regions, which may also be subject to remobilization of deposits by strong currents, waves, and episodic disturbances, such as storms (Figure 12). Similarly, deepwater deposits can be subject to energetic physical conditions (e.g., western boundary current regions; McCave et al., 2002), sediment reworking, and seasonal input of surface water-derived organic inputs, although physical disturbance is far less common in deep than shallow water. Seasonal increases of organic matter supply or distinct pulses of organic matter to the seabed are expressed in temporarily enhanced production of metabolic products, such as the production of CO_2 (Figure 12). Redox reactions can contract and expand in dominance in response to rapid changes in organic

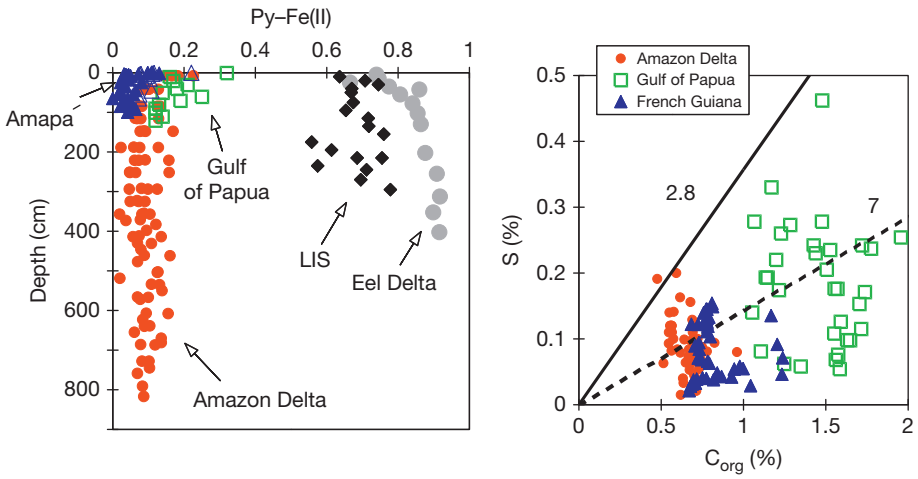

Figure 11 The composition and storage of solid phase reaction products reflect environmental conditions and diagenetic transport–reaction regimes. Examples: (a) The proportion of total diagenetically reduced Fe^{2+}, present as Fe sulfides (Py–Fe(II)), is typically low in marine mobile mud systems compared to more stable conditions of relatively steady accumulation (LIS, estuarine mud, Long Island Sound, Connecticut, Eel River delta, California; French Guiana coast; Amapá coast, Brazil (open triangles largely hidden behind French Guiana samples); Amazon delta, Brazil; and Gulf of Papua, Papua New Guinea). Total reduced Fe^{2+} is in the range of ~100–200 μmol g^{-1} in temperate estuarine and shelf mud deposits (LIS, Eel delta) and 300–400 μmol g^{-1} in tropical deltaic systems (e.g., Amazon and Gulf of Papua). Low Py–Fe(II) at high Fe^{2+} is indicative of highly reactive sediments and dominant suboxic diagenesis. (b) Normal marine shelf sediments average a C/S weight ratio of ~2.8, whereas mobile tropical deltaic muds retain C/S weight ratios in the range of ~7, a value also found in low-salinity environments. Reproduced from Aller RC, Hannides A, Heilbrun C, and Panzeca C (2004a) Coupling of early diagenetic processes and sedimentary dynamics in tropical shelf environments: the Gulf of Papua deltaic complex. *Continental Shelf Research* 24: 2455–2486; Aller RC, Heilbrun C, Panzeca C, Zhu ZB, and Baltzer F (2004b) Coupling between sedimentary dynamics, early diagenetic processes, and biogeochemical cycling in the Amazon-Guianas mobile mud belt: coastal French Guiana. *Marine Geology* 208: 331–360; Berner RA and Raiswell R (1984) C/S Method for distinguishing fresh-water from marine sedimentary-rocks. *Geology* 12: 365–368.

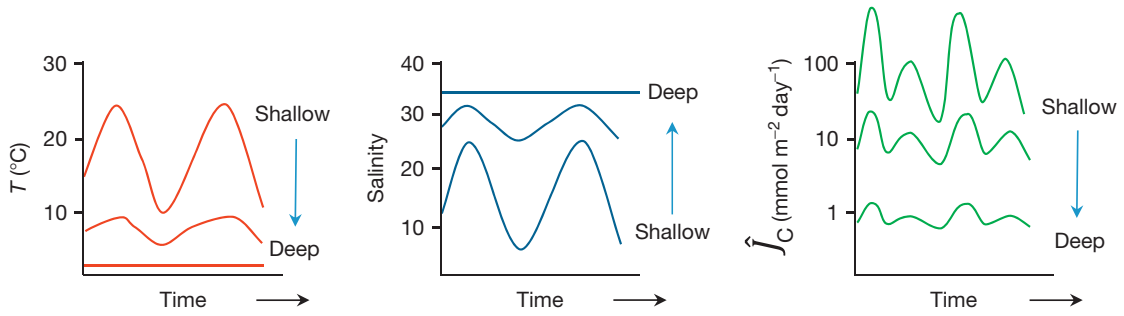

Figure 12 Boundary conditions on sedimentary deposits vary substantially depending on depositional environment. Temperate shallow coastal systems (<20 m) typically show wide seasonal variations in temperature and salinity, with mean temperatures varying inversely with latitude. In contrast, deepwater systems (>0.2 km) typically have stable temperature and salinity patterns. All environments are subject to variations in the input of reactive organic matter, (expressed as flux J_C), although the mean magnitude is ~100 × lower and absolute variations are damped in deep water relative to shallow systems (e.g., Smith et al., 2002). Boundary O_2 variations are absent in open ocean deep water, but extreme excursions in O_2 can occur in shallow water and upwelling margin systems.

reductant supply and also in response to temperature variations, which increase metabolic activity and relative reaction dominance during warmer relative to colder periods (e.g., Aller, 1980a; Crill and Martens, 1987; Klump and Martens, 1989; Thamdrup et al., 1994). These time-dependent redox reaction patterns are readily observed in shallow water systems, in phenomena, such as seasonal patterns of pore water Mn^{2+} (**Figure 13**; Thamdrup et al., 1994) or metabolic dissolution of $CaCO_3$ (Green and Aller, 1998, 2001), but they also characterize any deposit, shallow or deep water, in which distinct variations in boundary conditions occur (Pope et al., 1996; Sayles et al., 2001; Smith et al., 1996, 2002).

Variation in the oxygenation of overlying water is a major seasonal boundary factor in many shallow water systems where combinations of circulation, temperature, and metabolic activity result in significant changes in oxic–anoxic zonations in sediments and corresponding benthic fluxes of metabolites and trace metals released from episodically reduced Fe, Mn oxide carrier phases (e.g., Sholkovitz et al., 1992). Depending on the frequency, magnitude, and duration of variable boundary conditions relative to mean values and net sediment accumulation, such variation may or may not discernibly affect specific diagenetic properties and the preserved record; however, unsteady boundary conditions should always be explicitly considered as a potential factor before discounting them (Lasaga and Holland, 1976; Martin and Bender, 1988; Soetaert et al., 1996b).

A simple analytical diffusion–reaction model with regular periodic boundary conditions is used here to demonstrate some of the ways unsteady boundary conditions can affect distributions of reactive constituents near the sediment surface and under what general circumstances they can be ignored. Although the superposition of multiple periodic boundary functions allows consideration of any arbitrary condition using Fourier series, complicated, irregular transient, and exact boundary variations are best simulated and considered through numerical techniques (Soetaert et al., 1996b). In the present illustrative cases, let the upper boundary be subject to either of the regular periodic conditions:

Concentration condition:

$$C(t) = C_{T_0} + C_{T_1} \sin(\vartheta t) \qquad [11a]$$

Flux condition:

$$J(t) = J_0 + J_1 \sin(\vartheta t) \qquad [11b]$$

By further limiting consideration to length scales near the boundary where advection is relatively unimportant ($Pe \ll 1$), assuming no significant compaction, allowing for diffusive particle mixing (D_B) (or alternatively solute diffusion (D_s)), and first-order consumption with reaction coefficient k, the transport–reaction model (eqn [8]) becomes

$$\frac{\partial C}{\partial t} = D_B \frac{\partial^2 C}{\partial z^2} - kC \qquad [12]$$

The analytical solutions with lower boundary condition (BC) $z \to \infty; C \to 0$ and after the initial conditions no longer influence behavior (periodic part only) are

$$C = C_{T_0} e^{-\alpha_0 z} + C_{T_1} e^{-\alpha_1 z} \sin(\vartheta t - \alpha_2 z) \qquad [13a]\ [\text{BC } 11a]$$

$$C = \frac{J_0}{\alpha_0 D_B} e^{-\alpha_0 z} + \frac{J_1}{\alpha_1 D_B} e^{-\alpha_1 z} \sin(\vartheta t - \alpha_2 z - \varphi_1) \qquad [13b]\ [\text{BC } 11b]$$

where

$$\alpha_0 = \sqrt{\frac{k}{D_B}};\ \alpha_1 = \sqrt{\frac{\sqrt{k^2 + \vartheta^2} + k}{2D_B}};\ \alpha_2 = \sqrt{\frac{\sqrt{k^2 + \vartheta^2} - k}{2D_B}};$$

$$\varphi_1 = \tan^{-1} \frac{\alpha_2}{\alpha_1}$$

These solutions demonstrate that the amplitude of the propagating boundary signal is damped and that a phase shift in the periodicity (phase $-\alpha_2 z$, or, $-\alpha_2 z - \varphi_1$) occurs progressively with depth. Thus, any maximum at the boundary appears as a smaller amplitude at depth later in time. Critical factors governing transient behavior within deposits are the relative magnitudes of reactivity (k), frequency of oscillation (ϑ), and transport (D_B). The greatest impacts of variable boundary conditions are expected when the characteristic timescales of the reaction rate and the frequency are similar. If the component of interest is reactive organic matter, clearly, the highest reactivity material decomposes near the surface,

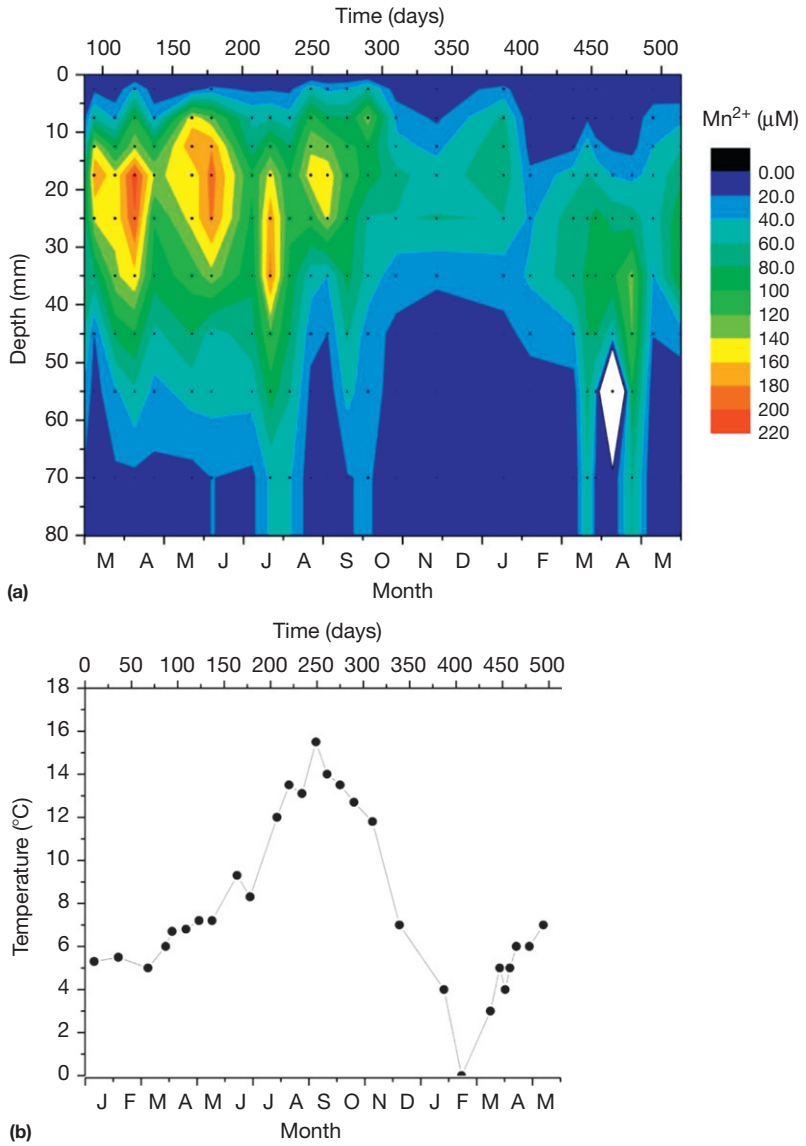

Figure 13 Seasonality in boundary conditions is strongly expressed in diagenetic properties of surface sediment and is progressively damped with depth in deposits (see eqns [10]–[12] in text). Example: (a) Seasonal variation in dissolved Mn^{2+} in deposits from Aarhus Bay, Denmark, responds to variations in temperature (metabolic activity), bioturbation (transport), and input of reactive organic matter (reductant supply) (no data = white diamond region). (b) Seasonal variation of temperature in Aarhus Bay corresponding to (a) and also demonstrating interannual variability (1990) typical of shallow water systems. Reproduced from Thamdrup B, Fossing H, and Jorgensen BB (1994) Manganese, iron, and sulfur cycling in a coastal marine sediment, Aarhus Bay, Denmark. *Geochimica et Cosmochimica Acta* 58: 5115–5129.

and rates (e.g., solute fluxes derived from decomposition) track the boundary input closely in time (i.e., fluxes appear approximately steady state with the immediate boundary condition). In contrast, relatively low-reactivity material decomposes at depth, and maximum reaction (and thus derived solute fluxes) can be substantially offset in time from the surface boundary. This offset may produce a lag in derived benthic solute flux and alter apparent depth dependence of the reaction if a steady boundary were assumed. Extremely high frequencies of boundary variation have minor impact (α_1 large; periodic term $\rightarrow 0$) on internal patterns, and only the mean condition is important in such cases.

8.11.6 C_{org} Burial and Preservation: Reactants and Diagenetic Regime

8.11.6.1 Patterns in C_{org} Distributions and Particle Associations

Various combinations of sedimentary C_{org} sources and reactivities, transport history, local boundary conditions (e.g., water column oxygen), and diagenetic regimes (e.g., sedimentary dynamics) produce a wide range of C_{org} concentrations and burial and preservation patterns within the oceans (Figure 14). Particular sets of conditions characterize different depositional environments, and the multiple factors governing C_{org}

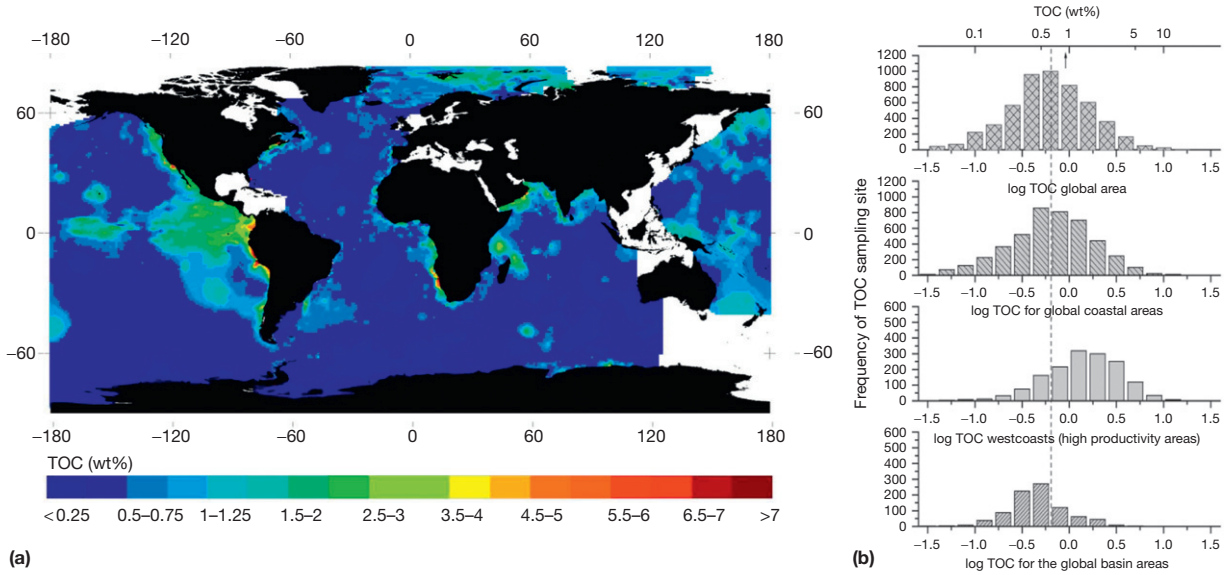

Figure 14 The delivery of reactive organic matter to the seafloor and diagenetic preservation patterns are reflected in sedimentary C_{org} concentration distributions. (a) Global patterns of total sedimentary organic C_{org} (TOC). (b) Statistical distributions of C_{org} in spatial samples as a function of depositional environment (log normal). Reproduced from Seiter K, Hensen C, Schroter E, and Zabel M (2004) Organic carbon content in surface sediments – Defining regional provinces. *Deep-Sea Research Part I* 51: 2001–2026.

burial often correlate. For example, low-oxygen conditions are commonly found in low-energy systems where physical and biological reworking of the seabed is also minimal and unidirectional accretion takes place. Association of C_{org} with particle surfaces can result in the preferential physical focusing of C_{org} into fine-grained deposits, which dominate storage (Premuzic et al., 1982; Trask, 1939). Organic–mineral complexes that characterize fine-grained mineralogies can also substantially lower the reactivity of C_{org} and enhance burial and preservation (Hedges and Keil, 1995; Mayer, 1994a,b).

The normalization of C_{org} content to particle surface area (SA) permits partial resolution of the relative roles of transport focusing of particles and net reactions in governing C_{org} distributions and preservation (**Figure 15**) (Mayer, 1994a,b). Particulate C_{org}/SA loading ratios in the range of 0.4–1.0 mg C_{org} m^{-2} are common in river-suspended material and at depth in shelf sediments (Mayer, 1994a,b). This observation led to the concept that this specific range reflects an asymptotic loading value characteristic of relatively stable organic–mineral associations having low reactivity and low availability for further diagenetic decomposition, that is, it represents a residual reactant background due largely to the protection of organic material by minerals (Hedges and Keil, 1995; Mayer, 1994a,b). Although organic–mineral associations clearly lower reactivity and affect reactive pool sizes, the fact that relatively depleted C_{org}/SA loading <0.4 mg m^{-2} is commonly found in deltaic deposits with high sedimentation rates that are frequently remobilized and reoxygenated, and also in deep-sea deposits with low sedimentation rates that are exposed to oxygenated conditions for extended periods, demonstrates both the conditional nature of decomposition and the lack of any absolute protective mechanisms (Aller and Blair, 2006). Similarly, C_{org} supply can exceed decomposition processes and sustain preservation of C_{org}/SA loading >1.0 mg C m^{-2} in classes of high-productivity environments, such as oxygenated (e.g., Cape Hatteras; Mayer et al., 2002) or low-oxygen continental margin regions (e.g., Peru upwelling; Hedges and Keil, 1995), illustrating that there are multiple stable high C_{org} loading states realized in specific sedimentary systems. In addition, it is known that substantial portions of sedimentary C_{org} are present in particle surface associations inconsistent with protection by minerals (Ransom et al., 1997). Thus, although globally they do not reflect any one specific protection or reaction mechanism, loading ratios provide a very useful way in which to differentiate environmental regions that reflect normal balances between supply and decomposition regimes found in many river, estuarine, and shelf environments (0.4–1.0 mg m^{-2}), balances found in regions of highly efficient net decomposition (0.1–0.4 mg m^{-2}), and balances found in regions of comparatively inefficient decomposition relative to supply (>1.0 mg m^{-2}) (Blair and Aller, 2012).

Overall, C_{org} *burial* fluxes vary directly with net sediment accumulation, and the primary sedimentary sinks for C_{org} are therefore dominated by the major fine-grained sediment depocenters associated with river deltas and continental margins, where ~90% of C_{org} storage occurs within ~15–20% of seafloor area (Berner, 1982; Burdige, 2007; Dunne et al., 2007; Hedges and Keil, 1995; Liu et al., 2010; Müller and Suess, 1979; Walsh, 1988; Wollast, 1998). The net accumulation rate of sediment is also a major control on the efficiency of C_{org} preservation, which is defined as the fraction of C_{org} buried relative to the total C_{org} flux initially supplied to the seabed (Canfield, 1993; Henrichs and Reeburgh, 1987). Under low-energy depositional conditions, high sediment accumulation rates tend to minimize local exposure to O_2 and the multiple impacts of bioturbation on remineralization (Keil et al., 2004; Tromp et al., 1995).

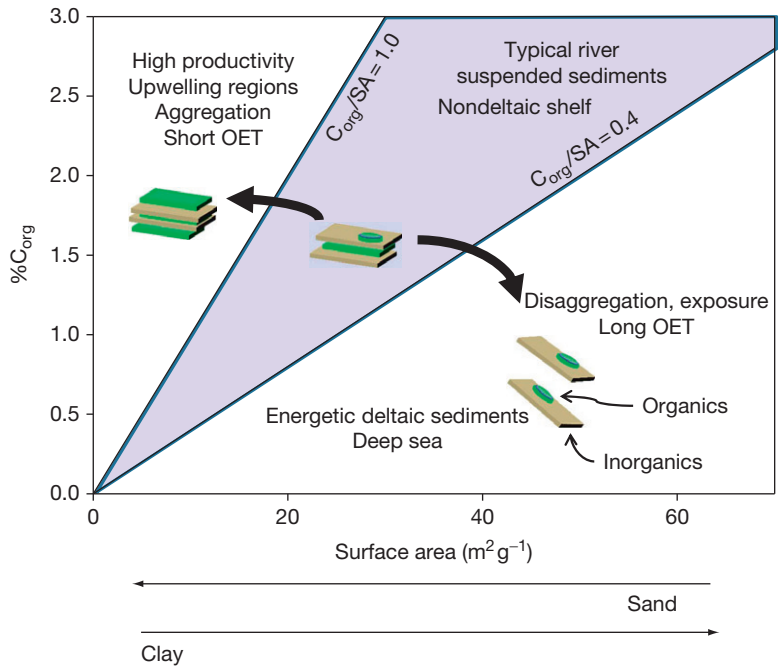

Figure 15 Sedimentary C_{org} contents generally correlate directly with sediment particle surface areas, consistent with dominant location of C_{org} on particle surfaces rather than interiors. Bulk sedimentary C_{org} is therefore determined in part by particle size and sediment segregation processes (transport sorting). Specific regions of surface loading (mg C_{org}/SA) on a C_{org} versus surface area (SA) plot characterize particular net balances between supply and remineralization reactions in different depositional environments (Hedges and Keil, 1995; Mayer, 1994a,b). Remineralization is inhibited by organo–mineral complexes (protection) and enhanced by oxygen exposure time (OET) and metabolite exchange. Data from Mayer (1994a,b), Mayer et al. (2002), Hedges and Keil (1995), Emerson and Hedges (2003), Goñi et al. (2008), Aller and Blair (2006), Aller et al. (2008). Reproduced from Blair NE and Aller RC (2012) The fate of terrestrial organic carbon in the marine environment. *Annual Reviews of Marine Science* 4: 401–423.

8.11.6.2 C_{org} Preservation: O_2, Accumulation Rates, and Diagenetic Regimes

Although accumulation rate is a major factor governing preservation, preservation patterns are more nuanced and complex than a single correlation with net sediment accumulation, particularly in deltaic environments where the highest sediment accumulation rates and C_{org} storage are found. Preservation is intimately tied to balances between C_{org} flux, oxygen exposure time, organic–mineral associations, and sedimentary dynamics. For example, extended exposure times of sedimentary organic matter to oxygenated conditions, however achieved, enhance remineralization and minimize the fraction of C_{org}, labile or refractory, that is preserved (Hedges and Keil, 1995; Hedges et al., 1999; Hulthe et al., 1998; Keil et al., 2004). Conditions of low preservation characterize much of the oxygenated deep sea, where combinations of relatively low C_{org} flux, low sedimentation rate, and oxygenated water promote extended oxygen exposure in surface deposits and thus low preservation (Hartnett et al., 1998; Hedges and Keil, 1995). The critical role of oxygen exposure and the nature of sediment deposition are particularly evident following pulsed input of sediment delivered as turbidites into the deep sea. The diffusion of oxygen into turbidite deposits between depositional events is clearly associated with the progressive burn down of C_{org} at downward migrating oxidation fronts, enhanced remineralization of sedimentary C_{org}, and minimal preservation (Cowie et al., 1995; Emerson and Hedges, 2003; Prahl et al., 1989, 1997; **Figure 16**).

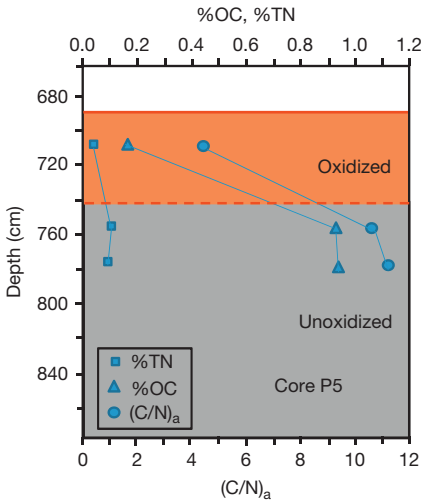

Figure 16 The critical roles of O_2 and O_2 exposure time (OET) as controls on remineralization and C_{org} preservation are readily demonstrated by unsteady diagenetic distributions of organic matter found in turbidite deposits in the deep sea. Extended exposure of reworked anoxic sediments to oxygenated overlying water, following pulsed deposition of turbidites, results in unsteady burn down of oxidation fronts during hiatal periods and a net loss of C_{org} (OC) and organic N ((C/N)a = mole ratio) in the oxidized zone. Remineralization of C_{org} during ~10 ky of secondary exposure to O_2 exceeds that achieved previously over ~140 ky under anoxic conditions. Reproduced from Cowie GL, Hedges JI, Prahl FG, and de Lance GJ (1995) Elemental and major biochemical changes across an oxidation front in a relict turbidite: An oxygen effect. *Geochimica et Cosmochimica Acta* 59: 33–46.

Remarkably, low C_{org} preservation diagenetic outcomes similar to those in the deep sea are also found in energetic deltaic systems where, despite extremely high C_{org} fluxes and sediment accumulation rates, C_{org} is efficiently remineralized regardless of the set of initial C_{org} reactivities supplied from either terrestrial or marine sources (**Figure 17**; Blair and Aller, 2012). In these depositional environments, the seabed acts as a batch sedimentary incinerator in which intense reworking of deposits promotes repeated episodic exposure to oxygen, reoxidation of reduced diagenetic products, flushing of metabolites, and incorporation of labile organic matter into the bulk sedimentary C_{org} mixture (**Figure 2(c)**; Aller and Blair, 2006; Aller et al., 2008). This latter condition results in a poorly understood process referred to as 'priming' in which the availability of labile C_{org} substrates enhances the decomposition of otherwise residual refractory organic components (Aller et al., 1996; Bianchi, 2011; Graf, 1992). When continental shelves are wide, such as characterize passive tectonic margins during periods of high sea stand, the residence time of sediment in these dynamic diagenetic conditions may be 100s–1000s of years, resulting in highly efficient remineralization of sedimentary organic material of all ages.

The highest C_{org} preservation efficiencies observed in the marine environment are found in association with mountainous rivers systems along tectonically active margins. In these systems, a large proportion of C_{org} is recycled refractory organic matter (e.g., kerogen) supplied relatively directly from sedimentary rock sources to the ocean from high-gradient drainage basins. Rapid delivery to marine sink regions following initial erosion results in comparatively minimal alteration of organic material in terrestrial environments, such as floodplains (Komada et al., 2004; Leithold et al., 2006). The bias to the supply of low reactivity, often ancient material is coupled with high accumulation rates in regions close to continental sources and with sediment deposition in relatively quiescent deep-water sites (narrow continental shelves), the latter minimizing the role of physical or biogenic reworking and O_2 exposure during transit and burial. This combination of factors tends to maximize C_{org} preservation along tectonically active margins and provides a long-term homeostat for atmospheric O_2 (Blair and Aller, 2012; Blair et al., 2004).

A third major group of high accumulation rate systems is intermediate in preservation behavior between those of the mobile mud environments or small mountainous rivers. These are generally large systems, such as the Ganges–Brahmaputra, Rhone, and Congo deltas, where sedimentary material incorporating both reactive and nonreactive components rapidly transits into quiescent deep water (Blair and Aller, 2012; Galy et al., 2007; Rabouille et al., 2009).

Although permeable sand deposits are often sites of intense remineralization and benthic fluxes, they are not significant storage sites for organic matter (Burdige, 2007; Jahnke, 2004; Middelburg and Soetaert, 2004; Walsh, 1988). The typical mineralogies of sands (e.g., quartz) preclude the kinds of close organic matter–mineral interactions and matrix incorporation found in clays that promote stabilization of organic matter during decomposition (Goñi et al., 2008; Hedges and Keil, 1995; Mayer, 1994a,b; Ransom et al., 1998). The efficient supply of O_2, labile organic particles, and exchange of metabolites associated with high permeability and advective pore water flow, combined with relative lack of protection of organic material by minerals, minimizes burial of residual refractory components, such as kerogen.

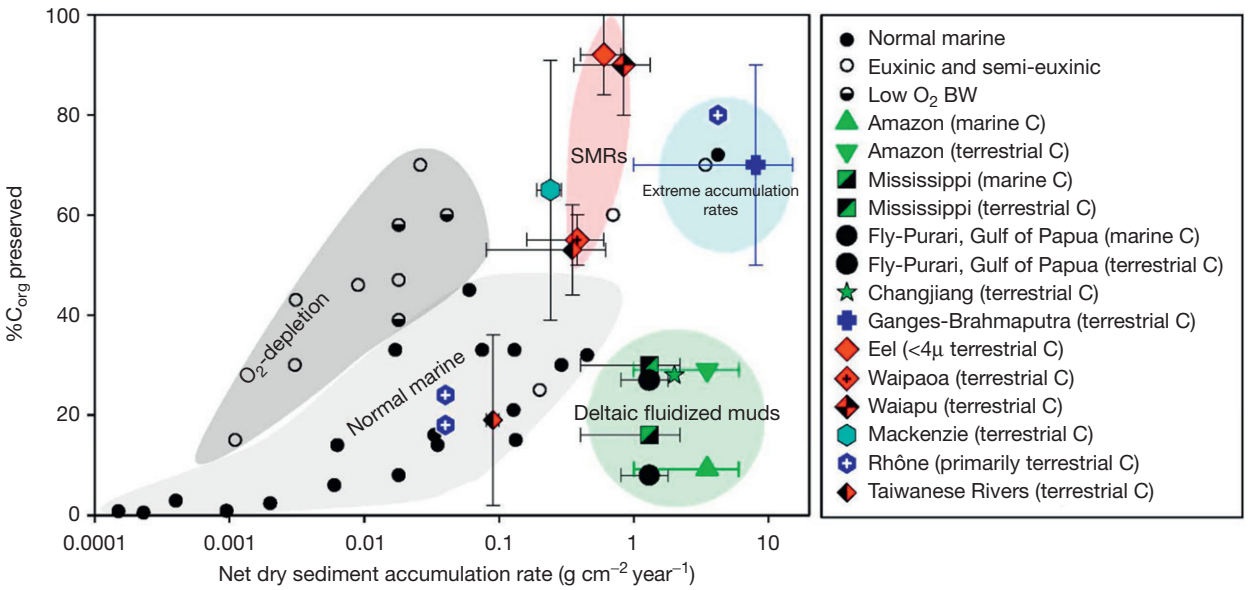

Figure 17 The percentage of C_{org} deposited on the seafloor that is buried (preserved) is a variable function of net sediment accumulation rate. Terrestrial C_{org} percent preservation estimates are derived from comparison of riverine C_{org} concentrations with seabed terrestrial C_{org} as determined by C isotopic mass balance calculations and assumed end-members. Remineralization (e.g., O_2 uptake and ΣCO_2 production), burial rates, and isotopic mixing models were used to estimate marine C_{org} preservation values (Data from Aller, 1998; Aller et al., 2008; Blair et al., 2003, 2010; Canfield, 1994; Galy et al., 2007; Goñi et al., 2005; Henrichs and Reeburgh, 1987; Huh et al., 2009; Kao et al., 2006; Pastor et al., 2011a,b; Thompson, 2009). Reproduced from Blair NE and Aller RC (2012) The fate of terrestrial organic carbon in the marine environment. *Annual Reviews of Marine Science* 4: 401–423.

8.11.7 Carbonate Mineral Dissolution–Alteration–Preservation

8.11.7.1 Coupling of Redox Reactions and Carbonate Diagenesis

The array of acids and bases formed during early diagenetic redox reactions strongly affects the dissolution, recrystallization, precipitation, and burial of sedimentary carbonate minerals. Thus, redox reaction patterns, transport regimes, and carbonate mineral diagenesis are very closely tied, spatially and temporally. As in the case of organic carbon, the availability, or not, of O_2 plays a particularly important but not exclusive role in governing carbonate mineral diagenetic behavior. In general, under oxic conditions, the oxidation of reduced components of sediments, C_{org}, NH_4^+, Mn^{2+}, Fe^{2+}, and H_2S–FeS_2, results in acid production (CO_2 (H_2CO_3), HNO_3, and H_2SO_4) and a tendency toward undersaturation and dissolution of carbonates focused into the zones of acid production near the oxic sediment–water interface and sedimentary redoxclines. Under suboxic and fully sulfidic conditions, the reduction of the weak conjugate bases NO_3^-, $Mn^{3+,4+}$ oxides, Fe^{3+} oxides, and SO_4^{2-} results in alkalinity production and a tendency toward supersaturation and precipitation of authigenic carbonates at depth. In the case of SO_4^{2-}, the exact patterns of carbonate saturation states during progressive stages of SO_4^{2-} reduction depend on the buildup of H_2S+HS^- in solution and the availability of reactive Fe to form Fe sulfides (Morse and Mackenzie, 1990; Walter and Burton, 1990). When reactive Fe is absent, such as in organic-rich shallow water carbonate mud deposits, the production and buildup of H_2S relative to carbonate alkalinity can result in undersaturation of common carbonate minerals during the initial stages of SO_4^{2-} reduction ($\Delta SO_4^{2-} \sim 2$ mM; Walter and Burton, 1990).

8.11.7.2 Carbonate Mineral Equilibria and Saturation States

Because the carbonate minerals initially present and undergoing reactions in surface deposits are dominated by biogenic material generated both in the water column by plankton and by benthic organisms on or in the seabed, the early diagenetic behaviors of biogenic low-Mg and high-Mg calcites and aragonite are critically important globally (Archer, 1996a; Morse et al., 2006). However, a range of additional Ca-, Mg-, Mn-, and Fe-rich carbonate minerals are also involved in early diagenetic reactions, particularly in the upper few centimeters to decimeters below the sediment surface in organic-rich, nearshore, and deeper margin deposits (Table 4). The likely diagenetic reactions of carbonates and their rates in sediments are inferred from pore water compositions, thermodynamic models of mineral stabilities, and kinetic models of dissolution–precipitation. The stabilities of different Ca carbonate minerals are commonly represented using dissociation reactions of the form

$$CaCO_3 \leftrightharpoons Ca^{2+} + CO_3^{2-}$$

and

$$Ca_xMg_{1-x}CO_3 \leftrightharpoons xCa^{2+} + (1-x)Mg^{2+} + CO_3^{2-}$$

Measured apparent or stoichiometric solubilities are used for most practical considerations in seawater, defined for calcite as

$$K'_{sp,\,cal} = [Ca^{2+}][CO_3^{2-}] = \frac{K_{sp,\,calc}}{[\gamma_{T,\,Ca^{2+}}][\gamma_{T,\,CO_3^{2-}}]} \qquad [14]$$

where $[Ca^{2+}]$, $[CO_3^{2-}]$ = total analytical concentrations at equilibrium, $K_{sp,cal}$ = thermodynamic ion activity solubility constant for calcite at defined T, P, and $\gamma_{T,Ca^{2+}}$, $\gamma_{T,CO_3^{2-}}$ = total activity coefficients of Ca^{2+} and CO_3^{2-} in seawater.

Similarly, for high-Mg calcite:

$$K'_{sp,\,hi-Mg\,Cal} = [Ca^{2+}]^x[Mg^{2+}]^{1-x}[CO_3^{2-}] \qquad [15]$$

In this latter case, however, there is no unique relationship to a thermodynamic constant in seawater (Morse et al., 2007). Thus, the solubilities of high-Mg calcite are usually evaluated as congruent stoichiometric solubilities and vary directly with Mg^{2+} content and biogenic or abiogenic source (Bischoff et al., 1987; Chave, 1954; Morse et al., 2006, 2007; Walter and Morse, 1985). High-Mg calcites and aragonites are more soluble than low-Mg calcite (Table 4) and are common constituents of nearshore deposits where overlying water is often supersaturated with respect to all biogenic carbonates (Andersson et al., 2008; Morse, 2003). Except where they are rapidly delivered by lateral transport from shallower regions,

Table 4 Solubilities of common carbonate minerals at 25 °C, 1 atm[a]

Phase	*Formula*	pK'_{sp} $((mol^2\,kg^{-2})x\,10^{-7})$	pK_{sp}
Aragonite	$CaCO_3$	6.65	8.30
Calcite	$CaCO_3$	4.39	8.48
Magnesite	$MgCO_3$		8.04
Magnesian calcites	$Ca_{0.94}Mg_{0.06}CO_3$–$Ca_{0.81}Mg_{0.19}CO_3$		8.08–8.38[b]
Siderite	$FeCO_3$		10.52 (10.43–11.2)
Rhodochrosite	$MnCO_3$	8.49	10.59 (9.47–12.51)
Dolomite	$CaMg(CO_3)_2$		18.15
Kutnahorite	$CaMn(CO_3)_2$	15.55[c]	21.81 (19.79–21.81)

[a] pK'_{sp} is the stoichiometric (apparent) molar solubility product in seawater; pK values are thermodynamic ion activity product solubilities: $-\log K_{sp}$. The range indicated in parentheses reflects effects of variable crystallinities, grain size, and particle surface alteration (after Jensen et al., 2002; Middelburg et al., 1987; Morse et al., 2007; Mucci, 1991).

[b] Biogenic Mg calcite stoichiometric ion activity products (Bischoff et al., 1987).

[c] Indicates estimated value from measured rhodochrosite and calcite stoichiometric solubilities (Aller and Rude, 1988).

these relatively soluble minerals are virtually absent from deep-water sediments because of water column undersaturation below ~0.5–1 km and dissolution reactions in both the water column and seabed. Thus, consideration of deep-sea carbonate diagenesis is usually restricted to the behavior of low-Mg calcite. The distribution of metabolic reaction rates, temperature, and pressure combines to produce a general pattern of Ca carbonate saturation states in the ocean in which supersaturated surface waters directly overlie undersaturated oxic sediments or deeper undersaturated oxic water and sediment, which in turn overlie supersaturated suboxic–anoxic deposits (**Figure 18**). Supersaturation in sediments results largely from the production of carbonate alkalinity during anaerobic metabolism and, in the case of Fe and Mn carbonates, from the release to solution of Mn^{2+} and Fe^{2+} during suboxic diagenesis.

The supersaturation of carbonate minerals during early diagenesis commonly results in the disseminated precipitation of a wide range of authigenic carbonates. The precipitation of Ca, Mg carbonate can be expressed through pore water depletions of Ca^{2+}, Mg^{2+}, loss of minor constituents of Ca, Mg carbonates, such as Sr^{2+}, Mn^{2+}, Fe^{2+}, and F^{-}, and stoichiometric deviations between pore water solutes, for example, alkalinity/SO_4^{2-} ratios <2 (Eq mol^{-1}) (e.g., Burdige et al., 2010; Rude and Aller, 1991; Sholkovitz, 1973). Fe^{2+} and Mn^{2+} carbonates also form in zones of suboxic, nonsulfidic diagenetic conditions where Fe^{2+}, Mn^{2+}, and CO_3^{2-} are elevated. Precipitation rates of Fe, Mn carbonates tend to be slower than Ca, Mg carbonate precipitation, but nevertheless, their occurrence is widespread (Jensen et al., 2002). Conditions favoring Fe, Mn carbonates are found in organic carbon-poor deep-sea deposits a few decimeters below the sediment surface (Arctic); in unusually Mn- and Fe-rich surface sediments from quiescent regions, such as the Panama Basin or Baltic Sea; in energetic shallow water mobile deltaic muds, such as the Amazon delta, Gulf of Papua, and Aru Sea; and a few centimeters below the sediment–water interface in lithogenic estuarine and deltaic deposits (Aller et al., 2004a; Alongi et al., 2012; Bricker and Troup, 1975; Holdren et al., 1975; Pedersen and Price, 1982; Suess, 1979; Zhu et al., 2002). Although these authigenic minerals can accumulate as distinct nodules, they are often disseminated throughout deposits or present as overgrowths on preexisting carbonate debris. If sulfide is present, Fe sulfides are more stable thermodynamically and form in preference to Fe carbonates (Garrels and Christ, 1965). Below the zone of SO_4^{2-} reduction, dolomite may also form, particularly in organic-rich margin deposits with elevated alkalinities (e.g., Baker and Burns, 1985; Machel, 2004). These diagenetic carbonates incorporate metabolic HCO_3^{-} from pore water, the proportional contribution of which depends on distance from the sediment–water interface and the local details of the transport–reaction regime. Authigenic carbonates formed during early diagenesis therefore often have relatively light $\delta^{13}C$ isotopic compositions ($\delta^{13}C < 0$) compared to overlying seawater and biogenic carbonates (Coleman, 1985). In deltaic environments, authigenic Ca, Mg, Mn, and Fe carbonates can represent a major fraction of total C burial (~25–30%). In the Amazon delta topset and downdrift coastal mudbanks, for example, authigenic carbonates account for ~70% of buried carbonate minerals at total inorganic C accumulation rates of ~5.7 mmol m^{-2} per day (Aller et al., 1996; Zhu et al., 2002).

8.11.7.3 Kinetics of Biogenic Carbonate Dissolution in Sediments

The global distribution of biogenic carbonates reflects balances between supply, dissolution, and dilution by lithogenic debris,

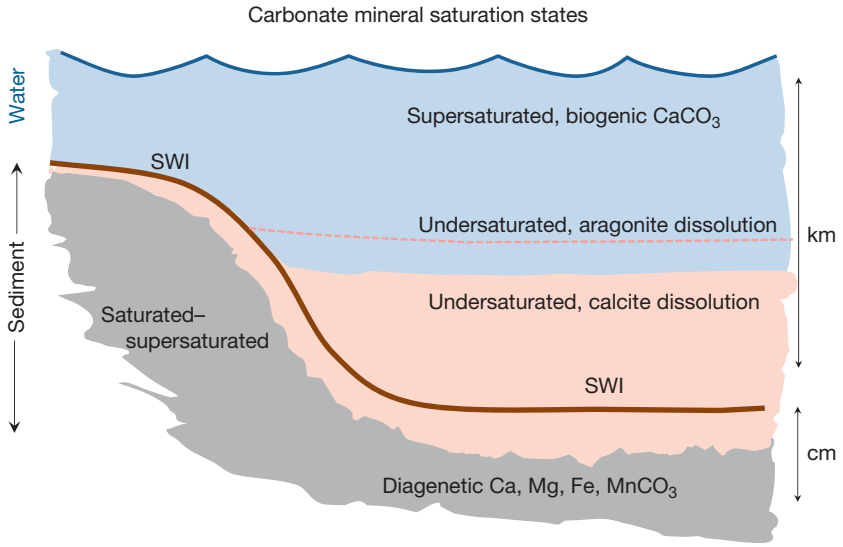

Figure 18 Carbonate mineral saturation states in the global ocean show a general spatial composite distribution of supersaturation, undersaturation, and supersaturation. Surface and upper ocean waters are supersaturated with respect to a wide range of biogenic carbonate minerals and overlie an undersaturated zone and dissolution in deeper waters and surficial sediments. The spatial scaling is determined by material fluxes, thermodynamic stabilities, reaction kinetics, and the buildup of metabolic acids (transport–reaction conditions). The exact zonations differ between specific minerals and are a function of the respective solubilities (e.g., aragonite relative to low-Mg calcite). Suboxic and anoxic diagenetic reactions typically result in supersaturation with respect to a wide range of carbonates within the upper few centimeters or meters of deposits and the diagenetic precipitation of authigenic carbonates below the surficial zone of dissolution (SWI, sediment–water interface).

the latter of consequence mainly near the continents (Figure 19) (Archer, 1996a; Seiter et al., 2004). Although often emphasized as a deep-sea process because of its role in determining the global distribution of carbonate compensation depth, the early diagenetic metabolic dissolution of biogenic carbonate is ubiquitous. The patterns of carbonate dissolution in surficial sedimentary deposits depend strongly on the diagenetic transport regime, including accumulation rate, particle bioturbation, and bioirrigation, and the relative reaction kinetics of carbonate dissolution, organic matter decomposition (CO_2 production) and the reoxidation of reduced metabolites, and overlying water saturation state. The reoxidation of reduced metabolites and associated strong acid production is of minor consequence in regions of low organic flux in the deep sea, but it is a significant mode of carbonate dissolution in shallow waters. Carbonate dissolution–precipitation distributions in surface deposits can be extremely complex, as illustrated by 3-D distributions of pH observed in bioturbated deposits, which imply close proximity of undersaturated and supersaturated microenvironments (Figure 6).

Calcite and aragonite particles undergo dissolution reactions, the rates of which depend on the departure of the contacting solutions from equilibrium saturations. Reaction kinetics have the general form

$$R_{CaCO_3} = k_{CaCO_3}\hat{C}_{CaCO_3}[1-\Omega]^n \qquad [16]$$

The reaction rate coefficient, k_{CaCO_3}, is typically expressed in units of % $CaCO_3$/time (mass $CaCO_3$ dissolved × 100/mass $CaCO_3$/time) (Keir, 1980). Alternative kinetic expressions are possible and often desirable depending on particular model applications (Emerson and Hedges, 2003). When carbonate particles are dispersed in undersaturated solutions, dissolution kinetics are high order, with $n = 3.5$–4 for calcites and aragonite, reflecting progressive change in the dominant dissolution mechanism at particle surfaces as a function of saturation state (Keir, 1980; Morse et al., 2007; Walter and Morse, 1985). Under diffusion-dominated sedimentary conditions, dissolution kinetics can apparently be reasonably approximated by $n = 1$ (Boudreau et al., 2010; Hales, 2003; Hales and Emerson, 1997) or 1–2 (Green and Aller, 2001). The reaction rate coefficients are strong functions of particle size (reactive surface area) and specific compositions and sources (Keir, 1980; Morse, 1978). Typically, but not always, reaction rate coefficients in sediments are ~10–10 000 × lower than those found in controlled laboratory conditions with relatively uniform particle sizes and mineralogy (Archer et al., 1989; Berelson et al., 1994b; Cai et al., 1995; Hales, 2003; Hales and Emerson, 1997; Pfeifer et al., 2002). The values of K_{sp}' (M^2) incorporated in eqn [16] for the biogenic carbonates vary as function of temperature and pressure, which can be closely approximated for calcite as a function of pressure ($p(z)$ atm, z = depth) and mean ocean temperature by

$$K_{sp}' \sim 4.3513 \times 10^{-7} e^{0.0019585p(z)} \qquad [17]$$

(Boudreau et al., 2010).

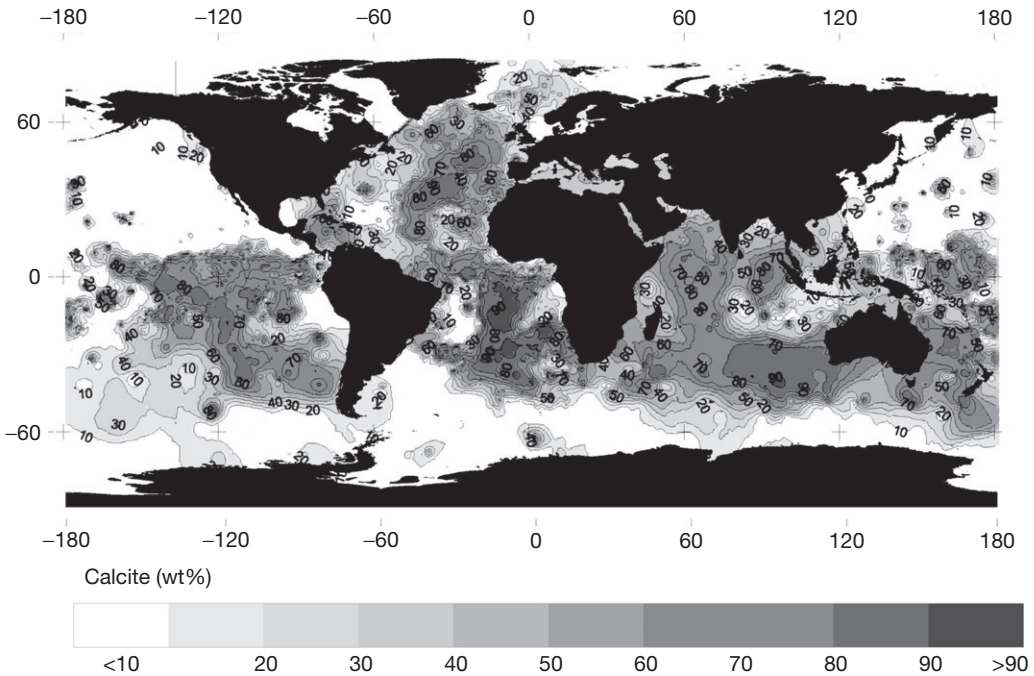

Figure 19 The global distribution of sedimentary biogenic $CaCO_3$ on a weight percentage basis reflects the relative rates of $CaCO_3$, C_{org}, and terrigenous sediment supply, and the dissolution of $CaCO_3$ in both the water column and surface sediments (water and sediment transport–reaction conditions). The highest percentages of $CaCO_3$ are found where terrigenous sediment supply is low and depth-integrated dissolution is minimized relative to the flux of $CaCO_3$ (after Seiter et al., 2004; see also Archer, 1996a). Reproduced from Seiter K, Hensen C, Schroter E, and Zabel M (2004) Organic carbon content in surface sediments – Defining regional provinces. *Deep-Sea Research Part I* 51: 2001–2026; Archer DE (1996a) An atlas of the distribution of calcium carbonate in sediments of the deep sea. *Global Biogeochemical Cycles* 10: 159–174.

8.11.7.4 Shallow Water Carbonate Dissolution

Shallow marine waters are generally supersaturated with respect to both calcite and aragonite, with saturations ranging from $\Omega_{cal} \sim 5.5$ and $\Omega_{arag} \sim 3.6$ in the tropics ($T = 25\,^{\circ}C$) to $\Omega_{cal} \sim 3.7$ and $\Omega_{arag} \sim 2.3$ in temperate regions ($T = 13\,^{\circ}C$) to $\Omega_{cal} \sim 2.6$ and $\Omega_{arag} \sim 1.6$ at high latitudes ($T = 4\,^{\circ}C$) (Andersson et al., 2008). Thus, in subtidal, surficial deposits, the sedimentary carbonate dissolution that occurs is closely tied to diagenetic metabolic acid production, metabolite reoxidation (e.g., sulfide oxidation and nitrification), and bioturbation, all of which can vary seasonally (Table 5). In temperate zone terrigenous estuarine deposits, where biogenic carbonate debris typically comprises ~1–10% by weight of surface sediments, net carbonate dissolution can be highest during the low temperature, well-oxygenated winter period, as shown by seasonal patterns of dissolution in central Long Island Sound, a representative temperate estuarine environment (Figure 20). Excess dissolved Ca^{2+} concentrations above that expected based on pore water Cl^- (salinity) track the degree of carbonate undersaturation during winter, when bioirrigation transport is minimal. Lack of strong biotransport allows reactions to be readily expressed in patterns of buildup or depletion of solute concentrations. Minor element components of carbonates, Sr^{2+} (aragonite) and F^- (calcite, aragonite), are also released into pore water and move into overlying water as carbonates dissolve (Figure 20(b)). The rapid deposition of organic matter during the seasonal spring bloom and the warming of overlying water bring the period of obvious diagenetic carbonate dissolution to an end, as anaerobic metabolism becomes dominant and bioturbation (bioirrigation) increases. Increased biogenic transport and biodeposition of carbonate (e.g., foraminifera and bivalves) in particular can mask the expression of carbonate dissolution, which occurs to some extent during all seasons in these types of deposits.

Much of the O_2 consumption by sediments during the colder periods in temperate deposits is due to reoxidation of Fe sulfides produced during previous warmer seasons, as well as to oxidation of upwardly diffusing NH_4^+, Mn^{2+}, and Fe^{2+} from depth. The transient buildup of metabolic products, such as Fe sulfides in sediments during one portion of the year, followed by net reoxidation during another, can result in substantial changes in the relative Ca^{2+} and HCO_3^- fluxes during each period. If, for example, carbonate dissolution is coupled to the reoxidation of Fe sulfides, the molar ratio of Ca^{2+} to alkalinity in the benthic flux at the time of reaction is 1:1 (mol Eq^{-1}). In contrast, aerobic respiration directly produces a Ca^{2+} to alkalinity ratio of 1:2 (mol Eq^{-1}; Table 4). Although the annual average flux ratio of Ca^{2+} to alkalinity may be close to 1:2 (i.e., no average annual storage of Fe sulfides), there can be substantial deviations in this ratio

Table 5 Coupled oxidation – carbonate dissolution reactions common in C_{org}-rich and bioturbated sediments underlying oxygenated water

(1) $O_2 + CH_2O + CaCO_3 \rightarrow Ca^{2+} + 2HCO_3^-$
(2) $FeS_2 + {}^{15}/_4\,O_2 + 4CaCO_3 + 7/2H_2O \rightarrow 4Ca^{2+} + 4HCO_3^- + 2SO_4^{2-} + Fe(OH)_3$
(3) $FeS + {}^{9}/_4\,O_2 + 2CaCO_3 + {}^{5}/_2H_2O \rightarrow 2Ca^{2+} + 2HCO_3^- + SO_4^{2-} + Fe(OH)_3$
(4) $NH_4^+ + 2O_2 + 2CaCO_3 \rightarrow NO_3^- + H_2O + 2HCO_3^- + 2Ca^{2+}$
(5) $2Mn^{2+} + O_2 + 4CaCO_3 + 2H_2O \rightarrow 2MnO_2 + 4Ca^{2+} + 4HCO_3^-$
(6) $2Fe^{2+} + O_2 + 4CaCO_3 + 5H_2O \rightarrow 2Fe(OH)_3 + 4Ca^{2+} + 4HCO_3^-$

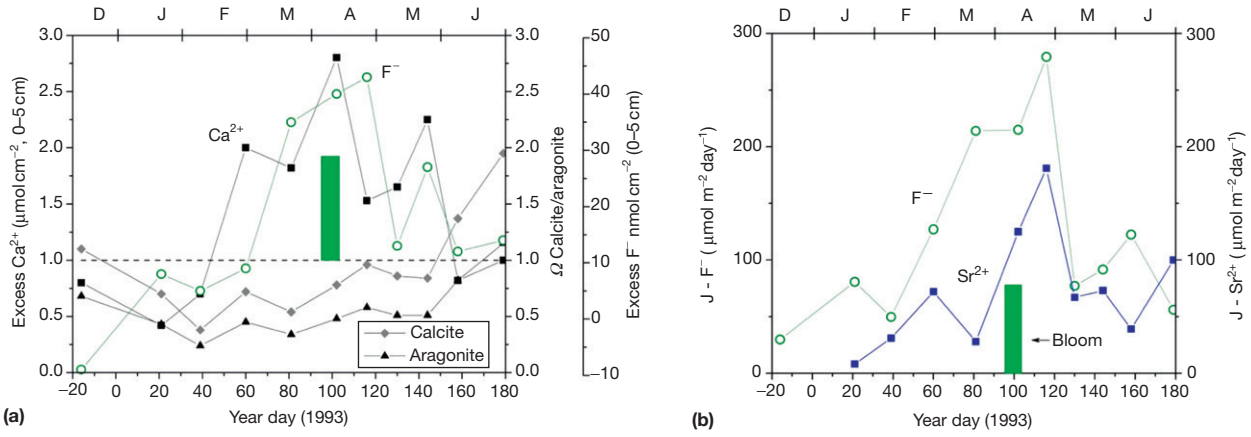

Figure 20 Extensive diagenetic dissolution of $CaCO_3$ takes place in estuarine and shelf deposits underlying supersaturated water, typically in the range of 5–15 mmol m^{-2} per day annual average (Burdige et al., 2010; Green and Aller, 2001). In temperate regions, net dissolution occurs year-round but is best expressed in pore water solute distributions during winter when bioturbation (bioirrigation) is minimal, carbonate mineral undersaturation is promoted by low temperatures, and net oxidation of sedimentary Fe sulfide dominates alkalinity production from reduction reactions. Example: (a) Seasonal pore water concentrations of excess Ca^{2+} and F^- (concentration above seawater salinity background) and carbonate mineral saturation states (Ω) in the upper 5 cm of mud deposits from central Long Island Sound. Net release of Ca^{2+} and F^- is supported by carbonate dissolution. The green bar indicates major deposition of detritus from the spring phytoplankton bloom. (b) Diffusive flux of Sr^{2-} (from aragonite) and F^- derived from $CaCO_3$ dissolution (F^- can also be released during Fe oxide reduction) calculated from concentration gradients (model eqn [4] in text). Reproduced from Green MA and Aller RC (1998) Seasonal patterns of carbonate diagenesis in nearshore terrigenous muds: Relation to spring phytoplankton bloom and temperature. *Journal of Marine Research* 56: 1097–1123; Green MA and Aller RC (2001) Early diagenesis of calcium carbonate in Long Island Sound sediments: Benthic fluxes of Ca^{2+} and minor elements during seasonal periods of net dissolution. *Journal of Marine Research* 59: 769–794.

from 1:2 during any given season. Similarly, microscale biogenic mixing events that reexpose reduced material directly to oxygenated overlying water (e.g., Fe sulfide-rich fecal piles) can produce local carbonate dissolution, which presumably can produce small local excursions in the Ca^{2+}/alkalinity ratio. Transient reoxidation processes coupled with $CaCO_3$ dissolution may explain reported Ca^{2+}/alkalinity ratios of 1:1 rather than 1:2 in benthic chamber incubations over highly bioturbated, organic carbon-rich margin deposits (Jahnke and Jahnke, 2004). Carbonate precipitation and/or proton exchange reactions may also account for these deviations (Jahnke and Jahnke, 2004; Jahnke et al., 1997).

These diagenetic processes and the associated extensive carbonate dissolution occur in both shallow water carbonate and terrigenous deposits (Aller, 1982a; Walter and Burton, 1990). For example, carbonate dissolution in Bahamian platform deposits averages 7.8 ± 4.5 mmol m^{-2} per day, ranging to as high as ~80 mmol m^{-2} per day (Burdige, 2010). Similar magnitudes of dissolution fluxes characterize terrigenous shelf and estuarine deposits, for example, with annual averages in central Long Island Sound of ~5.2 mmol m^{-2} per day and estimates ranging to 13 (Green and Aller, 2001). The injection of O_2 by bioirrigation and seagrass roots into otherwise anoxic zones greatly enhances dissolution in deposits (Burdige et al., 2008, 2010; Ku et al., 1999). Dissolution in shallow water carbonate depositional environments is also clearly accompanied by extensive reprecipitation and recrystallization (reprecipitation/dissolution ratios ~3–6), representing both Ostwald ripening of fine-grained debris and the localized replacement–recrystallization of relatively unstable by more stable phases (Burdige et al., 2010; Hover et al., 2001; Rude and Aller, 1991; Walter et al., 1993). The coupling of dissolution–reprecipitation can result in substantial isotopic alteration of the residual carbonate (Burdige et al., 2010; Patterson and Walter, 1994; Walter et al., 1993).

8.11.7.5 Dissolution of Carbonate in Deep-Sea Deposits and Internal Reaction Patterns

Deep-sea deposits are subject to both saturated and undersaturated boundary conditions with respect to biogenic carbonates, and metabolic dissolution processes driven by C_{org} remineralization are 10–100× lower than in shallow water systems (Figure 8). Pressure and temperature effects on carbonate equilibria and other labile sediment properties require that measurements of core compositions and benthic solute fluxes related to $CaCO_3$ diagenesis be made in situ to avoid substantial artifacts associated with depressurization and warming (Berelson et al., 1994a; Emerson et al., 1982). The distribution of remineralization and metabolic acid production with depth in sediments interacts with overlying water boundary conditions and $CaCO_3$ dissolution kinetics to produce various patterns of $CaCO_3$ loss or storage (Adler et al., 2001; Archer, 1996b; Boudreau et al., 2010; Hales, 2003; Keir and Michel, 1993; Martin et al., 2000). The proportions of highly labile and refractory organic matter, coupled with sediment accumulation rates and bioturbation rates, determine whether most metabolic acid production takes place at the sediment–water interface or deeper (several centimeters) within deposits (i.e., low or high Damköhler numbers) (Section 8.11.4.1). When reactions are focused primarily at the sediment–water interface and the overlying water is saturated, metabolic acids are neutralized in large part by CO_3^{2-} in overlying water rather than sedimentary $CaCO_3$, so that dissolution is relatively inefficient with respect to diagenetic remineralization (Emerson and Bender, 1981; Hales, 2003; Martin and Sayles, 2003). Undersaturated overlying water and long residence times of $CaCO_3$ at the interface promote dissolution regardless of additional sedimentary metabolic acids. When metabolic acid production occurs several centimeters or deeper in deposits, diagenetic dissolution can be substantial for both saturated and undersaturated boundary conditions. Reactions involving both dissolution and precipitation of carbonates coupled to remineralization result in characteristic pH, pCO_2, and Ca^{2+} distributions with depth in deposits (Figure 21).

8.11.7.6 Benthic Alkalinity Fluxes

The alkalinity flux (~carbonate alkalinity = $HCO_3^- + 2CO_3^{2-}$) from sediments is often dominated by carbonate dissolution (Archer, 1996b; Berelson et al., 1994b, 2007; Jahnke and Jahnke, 2004; Jahnke et al., 1994, 1997). The net burial of reduced diagenetic products, such as sulfide (Fe sulfides), may also support an alkalinity flux in continental margin-shelf regions; however, under oxygenated overlying water, this direct contribution is often minimized because of extensive reoxidation of metabolites during bioturbation in surface sediments and also the precipitation of authigenic carbonates at depth in deposits. The global patterns of depth dependence and magnitude of benthic alkalinity fluxes expressed as $CaCO_3$ dissolution rates (i.e., ½ alkalinity flux) largely follow the expected interactions between biogenic carbonate supply, rates of metabolic CO_2 production, depth-dependent solubilities, and overlying water saturation states: they are highest at the margins where metabolic activity and $CaCO_3$ supply are high, increased slightly where undersaturated boundary conditions are present, and decreased at abyssal depths as sources of $CaCO_3$ are depleted (Figure 22; Berelson et al., 2007). The magnitudes in abyssal regions >2000 m depth range from ~0.2 to 0.3 and at the margins (<2000 m) from ~0.6 (Pacific) to 2.8 (Atlantic) mmol $CaCO_3$ m^{-2} per day. These values contrast with estuarine and shelf regions (<200 m), where annual average values of ~5–15 mmol $CaCO_3$ m^{-2} per day or higher are typical (Berelson et al., 2007; Burdige et al., 2010; Green and Aller, 2001; Powell et al., 1989). Although shallow water systems are of comparable magnitude to pelagic sediments with respect to $CaCO_3$ accumulation rates (shallow → ~15; pelagic → ~11–19 × 10^{12} mol $year^{-1}$) (Schneider et al., 2006), carbonate production and dissolution budgets in shallow water (<200 m), particularly for terrigenous deposits, remain very poorly constrained (Milliman and Droxler, 1996; Schneider et al., 2006). As surface ocean saturation states continue to decrease as a result of anthropogenic activities, both shallow water and deepwater diagenetic dissolution rates will increase, the former perhaps particularly dramatically because of abundant, relatively soluble high-Mg calcite and aragonite present in shelf and platform regions (Andersson et al., 2008; Burdige et al., 2010; Morse et al., 2006).

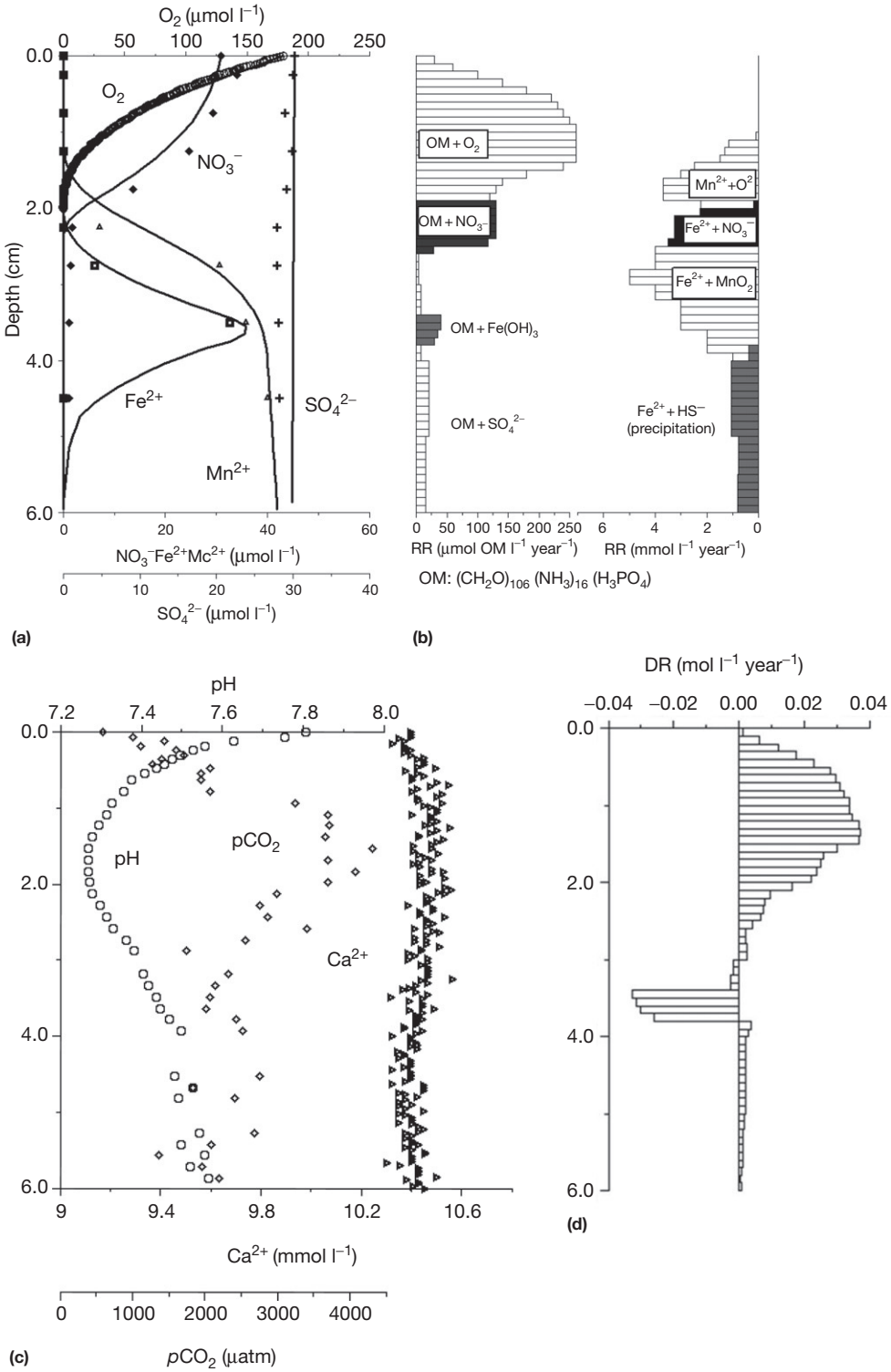

Figure 21 Steady-state diagenetic models allow quantification of general metabolic reactions and coupled $CaCO_3$ dissolution and precipitation. Example: (a) Pore water solute profiles and numerical diagenetic model fits at a continental margin station off Gabon, West Africa, in 1251 m water depth. O_2 profiles were obtained in situ: all other constituents are from retrieved cores (Pfeifer et al., 2002). (b) Modeled reaction rates associated with C_{org} (OM) remineralization (**Table 3**) and secondary reoxidation reactions (Mn^{2+}–O_2, Fe^{2+}–NO_3^-, and Fe^{2+}–MnO_2; **Table 2**). (c) In situ pH, pCO_2, and Ca^{2+} profiles. Overlying water $\Omega_{cal} = 1.07$. These profiles demonstrate net dissolution over the 0–3 cm depth interval and authigenic carbonate precipitation below 3 cm. (d) Modeled net dissolution (DR+) and net precipitation rates (DR−) of $CaCO_3$ (authigenic carbonates may be partially composed of Fe, Mn carbonates). Weight percent carbonate distributions (not shown) are consistent with both surficial dissolution (0–3 cm) and subsurface precipitation. Reproduced from Pfeifer K, Hensen C, Adler M, Wenzhofer F, Weber B, and Schulz HD (2002) Modeling of subsurface calcite dissolution, including the respiration and reoxidation processes of marine sediments in the region of equatorial upwelling off Gabon. *Geochimica et Cosmochimica Acta* 66: 4247–4259.

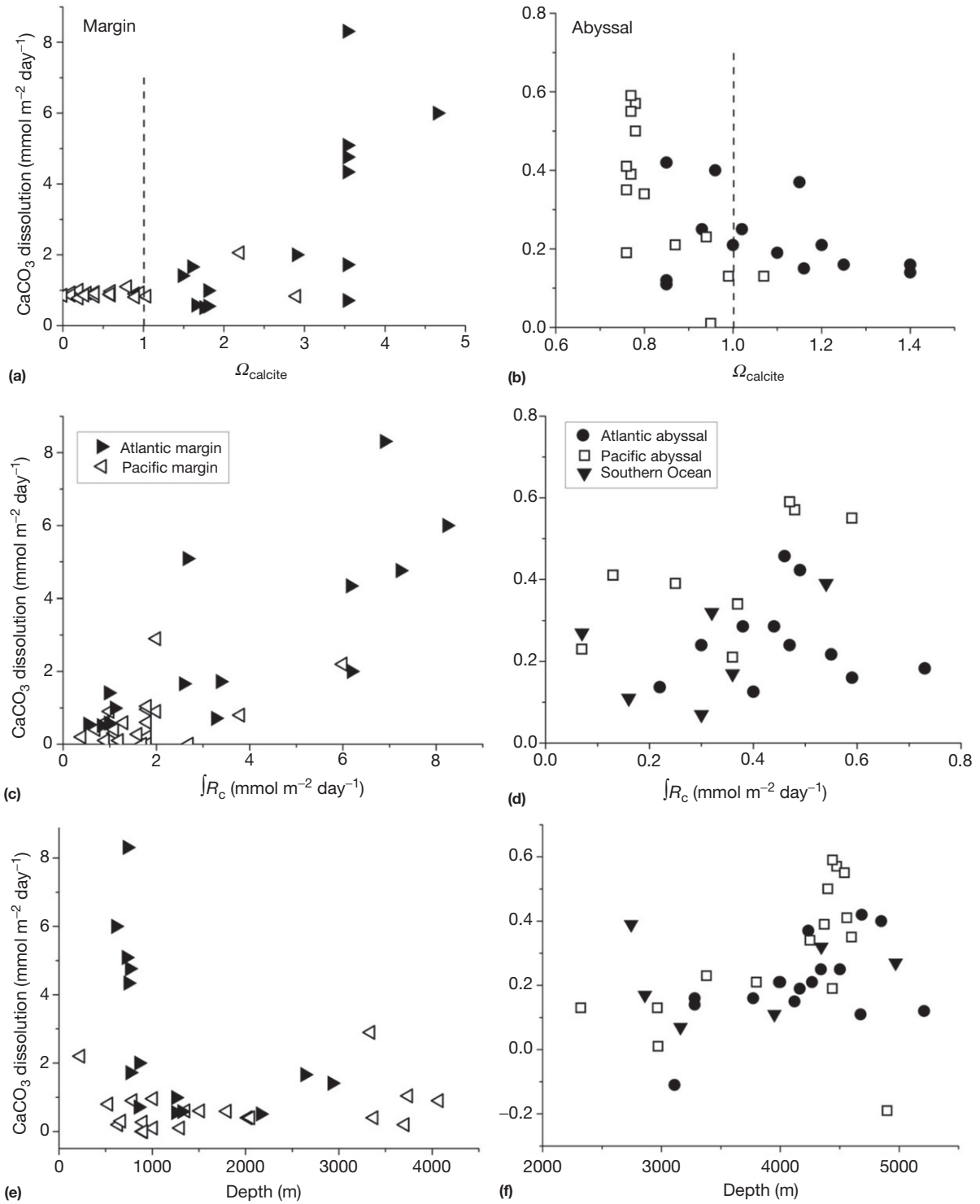

Figure 22 When $CaCO_3$ and reactive C_{org} are present, diagenetic dissolution is ubiquitous. (a) As shown by plotting dissolution rates versus saturation state in overlying water, deepwater benthic $CaCO_3$ dissolution (1–8 mmol m^{-2} per day) is most intense along continental margins where it is largely independent of overlying water saturation state (Ω_{cal}). (b) Abyssal diagenetic dissolution ranges from ~0.1 to 0.6, averaging ~0.2 mmol m^{-2} per day. A major effect of undersaturated overlying water is evident only at low Ω_{cal} ($\leq$0.8) in abyssal regions of the Pacific. (c) $CaCO_3$ dissolution in continental margin deposits varies directly with benthic metabolic activity as expressed by correlation with the depth-integrated C_{org} remineralization rate ($\int R_C$- (mmol m^{-2} per day), derived from O_2 flux). (d) $CaCO_3$ dissolution at abyssal depths within individual ocean basins also generally correlates directly with C_{org} remineralization. (e) The highest $CaCO_3$ dissolution fluxes along continental margins take place at $<$1 km bathymetric depth where metabolic activity is highest. (f) Dissolution increases slightly at the deepest abyssal depths as the role of overlying water saturation becomes relatively important and then decreases as all available $CaCO_3$ is reacted. Modified from Berelson WM, Balch WM, Najjar R, Feely RA, Sabine C, and Lee K (2007) Relating estimates of $CaCO_3$ production, export, and dissolution in the water column to measurements of $CaCO_3$ rain into sediment traps and dissolution on the sea floor: A revised global carbonate budget. *Global Biogeochemical Cycles* 21: GB1024.

8.11.8 Biogenic Silica and Reverse Weathering

8.11.8.1 Patterns in Biogenic SiO_2 Distributions

The fluxes into the ocean of dissolved silica and silicate debris from rock weathering are balanced in large part by the formation, the deposition, and the burial of biogenic silica and its early diagenetic products in marine sediments (see Chapter 9.4). Thus, understanding and quantifying diagenetic reactions and early diagenetic behavior of Si takes on major importance because of its central role in elemental cycling associated with controls on oceanic productivity (e.g., diatoms), on seawater composition through authigenic aluminosilicate formation (HCO_3^-, K^+, Li^+, and F^-), and also on the paleoceanographic record of ancient productivity and weathering patterns (e.g., Misra and Froelich, 2012). Deposition and burial of biogenic silica are directly reflected by the dominance of opaline silica-rich deposits over large areas of the seafloor, particularly in the Southern Ocean, equatorial Pacific, and eastern boundary upwelling regions of low lithogenic particle supply (Figure 23). As in the case of organic matter and carbonates, however, the small percentages by weight (1–3%) of opaline silica in continental margin deposits with high sedimentation rate are of equivalent or greater importance to global biogenic silica storage than the far more obvious and extensive areas of siliceous sediments in the deep sea (DeMaster, 2002).

8.11.8.2 Diagenetic Fates, Equilibria, and Dissolution Reaction Kinetics of Biogenic SiO_2

Like other reactive components of sediments, the early diagenetic reactions of biogenic silica are characterized by complex balances between dissolution, surface alteration, and synthetic-precipitation reactions, and a wide range of possible diagenetic fates (Figure 24). The absolute and relative balances between these myriad reactions vary substantially in different depositional environments and depend strongly on the relative availability and mixtures of reactants (e.g., Aplin, 1993). Acid–base reactions play less of a direct role in silica diagenesis than for carbonates, but there is a close coupling to sedimentary redox reactions through the mobilization of Fe^{2+} and Al^{3+}, which can readily react with biogenic silica (Dixit et al., 2001; Lewin, 1961; Mackin and Aller, 1989; Van Bennekom et al., 1989), the decomposition of organic matrix components of biogenic silica, which can alter dissolution kinetics (Bidle and Azam, 2001; Lewin, 1961; Van Cappellen and Qiu, 1997a), and the production of HS^-, the latter affecting the concentrations and behavior of $Fe^{2+,3+}$, which might otherwise react with silica (Figure 25).

The diagenetic behavior and sedimentary storage of silica has been traditionally examined from the standpoint of reactions expected for biogenic opaline silica (bSi), deviations from which are used to infer additional processes, such as

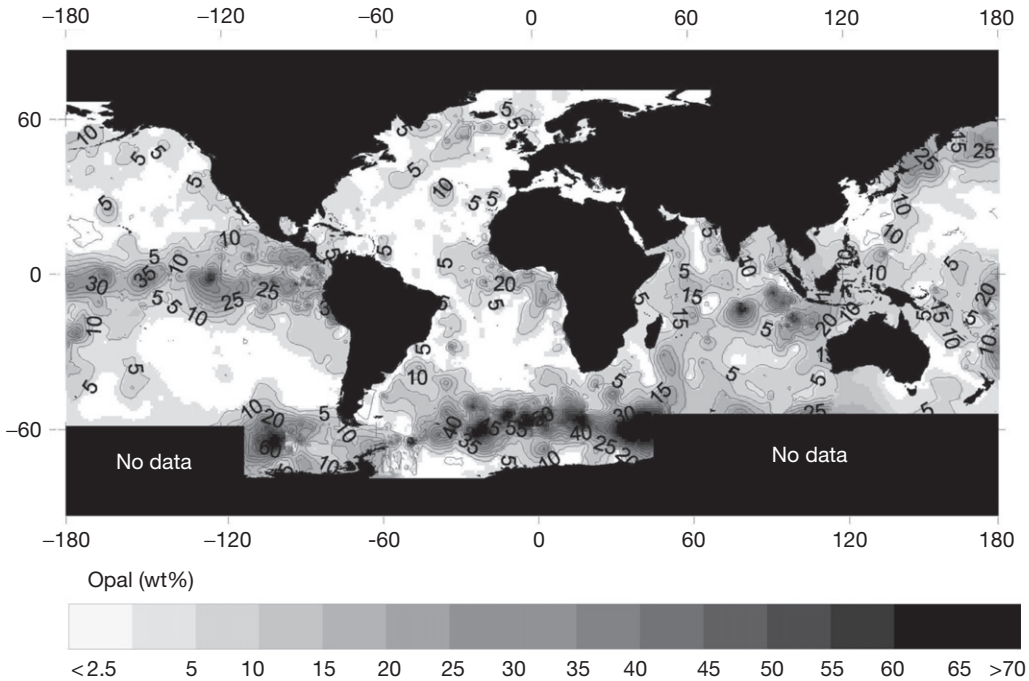

Figure 23 The global distribution of sedimentary biogenic SiO_2 (bSi) on a weight percentage basis reflects the relative rates of biogenic opaline SiO_2 and terrigenous sediment supply and the dissolution–alteration of SiO_2 in both the water column and surface sediments (water column and sediment transport–reaction conditions). The highest percentages of SiO_2 are found where terrigenous sediment supply is low and depth-integrated dissolution is minimized relative to the flux of SiO_2 (e.g., Southern Ocean and Equatorial Pacific) (after Seiter et al., 2004; see also Broecker and Peng, 1982). Reproduced from Seiter K, Hensen C, Schroter E, and Zabel M (2004) Organic carbon content in surface sediments – Defining regional provinces. *Deep-Sea Research Part I* 51: 2001–2026; See also: Broecker WS and Peng TH (1982) *Tracers in the Sea*. New York: Eldigio Press, Lamont Doherty Geological Observatory.

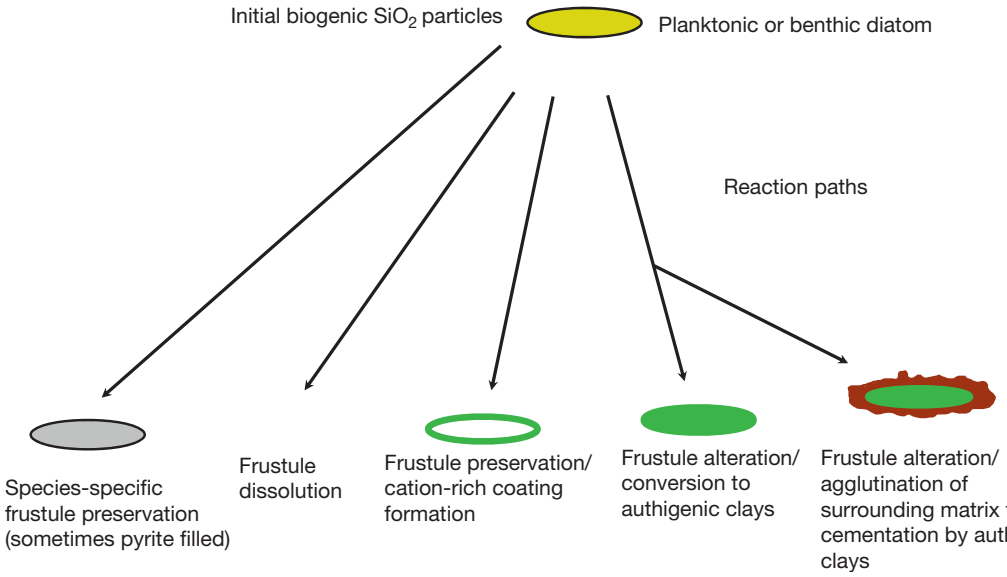

Figure 24 Schematic diagram illustrating the multiple possible diagenetic fates of biogenic SiO_2 particles in sediments. Reproduced from Michalopoulos P and Aller RC (2004) Early diagenesis of biogenic silica in the Amazon Delta: Alteration, authigenic clay formation, and storage. *Geochimica et Cosmochimica Acta* 68: 1061–1085.

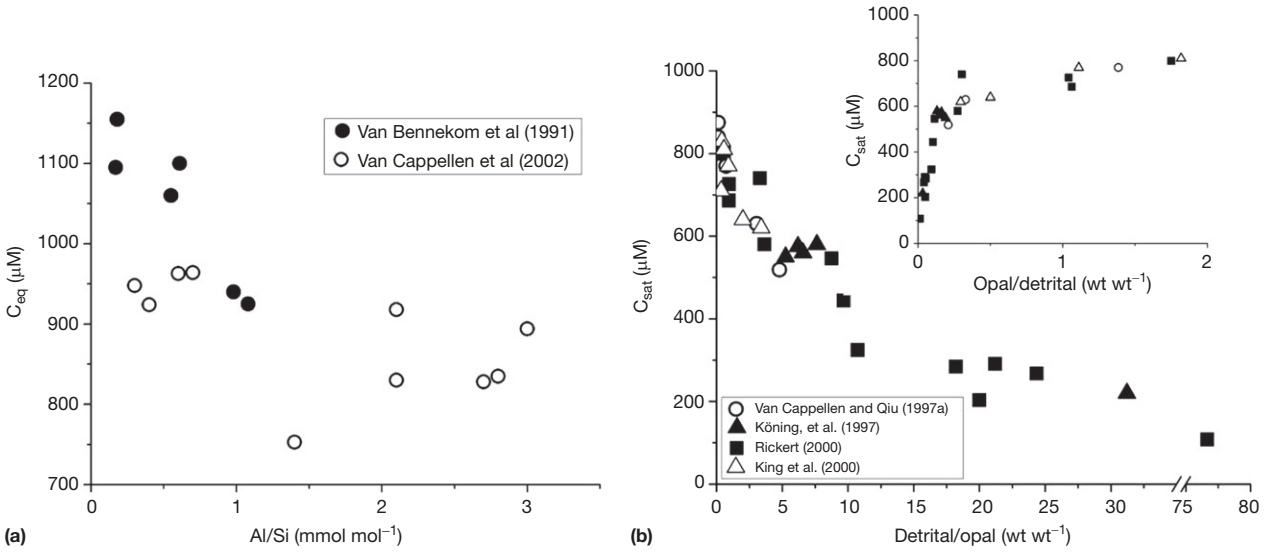

Figure 25 The interaction of reactive Si with Al plays a particularly important role during the diagenesis of biogenic SiO_2. (a) The concentration of $Si(OH)_4$ in saturation equilibrium with diatom debris decreases substantially as the Al/Si ratio in frustules increases from ~0.1 mmol mol^{-1} (water column) to ~3 (core top sediment). (b) The concentration of $Si(OH)_4$ in saturation equilibrium with sediments, determined using flow-through reactors, varies regularly as a function of the ratio of detrital/opal weight ratio, consistent with lithogenic dissolved Al sources, bSi surface alteration reactions, and authigenic clay formation. The inset illustrates the behavior at high opal/detrital ratios (region of main graph near 0 detrital/opal ratio) (Data from King et al., 2000; Köning et al., 1997; Rickert, 2000; Van Bennekom et al., 1991; Van Cappellen and Qiu, 1997b; Van Cappellen et al., 2002). Reproduced from Loucaides S, Cappellen P, Roubeix V, Moriceau B, and Ragueneau O (2012a) Controls on the recycling and preservation of biogenic silica from biomineralization to burial. *Silicon* 4: 7–22.

alteration or authigenic mineral formation. Thus, the kinetics of dissolution and the equilibrium behavior of opaline silica have been incorporated into transport–reaction models in order to predict and interpret the pore water $Si(OH)_4$ distributions, the recycling fluxes, the spatial patterns of siliceous sediments, and the storage of biogenic silica (Archer et al., 1993; McManus et al., 1995; Rabouille et al., 1997; Schink et al., 1975; Seiter et al., 2010). A typical general kinetic equation quantifying dissolution is (Hurd, 1973; Rickert et al., 2002; Schink et al., 1975; see also **Chapter 9.4**)

$$R_{Si} = k_{Si}\hat{C}_{Si}[1-\Omega]^n \qquad [18]$$

where: R_{Si} = production rate of dissolved $Si(OH)_4$ (mass/volume pore water); k_{Si} = first-order rate coefficient (mass *b*Si/reactive

area *b*Si/time); $\hat{C}_{Si}$ = reactive surface area *b*Si/volume pore water (= (reactive surface area *b*Si/mass *b*Si) · (mass *b*Si/volume pore water)); $\Omega = C_{Si}/C_{eq}$, and C_{eq} is the equilibrium concentration of opaline Si. (Note that $Si(OH)_4$ is also written equivalently as H_4SiO_4; the latter expression emphasizes acid behavior in solution, and the former emphasizes the tetrahedral molecular structure and metalloid properties critical to authigenesis.)

When bSi is not limiting, the behavior is sometimes simply approximated by (e.g., Kamatani and Riley, 1979)

$$R_{Si} = k^*_{Si}\left[C_{eq} - C_{Si}\right] \qquad [19]$$

The pseudo-first-order reaction rate coefficient, k^*_{Si}, incorporates the reactive surface area of biogenic silica/volume solution, a formulation which compromises direct comparison of values of k^*_{Si} between sites (Hurd and Theyer, 1975). The reaction order, n, is 1 when $\Omega > 0.3$–0.4 (eqn [18]), so that first-order kinetics characterizes most sedimentary conditions. As in the case of carbonate particles, higher-order kinetics is observed in suspensions at greater degrees of undersaturation ($\Omega < 0.3$–0.4) (Rickert et al., 2002; Van Cappellen and Qiu, 1997b). Concentrations of $Si(OH)_4$ at equilibrium with recently formed biogenic opaline silica particles are ~1080 to ~1730 μM over 2–25 °C at pH 8 (Hurd, 1973; Rickert et al., 2002; Van Cappellen and Qiu, 1997b). Pressure effects on equilibrium are of relatively minor importance (±15%) over oceanic ranges relative to temperature (Fanning and Pilson, 1974; Loucaides et al., 2012b). The kinetic and equilibrium relationships of Si in deposits, like other reactive sedimentary components, vary substantially, reflecting the weighted behavior of a mixture of particles having varied compositions and kinetic properties (e.g., initial biogenic particle source characteristics, alteration history) (Hurd and Theyer, 1975; Van Bennekom et al., 1989; Van Cappellen et al., 2002).

Pore water $Si(OH)_4$ concentrations near equilibrium with opaline silica are seldom attained by pore waters in either shallow water or deep-sea deposits (Hurd, 1973; Loucaides et al., 2012a; Mackin and Aller, 1989; McManus et al., 1995; Rabouille et al., 1997; Van Bennekom et al., 1989). In addition to factors, such as reactive surface area related to the specific biological source of Si, it is well established that the surfaces of biogenic silica particles often quickly incorporate and become enriched in Al^{3+}, Fe^{2+}, and Mg^{2+}, dramatically affecting solubilities and dissolution behavior of Si in both the oceanic water column and within sedimentary deposits (Hurd, 1973; Kamatani et al., 1988; Lewin, 1961; Loucaides et al., 2010; Rickert, 2000; Van Bennekom et al., 1989; Willey, 1975, 1978, 1980). Al in particular can progressively permeate siliceous tests during initial deposition and burial (Dixit and Van Cappellen, 2002; Dixit et al., 2001; Van Bennekom et al., 1989, 1991). The incorporation of Al substantially lowers the reactivity and solubility of biogenic silica and can promote preservation and initial burial as slightly altered Al-enriched bSi (**Figure 26(a)**). Conversion to less soluble, more crystallized forms, opal CT and quartz, takes place during later stages of opaline Si diagenesis (e.g., Hurd and Theyer, 1975; Kastner et al., 1977; Williams et al., 1985; see also **Chapter 9.4**).

8.11.8.3 Authigenic Silicate Formation and Reverse Weathering

Although the major sedimentary storage mode for biogenic silica is as opaline or slightly altered opaline silica (see **Chapter 9.4**), there are multiple alternative diagenetic reaction paths that can result in partial or complete conversion of silica into authigenic aluminosilicates (**Figures 1** and **24**). Close associations of biogenic silica with distinct authigenic aluminosilicate minerals have long been reported from a variety of depositional environments. For example, Hurd (1973) described the intimate intergrowth of authigenic Al, Si phases with radiolarian tests in Pacific deep-sea sediments, and proposed equilibration with such phases as one possible control on pore water $Si(OH)_4$ concentrations. Similar associations of authigenic clay and siliceous biogenic debris have been documented at numerous additional deep-sea sites (Cole, 1985; Heath and Dymond, 1977; Hein et al., 1979; Johnson, 1976; Odin and Frohlich, 1988; Sayles and Bischoff, 1973). Aluminosilicates have also been reported associated intimately with living diatoms in nearshore marine waters (Van Bennekom and Van der Gast, 1976), and obvious replacement of diatom frustules by poorly crystalline authigenic clay minerals occurs rapidly in saline lakes (Badaut and Risacher, 1983). Experimental incubations of marine sediments and diatoms readily demonstrate rapid (0.1–2 year) nucleation and growth of aluminosilicates on frustules and other reactive siliceous substrates in seawater at low temperature ($T < 30$ °C) (Loucaides et al., 2010; Michalopoulos and Aller, 1995; Michalopoulos et al., 2000). Consistent with observations of solids, studies of diatom frustule-rich Southern Ocean deposits have implicated control of pore water silicate concentrations by authigenic aluminosilicate formation during early diagenesis (Dixit et al., 2001; King et al., 2000; Rabouille et al., 1997; Van Beusekom et al., 1997; Van Cappellen and Qiu, 1997a,b). Perhaps most importantly in terms of global mass balance considerations, bottom waters and pore waters in a wide range of nearshore high sedimentation rate deltaic and estuarine environments also typically show regular stoichiometric relationships between dissolved Al and Si, indicative of extremely rapid, early diagenetic formation of authigenic aluminosilicates (Mackin, 1986; Mackin and Aller, 1984, 1986, 1989).

The involvement of biogenic silica in the formation of aluminosilicate phases represents a form of reverse weathering *sensu* Mackenzie and Garrels (Mackenzie and Garrels, 1966; Mackenzie et al., 1981; Michalopoulos and Aller, 1995; Wollast, 1974; Wollast and Mackenzie, 1983). These reactions have the general form

$$\text{Reactive } SiO_2 + Al(OH)_4^- + \left(Fe^{2+3+}, Mg^{2+}, K^+, Li^+\right) + F^- + HCO_3^- \rightarrow \text{aluminosilicates} + CO_2 + H_2O \qquad [20]$$

Reverse weathering reactions result in the formation of relatively cation-rich aluminosilicate phases at the expense of reactive SiO_2 phases, such as biogenic silica and degraded clays during early diagenesis in seawater, and these reactions have been proposed as a significant component of oceanic elemental mass balances (Mackenzie and Garrels, 1966). The apparent lack of confirming evidence in the initial searches for such reactions in the oceans (e.g., Dasch, 1969; Russell, 1970), coupled with obvious alternative elemental sinks evident in hydrothermal systems, resulted in a tendency to discount their existence and to ignore many subsequent indications to the contrary (Hurd, 1973; Mackenzie et al., 1981; Mackin and

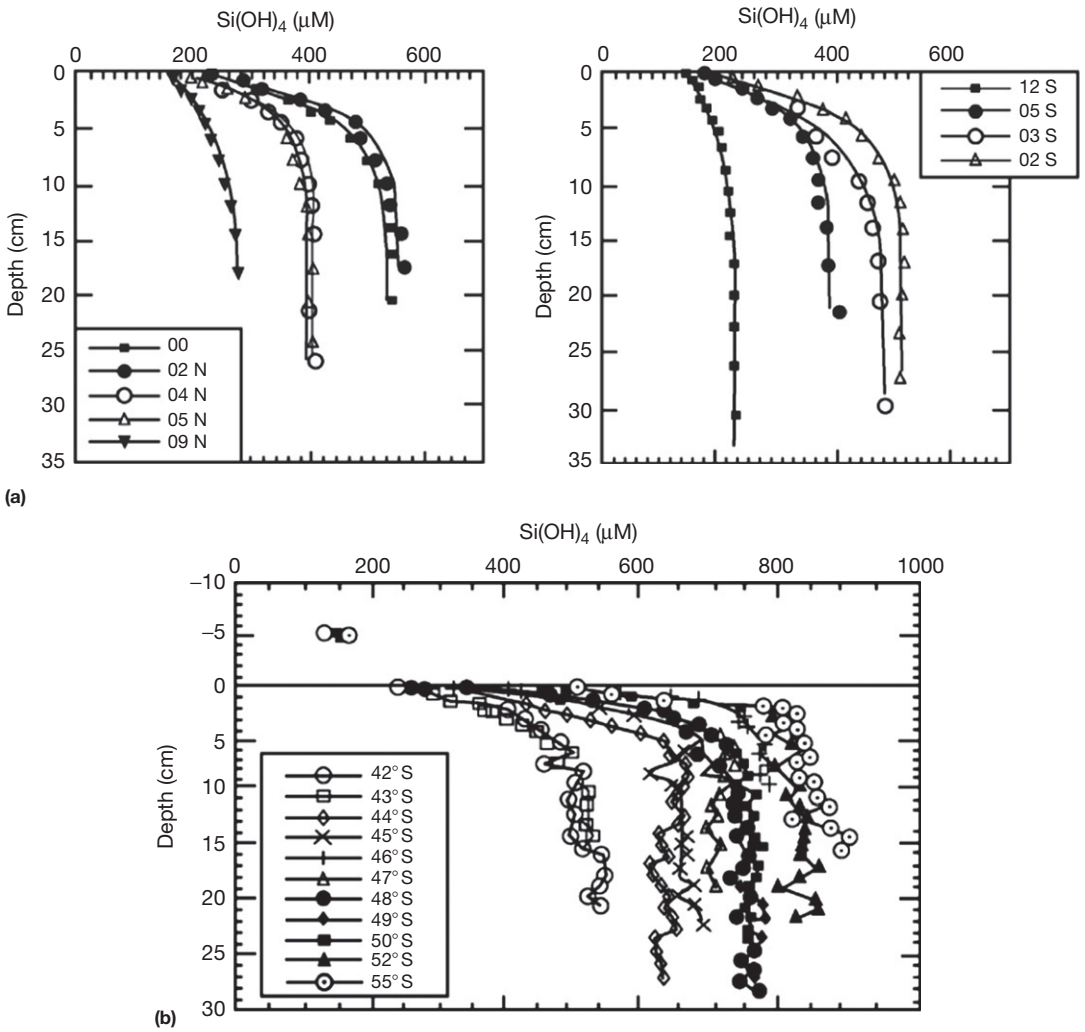

Figure 26 Pore water $Si(OH)_4$ concentrations typically asymptote to different values in different geographic regions, reflecting balances between supply, dissolution reaction kinetics (e.g., initial source particles and alteration), surface alteration, and secondary mineral formation. Examples: (a) stations along a north–south transect along 140° W in the equatorial Pacific (after McManus et al., 1995) and (b) stations along a north–south transect through the Indian Ocean sector of the southern Polar Front. Reproduced from Rabouille C, Gaillard JF, Treguer P, and Vincendeau MA (1997) Biogenic silica recycling in surficial sediments across the Polar Front of the Southern Ocean (Indian Sector). *Deep-Sea Research Part II* 44: 1151–1176.

Aller, 1989; Risvet, 1978; Savin and Epstein, 1970; Sayles, 1979; Yeh and Eslinger, 1986). Sayles (1979), for example, reported extensive evidence from pore waters obtained throughout the deep sea indicating the common occurrence of silicate authigenesis. It has also long been recognized that authigenic silicates are widely present and formed on continental shelves (e.g., green marine clays), but the timescales of formation, like those inferred from the deep sea, were traditionally assumed to be of order 10^3–10^6 years (Odin, 1988; see **Chapter 9.12**).

A major conceptual change in the last few decades has come from experimental and field studies of deltaic sediments mentioned previously that have directly demonstrated the existence of rapid, early diagenetic reverse weathering reactions in deposits with extremely high sediment accumulation rates, such as the Amazon, Mississippi, and Congo deltas. These studies indicate that in at least some Fe, Al oxide-rich environments, such as tropical and subtropical deltas, reactive biogenic silica availability could be the limiting factor for the formation of authigenic aluminosilicate phases (Ku and Walter, 2003; Loucaides et al., 2010; Michalopoulos and Aller, 1995, 2004; Presti and Michalopoulos, 2008). Reaction limitation by biogenic silica in deltaic systems contrasts with regions that have low sediment accumulation rates, such as the Southern Ocean, where the availability of lithogenic (Al, Fe) debris is limiting (Aplin, 1993; Van Cappellen and Qiu, 1997b). The roles of high sediment accumulation sinks for biogenic silica in the form of authigenic aluminosilicates, and for seawater solutes, such as K^+, Li^+, Mg^{2+}, and F^-, that are incorporated into clays, remain an exciting frontier of early diagenetic and elemental cycling research (e.g., **Figure 27**) (Michalopoulos and Aller, 2004; Rude and Aller, 1994). It is clear, however, that in environments with high sediment accumulation rates such as deltas, the alteration of biogenic silica and formation of authigenic silicates can increase net storage by factors of 2–3× (Mississippi delta) or 5–10× (Amazon

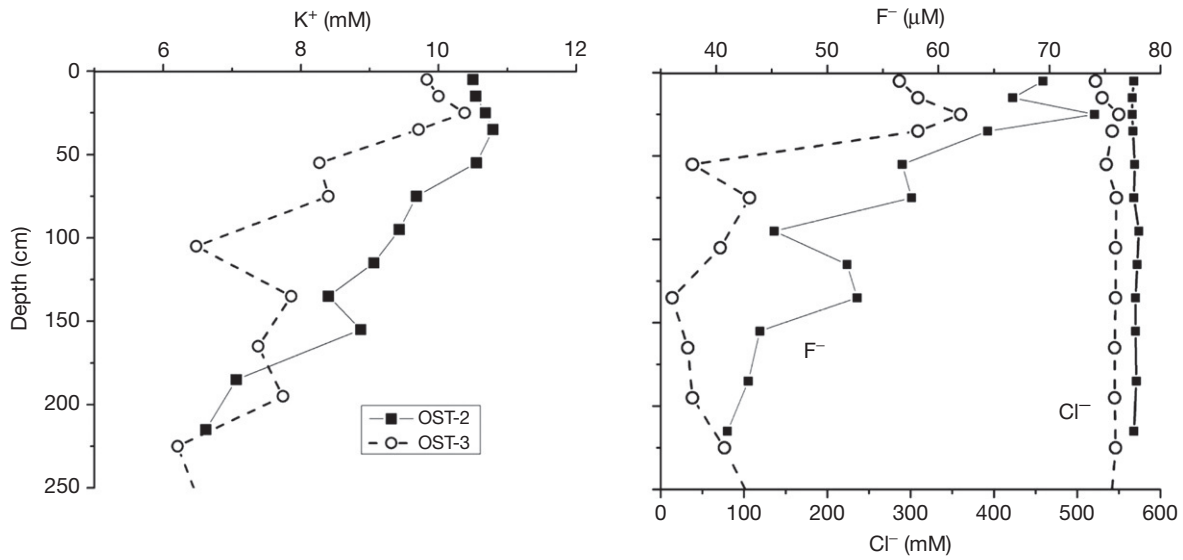

Figure 27 Pore water profiles of minor elements in rapidly accumulating and highly mobile deltaic sediments often demonstrate extensive uptake of seawater solutes associated with authigenic clay formation over seasonal timescales. Example: (a) K^+ and (b) F^- concentration profiles from two sites on the Amazon delta topset (February 1990; OST-2, 20 m; OST-3, 40 m depth; $\omega = 1.4–4.8\ g\,cm^{-2}$ per year at OST-2, OST-3, respectively). Stoichiometric loss ratios are consistent with a 'glauconitic' clay. Cl^- profiles demonstrate that reaction rather than salinity controls K^+ and F^- gradients. Reproduced from Rude PD and Aller RC (1994) Fluroine uptake by Amazon Continental-Shelf sediment and its impact on the global fluorine cycle. *Continental Shelf Research* 14: 883–907.

delta) from what might otherwise be estimated from relatively unaltered biogenic silica burial (Michalopoulos and Aller, 2004; Presti and Michalopoulos, 2008). When such diagenetic alteration of biogenic silica to aluminosilicates is incorporated into global budgets for Si, the continental margins become at least comparable in importance to the deep sea for biogenic Si storage (Laruelle et al., 2010).

8.11.9 Future Directions

Human activities are substantially and dramatically affecting the Earth surface system and driving major global environmental changes. Many of these changes are strongly focused into the coastal and continental boundary regions where biogeochemical interactions are most intense and diagenetic processes are critical components of biogeochemical cycling across a broad range of timescales. The continental margins, including shelves and deltaic systems, are disproportionally important in bioactive elemental cycling relative to the vast global ocean. Representing ~15–20% of the seafloor area, the boundary regions accumulate ~90% of the sedimentary debris entering or generated in the sea and store 50–80% of bioactive elements, such as reactive C and Si, in various forms (Berner, 1982; Dunne et al., 2007; Jahnke, 2010; Liu et al., 2010; Laruelle et al., 2010; Milliman and Farnsworth, 2011; Wollast, 1998). These regions are characterized by the greatest diversity and most complex configurations of diagenetic regimes on Earth and, in contrast to the deeper, open ocean, are not particularly amenable to simple, steady-state diagenetic modeling (**Figure 2**). Technological developments, such as new optical, immunological, and electrochemical sensors, eddy correlation techniques, miniaturized mass spectrometers for in situ applications (Camilli and Duryea, 2009), kinetic studies, and sophisticated numerical models, will provide a basis for accurately constraining unsteady, heterogeneous processes in these dynamic boundary environments. Increasingly close integration of diagenetic, ocean–atmosphere–sediment dynamics, and ecosystem models (e.g., Middelburg and Soetaert, 2004; Soetaert et al., 2000), together with the intuition derived from experience and observation, will be required to understand and evaluate the impacts and predict the future consequences of unfettered anthropogenic forcing on complex margin systems and thus global biogeochemical cycles (Liu et al., 2010).

Acknowledgments

This chapter is patterned after the earlier contribution by Emerson and Hedges (2003), Chapter 6.11 in the first edition of the *Treatise*, which stands on its own. It has been extended in some alternative directions, however, as it places greater emphasis on deltaic and shallow water depositional systems and unsteady diagenesis, and it incorporates more recent data obtained through technical advances, such as planar optodes and eddy correlation. It does this in part at the expense of more detailed coverage of deep-sea processes and organic geochemistry for which the chapters by Emerson and Hedges (2003) and by Martin and Sayles (**Chapter 9.2**) should be further examined for perspective. I thank editors Mike Mottl and Karl K. Turekian for their patience, support, and review, multiple authors for supplying original data (J. Middelburg; C. Hensen; K. Seiter; K. Soetaert; B. Thamdrup; M. Zabel), and J.Y. Aller for assistance. R. C.A. has been funded largely through NSF OCE programs. This chapter is dedicated to the late Karl K. Turekian, mentor and friend.

References

Adler M, Hensen C, Wenzhöfer F, et al. (2001) Modeling of calcite dissolution by oxic respiration in supralysoclinal deep-sea sediments. *Marine Geology* 177: 167–189.

Allen GP, Salomon JC, Bassoullet P, et al. (1980) Effects of tides on mixing and suspended sediment transport in macro-tidal estuaries. *Sedimentary Geology* 26: 69–90.

Aller RC (1980a) Diagenetic processes near the sediment-water interface of Long Island Sound, I. Decomposition and nutrient element geochemistry. In: Saltzman B (ed.) *Advances in Geophysics*, pp. 235–348. New York: Academic Press.

Aller RC (1980b) Quantifying solute distributions in the bioturbated zone of marine-sediments by defining an average micro-environment. *Geochimica et Cosmochimica Acta* 44: 1955–1965.

Aller RC (1982a) Carbonate dissolution in nearshore terrigenous muds: The role of physical and biological reworking. *Journal of Geology* 90: 79–95.

Aller RC (1982b) The effects of macrobenthos on chemical properties of marine sediments and overlying waters. In: McCall PL and Tevesz MJS (eds.) *Animal-Sediment Relations: The Biogenic Alteration of Sediments*, pp. 53–102. New York: Plenum.

Aller RC (1994a) Bioturbation and remineralization of sedimentary organic-matter – Effects of redox oscillation. *Chemical Geology* 114: 331–345.

Aller RC (1994b) The sedimentary Mn cycle in Long Island Sound – Its role as intermediate oxidant and the influence of bioturbation, O2, and C(org) flux on diagenetic reaction balances. *Journal of Marine Research* 52: 259–295.

Aller RC (1998) Mobile deltaic and continental shelf muds as suboxic, fluidized bed reactors. *Marine Chemistry* 61: 143–155.

Aller RC (2001) Transport and reactions in the bioirrigated zone. In: Boudreau BP and Jorgensen BB (eds.) *The Benthic Boundary Layer*, pp. 269–301. Oxford: Oxford University Press.

Aller RC (2004) Conceptual models of early diagenetic processes: The muddy seafloor as an unsteady, batch reactor. *Journal of Marine Research* 62: 815–835.

Aller JY and Aller RC (2004) Physical disturbance creates bacterial dominance of benthic biological communities in tropical deltaic environments of the Gulf of Papua. *Continental Shelf Research* 24: 2395–2416.

Aller JY, Aller RC, Kemp PF, et al. (2010) Fluidized muds: A novel setting for the generation of biosphere diversity through geologic time. *Geobiology* 8: 169–178.

Aller RC and Blair NE (1996) Sulfur diagenesis and burial on the Amazon shelf: Major control by physical sedimentation processes. *Geo-Marine Letters* 16: 3–10.

Aller RC and Blair NE (2006) Carbon remineralization in the Amazon-Guianas tropical mobile mudbelt: A sedimentary incinerator. *Continental Shelf Research* 26: 2241–2259.

Aller RC, Blair NE, and Brunskill GJ (2008) Early diagenetic cycling, incineration, and burial of sedimentary organic carbon in the central Gulf of Papua (Papua New Guinea). *Journal of Geophysical Research Earth Surface* 113. http://dx.doi.org/10.1029/2006JF000689.

Aller RC, Blair NE, Xia Q, et al. (1996) Remineralization rates, recycling, and storage of carbon in Amazon shelf sediments. *Continental Shelf Research* 16: 753–786.

Aller RC, Hannides A, Heilbrun C, et al. (2004a) Coupling of early diagenetic processes and sedimentary dynamics in tropical shelf environments: The Gulf of Papua deltaic complex. *Continental Shelf Research* 24: 2455–2486.

Aller RC, Heilbrun C, Panzeca C, et al. (2004b) Coupling between sedimentary dynamics, early diagenetic processes, and biogeochemical cycling in the Amazon-Guianas mobile mud belt: Coastal French Guiana. *Marine Geology* 208: 331–360.

Aller RC and Rude PD (1988) Complete oxidation of solid-phase sulfides by manganese and bacteria in anoxic marine-sediments. *Geochimica et Cosmochimica Acta* 52: 751–765.

Alongi DM (1991) The role of intertidal mudbanks in the diagenesis and export of dissolved and particulate materials from the Fly-Delta, Papua- New-Guinea. *Journal of Experimental Marine Biology and Ecology* 149: 81–107.

Alongi DM, Wirasantosa S, Wagey T, et al. (2012) Early diagenetic processes in relation to river discharge and coastal upwelling in the Aru Sea, Indonesia. *Marine Chemistry* 140–141: 10–23.

Alsharhan AS and Kendall CGS (2003) Holocene coastal carbonates and evaporites of the southern Arabian Gulf and their ancient analogues. *Earth-Science Reviews* 61: 191–243.

Andersson AJ, Mackenzie FT, and Bates NR (2008) Life on the margin: Implications of ocean acidification on Mg-calcite, high latitude and cold-water marine calcifiers. *Marine Ecology Progress Series* 373: 265–273.

Andrews D and Bennett A (1981) Measurements of diffusivity near the sediment-water interface with a fine-scale resistivity probe. *Geochimica et Cosmochimica Acta* 45: 2169–2175.

Anschutz P, Jorissen FJ, Chaillou G, et al. (2002) Recent turbidite deposition in the eastern Atlantic: Early diagenesis and biotic recovery. *Journal of Marine Research* 60: 835–854.

Aplin AC (1993) The composition of authigenic clay minerals in recent sediments: Links to the supply of unstable reactants. In: Manning DAC, Hall PL, and Hughes CR (eds.) *Geochemistry of Clay-Pore Fluid Interactions*, pp. 81–106. London: Chapman and Hall.

Archer DE (1996a) An atlas of the distribution of calcium carbonate in sediments of the deep sea. *Global Biogeochemical Cycles* 10: 159–174.

Archer DE (1996b) A data-driven model of the global calcite lysocline. *Global Biogeochemical Cycles* 10: 511–526.

Archer DE, Emerson S, and Reimers C (1989) Dissolution of calcite in deep-sea sediments: pH and O_2 microelectrode results. *Geochimica et Cosmochimica Acta* 53: 2831–2845.

Archer DE, Lyle M, Rodgers K, et al. (1993) What controls opal preservation in tropical deep-sea sediments. *Paleoceanography* 8: 7–21.

Archer DE, Morford JL, and Emerson SR (2002) A model of suboxic sedimentary diagenesis suitable for automatic tuning and gridded global domains. *Global Biogeochemical Cycles* 16: 1017.

Badaut D and Risacher F (1983) Authigenic smectite on diatom frustules in Bolivian saline lakes. *Geochimica et Cosmochimica Acta* 47: 363–375.

Bailey JE and Ollis DF (1986) *Biochemical Engineering Fundamentals*. New York: McGraw-Hill.

Baker PA and Burns SJ (1985) Occurrence and formation of dolomite in organic-rich continental margin sediments. *AAPG Bulletin* 69: 1917–1930.

Bear J (1972) *Dynamics of Fluids in Porous Media*. New York: American Elsevier.

Berelson WM, Balch WM, Najjar R, et al. (2007) Relating estimates of $CaCO_3$ production, export, and dissolution in the water column to measurements of $CaCO_3$ rain into sediment traps and dissolution on the sea floor: A revised global carbonate budget. *Global Biogeochemical Cycles* 21: GB1024.

Berelson WM, Hammond DE, McManus J, et al. (1994a) Dissolution kinetics of calcium carbonate in equatorial Pacific sediments. *Global Biogeochemical Cycles* 8: 219–235.

Berelson WM, Hammond DE, O'Neill D, et al. (1994b) Benthic fluxes and pore water studies from sediments of the central equatorial north Pacific: Nutrient diagenesis. *Geochimica et Cosmochimica Acta* 54: 3001–3912.

Berg P, Glud RN, Hume A, et al. (2009) Eddy correlation measurements of oxygen uptake in deep ocean sediments. *Limnology and Oceanography – Methods* 7: 576–584.

Berg P and Huettel M (2008) Monitoring the seafloor using the noninvasive eddy correlation technique: Integrated benthic exchange dynamics. *Oceanography* 21: 164–167.

Berg P, Risgaard-Petersen N, and Rysgaard S (1998) Interpretation of measured concentration profiles in sediment pore water. *Limnology and Oceanography* 43: 1500–1510.

Berg P, Roy H, and Wiberg PL (2007) Eddy correlation flux measurements: The sediment surface area that contributes to the flux. *Limnology and Oceanography* 52: 1672–1684.

Berner RA (1964) An idealized model of dissolved sulfate distribution in recent sediments. *Geochimica et Cosmochimica Acta* 28: 1497–1503.

Berner RA (1980) *Early Diagenesis: A Theoretical Approach*. Princeton, NJ: Princeton University Press.

Berner RA (1981) A new geochemical classification of sedimentary environments. *Journal of Sedimentary Petrology* 51: 359–365.

Berner RA (1982) Burial of organic-carbon and pyrite sulfur in the modern ocean – Its geochemical and environmental significance. *American Journal of Science* 282: 451–473.

Berner RA (1984) Sedimentary pyrite formation: An update. *Geochimica et Cosmochimica Acta* 48: 605–615.

Berner RA (2004) *The Phanerozoic Carbon Cycle: CO_2 and O_2*. New York: Oxford University Press.

Berner RA and Raiswell R (1984) C/S Method for distinguishing fresh-water from marine sedimentary-rocks. *Geology* 12: 365–368.

Bertics VJ and Ziebis W (2010) Bioturbation and the role of microniches for sulfate reduction in coastal marine sediments. *Environmental Microbiology* 12: 3022–3034.

Bianchi TS (2011) The role of terrestrially derived organic carbon in the coastal ocean: A changing paradigm and the priming effect. *Proceedings of the National Academy of Sciences of the United States of America* 108: 19473–19481.

Bidle KD and Azam F (2001) Bacterial control of silicon regeneration from diatom detritus: Significance of bacterial ectohydrolases and species identity. *Limnology and Oceanography* 46: 1606–1623.

Billen G (1982) An idealized model of nitrogen recycling in marine sediments. *American Journal of Science* 282: 512–541.

Bischoff WD, Mackenzie FT, and Bishop FC (1987) Stabilities of synthetic magnesian calcites in aqueous solution: Comparison with biogenic materials. *Geochimica et Cosmochimica Acta* 51: 1413–1423.

Blair NE and Aller RC (2012) The fate of terrestrial organic carbon in the marine environment. *Annual Review of Marine Science* 4: 401–423.

Blair NE, Leithold EL, and Aller RC (2004) From bedrock to burial: The evolution of particulate organic carbon across coupled watershed-continental margin systems. *Marine Chemistry* 92: 141–156.

Blair NE, Leithold EL, Brackley H, et al. (2010) Terrestrial sources and export of particulate organic carbon in the Waipaoa sedimentary system: Problems, progress and processes. *Marine Geology* 270: 108–118.

Blair NE, Leithold EL, Ford ST, et al. (2003) The persistence of memory: The fate of ancient sedimentary organic carbon in a modern sedimentary system. *Geochimica et Cosmochimica Acta* 67: 63–73.

Bollinger MS and Moore WS (1993) Evaluation of salt-marsh hydrology using radium as a tracer. *Geochimica et Cosmochimica Acta* 57: 2203–2212.

Boudreau BP (1986) Mathematics of tracer mixing in sediments. 1. Spatially-dependent, diffusive mixing. *American Journal of Science* 286: 161–198.

Boudreau BP (1994) Is burial velocity a master parameter for bioturbation. *Geochimica et Cosmochimica Acta* 58: 1243–1249.

Boudreau BP (1997) *Diagenetic Models and Their Implementation: Modelling Transport and Reactions in Aquatic Sediments*. Berlin: Springer.

Boudreau BP and Imboden DM (1987) Mathematics of tracer mixing in sediments. 3. The theory of nonlocal mixing within sediments. *American Journal of Science* 287: 693–719.

Boudreau BP, Middelburg JJ, and Meysman FJR (2010) Carbonate compensation dynamics. *Geophysical Research Letters* 37: L03603.

Boudreau BP and Ruddick BR (1991) On a reactive continuum representation of organic-matter diagenesis. *American Journal of Science* 291: 507–538.

Boudreau BP and Westrich JT (1984) The dependence of bacterial sulfate reduction on sulfate concentration in marine sediments. *Geochimica et Cosmochimica Acta* 48: 2503–2516.

Brandes JA and Devol AH (1995) Simultaneous nitrate and oxygen respiration in coastal sediments: Evidence for discrete diagenesis. *Journal of Marine Research* 53: 771–797.

Bricker OP and Troup BN (1975) Sediment-water exchange in Chesapeake Bay. In: Cronin LE (ed.) *Estuarine Research, 1. Chemistry, Biology, and the Estuarine System*, pp. 3–27. New York: Academic Press.

Broecker WS and Peng TH (1982) *Tracers in the Sea*. New York: Eldigio Press, Lamont Doherty Geological Observatory.

Brunskill GJ, Zagorskis I, and Pfitzner J (2003) Geochemical mass balance for lithium, boron, and strontium in the Gulf of Papua, Papua New Guinea (Project TROPICS). *Geochimica et Cosmochimica Acta* 67: 3365–3383.

Burdige DJ (2006) *Geochemistry of Marine Sediments*. Princeton, NJ: Princeton University Press.

Burdige DJ (2007) Preservation of organic matter in marine sediments: Controls, mechanisms, and an imbalance in sediment organic carbon budgets? *Chemical Reviews* 107: 467–485.

Burdige DJ (2010) A modeling study of organic matter remineralization in deeply-buried marine sediments. *Geochimica et Cosmochimica Acta* 74: A127–A127.

Burdige DJ (2012) *Estuarine and Coastal Sediments – Coupled Biogeochemical Cycling*. Amsterdam: Elsevier.

Burdige DJ, Hu X, and Zimmerman RC (2010) The widespread occurrence of coupled carbonate dissolution/reprecipitation in surface sediments on the Bahamas Bank. *American Journal of Science* 310: 492–521.

Burdige DJ, Zimmerman RC, and Hu X (2008) Rates of carbonate dissolution in permeable sediments estimated from pore-water profiles: The role of sea grasses. *Limnology and Oceanography* 53: 549–565.

Cai WJ and Reimers CE (1995) Benthic oxygen flux, bottom water oxygen concentration and core top organic carbon content in the deep northeast Pacific Ocean. *Deep-Sea Research Part I* 42: 1681–1699.

Cai WJ, Reimers CE, and Shaw T (1995) Microelectrode studies of organic carbon degradation and calcite dissolution at a California Continental rise site. *Geochimica et Cosmochimica Acta* 59: 497–511.

Camilli R and Duryea AN (2009) Characterizing spatial and temporal variability of dissolved gases in aquatic environments with in situ mass spectrometry. *Environmental Science and Technology* 43: 5014.

Canfield DE (1993) Organic matter oxidation in marine sediments. In: Wollast R, Mackenzie FT, and Chou L (eds.) *Interaction of C, N, P, and S Biogeochemical Cycles and Global Change*, pp. 333–363. Berlin: Springer.

Canfield DE (1994) Factors influencing organic-carbon preservation in marine-sediments. *Chemical Geology* 114: 315–329.

Canfield DE, Kristensen E, and Thamdrup B (2005) *Aquatic Geomicrobiology*. San Diego: Elsevier.

Canfield DE, Raiswell R, and Bottrell S (1992) The reactivity of sedimentary iron minerals toward sulfide. *American Journal of Science* 292: 659–683.

Canfield DE and Thamdrup B (2009) Towards a consistent classification scheme for geochemical environments, or, why we wish the term 'suboxic' would go away. *Geobiology* 7: 385–392.

Cao Z-R, Zhu Q-Z, Aller RC, et al. (2011) A fluorosensor for two-dimensional measurements of extracellular enzyme activity in marine sediments. *Marine Chemistry* 123: 23–31.

Chang BX and Devol AH (2009) Seasonal and spatial patterns of sedimentary denitrification rates in the Chukchi sea. *Deep-Sea Research Part II* 56: 1339–1350.

Chave KE (1954) Aspects of the biogeochemistry of magnesium 2. Calcareous sediments and rocks. *The Journal of Geology* 62: 587–599.

Claypool JK and Kaplan IR (1974) The origin and distribution of methane in marine sediments. In: Kaplan IR (ed.) *Natural Gases in Marine Sediments*, pp. 99–139. New York: Plenum.

Cole TG (1985) Composition, oxygen isotope geochemistry, and origin of smectite in the metalliferous sediments of the Bauer Deep, Southeast Pacific. *Geochimica et Cosmochimica Acta* 49: 221–235.

Coleman ML (1985) Geochemistry of diagenetic nonsilicate minerals. Kinetic considerations. *Philosophical Transactions of the Royal Society of London, A* 315: 39–56.

Corbett DR, McKee B, and Allison M (2006) Nature of decadal-scale sediment accumulation on the western shelf of the Mississippi River delta. *Continental Shelf Research* 26: 2125–2140.

Cowie GL, Hedges JI, Prahl FG, et al. (1995) Elemental and major biochemical changes across an oxidation front in a relict turbidite: An oxygen effect. *Geochimica et Cosmochimica Acta* 59: 33–46.

Crill PM and Martens CS (1987) Biogeochemical cycling in an organic-rich coastal marine basin. 6. Temporal and spatial variations in sulfate reduction rates. *Geochimica et Cosmochimica Acta* 51: 1175–1186.

Curry KJ, Bennett RH, Mayer LM, et al. (2007) Direct visualization of clay microfabric signatures driving organic matter preservation in fine-grained sediment. *Geochimica et Cosmochimica Acta* 71: 1709–1720.

Dasch EJ (1969) Strontium isotopes in weathering profiles, deep-sea sediments, and sedimentary rocks. *Geochimica et Cosmochimica Acta* 33: 1521–1532.

DeMaster DJ (2002) The accumulation and cycling of biogenic silica in the Southern Ocean: Revisiting the marine silica budget. *Deep-Sea Research Part II* 49: 3155–3167.

Dixit S and Van Cappellen P (2002) Surface chemistry and reactivity of biogenic silica. *Geochimica et Cosmochimica Acta* 66: 2559–2568.

Dixit S, Van Cappellen P, and Van Bennekom AJ (2001) Processes controlling solubility of biogenic silica and pore water build-up of silicic acid in marine sediments. *Marine Chemistry* 73: 333–352.

Drever JI, Li Y-H, and Maynard JB (1988) Geochemical cycles: The continental crust and the oceans. In: Gregor CB, Garrels RM, Mackenzie FT, and Maynard JB (eds.) *Chemical Cycles in the Evolution of the Earth*, pp. 17–53. New York: Wiley.

Dukat DA and Kuehl SA (1995) Non-steady-state 210Pb flux and the use of 228Ra/226Ra as a geochronometer on the Amazon continental shelf. *Marine Geology* 125: 329–350.

Dunne JP, Sarmiento JL, and Gnanadesikan A (2007) A synthesis of global particle export from the surface ocean and cycling through the ocean interior and on the seafloor. *Global Biogeochemical Cycles* 21: GB4006.

Einsele G (2000) *Sedimentary Basins: Evolution, Facies, and Sediment Budget*, 2nd edn. Berlin: Springer.

Emerson S (1985) Organic carbon dynamics and preservation in deep-sea sediments. *Deep-Sea Research* 32: 1–21.

Emerson S and Bender M (1981) Carbon fluxes at the sediment-water interface of the deep-sea: Calcium carbonate preservation. *Journal of Marine Research* 39: 139–162.

Emerson S, Fischer K, Reimers C, et al. (1985) Organic-carbon dynamics and preservation in deep-sea sediments. *Deep Sea Research* 32: 1–21.

Emerson S, Grundmanis V, and Graham D (1982) Carbonate chemistry in marine pore waters: MANOP sites C and S. *Earth and Planetary Science Letters* 61: 220–232.

Emerson S and Hedges J (2003) Sediment diagenesis and benthic flux. In: Holland HD and Turekian KK (eds.) *Treatise on Geochemistry*, pp. 293–319. Oxford: Pergamon.

Emerson S, Jahnke R, and Heggie D (1984) Sediment-water exchange in shallow water estuarine sediments. *Journal of Marine Research* 42: 709–730.

Emerson S, Stump C, Grootes PM, et al. (1987) Estimates of degradable organic carbon in deep-sea surface sediments from ^{14}C concentrations. *Nature* 329: 51–53.

Fan YZ, Zhu QZ, Aller RC, et al. (2011) An in situ multispectral imaging system for planar optodes in sediments: Examples of high-resolution seasonal patterns of pH. *Aquatic Geochemistry* 17: 457–471.
Fanning KA and Pilson MEQ (1974) Diffusion of dissolved silica out of deep-sea sediments. *Journal of Geophysical Research* 79: 1293–1297.
Forster S and Graf G (1992) Continuously measured changes in redox potential influenced by oxygen penetrating from burrows of *Callianassa subterranea*. *Hydrobiologia* 235/236: 517–532.
Froelich PN, Klinkhammer GP, Bender ML, et al. (1979) Early oxidation of organic-matter in pelagic sediments of the Eastern Equatorial Atlantic-Suboxic diagenesis. *Geochimica et Cosmochimica Acta* 43: 1075–1090.
Galy V, France-Lanord C, Beyssac O, et al. (2007) Efficient organic carbon burial in the Bengal fan sustained by the Himalayan erosional system. *Nature* 450: 407–410.
Garrels RM and Christ CL (1965) *Solutions, Minerals, and Equilibria*. New York: Harper and Row.
Gilbert F, Hulth S, Grossi V, Aller RC (2013) Redox oscillation and benthic nitrogen mineralization within burrowed sediments: An experimental simulation. *Marine Ecology Progress Series*.
Glud RN (2008) Oxygen dynamics of marine sediments. *Marine Biology Research* 4: 243–289.
Glud RN, Berg P, Hume A, et al. (2010) Benthic O_2 exchange across hard-bottom substrates quantified by eddy correlation in a sub-Arctic fjord. *Marine Ecology Progress Series* 417: 1–12.
Glud RN, Ramsing NB, Gundersen JK, et al. (1996) Planar optrodes: A new tool for fine scale measurements of two-dimensional O_2 distribution in benthic communities. *Marine Ecology Progress Series* 140: 217–226.
Goldhaber MB (2003) Sulfur-rich sediments. In: Holland HD and Turekian KK (eds.) *Treatise on Geochemistry*, pp. 257–288. Oxford: Pergamon.
Goldhaber MB, Aller RC, Cochran JK, et al. (1977) Sulfate reduction, diffusion, and bioturbation in Long Island Sound sediments; report of the FOAM Group. *American Journal of Science* 277: 193–237.
Goldhaber MB and Kaplan IR (1974) The sulfur cycle. In: Goldberg ED (ed.) *The Sea*, pp. 569–654. New York: Wiley.
Goñi MA, Monacci N, Gisewhite R, et al. (2008) Terrigenous organic matter in sediments from the Fly River delta-clinoform system (Papua New Guinea). *Journal of Geophysical Research Earth Surface* 113: F01S10.
Goñi MA, Yunker MB, Macdonald RW, et al. (2005) The supply and preservation of ancient and modern components of organic carbon in the Canadian Beaufort Shelf of the Arctic Ocean. *Marine Chemistry* 93: 53–73.
Graf G (1992) Benthic-pelagic coupling – A benthic view. *Oceanography and Marine Biology* 30: 149–190.
Green MA and Aller RC (1998) Seasonal patterns of carbonate diagenesis in nearshore terrigenous muds: Relation to spring phytoplankton bloom and temperature. *Journal of Marine Research* 56: 1097–1123.
Green MA and Aller RC (2001) Early diagenesis of calcium carbonate in Long Island Sound sediments: Benthic fluxes of Ca^{2+} and minor elements during seasonal periods of net dissolution. *Journal of Marine Research* 59: 769–794.
Habicht KS, Gade M, Thamdrup B, et al. (2002) Calibration of sulfate levels in the Archean Ocean. *Science* 298: 2372–2374.
Hales B (2003) Respiration, dissolution, and the lysocline. *Paleoceanography* 18: 1099.
Hales B and Emerson S (1997) Evidence in support of first-order dissolution kinetics of calcite in seawater. *Earth and Planetary Science Letters* 148: 317–327.
Hartnett HE, Keil RG, Hedges JI, et al. (1998) Influence of oxygen exposure time on organic carbon preservation in continental margin sediments. *Nature* 391: 572–574.
Hayes MO (1967) Relationship between coastal climate and bottom sediment type on the inner continental shelf. *Marine Geology* 5: 111–132.
Heath GR and Dymond J (1977) Genesis and transformation of metalliferous sediments from the East Pacific Rise, Bauer Deep and Central Basin, Northwest Nazca Plate. *Geological Society of America Bulletin* 88: 723–733.
Hedges JI, Hu FS, Devol AH, et al. (1999) Sedimentary organic matter preservation: A test for selective degradation under oxic conditions. *American Journal of Science* 299: 529–555.
Hedges JI and Keil RG (1995) Sedimentary organic matter preservation: An assessment and speculative synthesis. *Marine Chemistry* 49: 81–115.
Hein JR and Griggs GB (1972) Distribution and scanning electron microscope (SEM) observations of authigenic pyrite from a Pacific deep-sea core. *Deep Sea Research* 19: 133–138.
Hein JR, Yeh HW, and Alexander E (1979) Origin of iron-rich montmorillonite from the manganese nodule belt of the North Equatorial Pacific. *Clays and Clay Minerals* 27: 185–194.
Heip CHR, Goosen NK, Herman PMJ, et al. (1995) Production and consumption of biological particles in temperate tidal estuaries. In: Ansell AD, Gibson RN, and Barnes M (eds.) *Oceanography and Marine Biology – An Annual Review*, vol. 33, pp. 1–149. London: University College London Press.
Henrichs SM and Reeburgh WS (1987) Anaerobic mineralization of marine sediment organic-matter-rates and role of anaerobic processes in the oceanic carbon economy. *Geomicrobiology Journal* 5: 191–237.
Holdren GR Jr., Bricker OP, and Matisoff G (1975) A model for the control of dissolved manganese in the interstitial waters of Chesapeake Bay. In: Church TM (ed.) *Marine Chemistry in the Coastal Environment*, pp. 364–381. Washington, DC: American Chemical Society.
Holland HD (1984) *The Chemistry of the Atmosphere and Oceans*. New York: Wiley.
Hover VC, Walter LM, and Peacor DR (2001) Early marine diagenesis of biogenic aragonite and Mg-calcite: New constraints from high-resolution STEM and AEM analyses of modern platform carbonates. *Chemical Geology* 175: 221–248.
Howarth RW (1993) Microbial processes in salt-marsh sediments. In: Ford TE (ed.) *Aquatic Microbiology: An Ecological Approach*, pp. 239–259. Boston: Blackwell.
Huettel M, Cook P, Janssen F, et al. (2007) Transport and degradation of a dinoflagellate bloom in permeable sublittoral sediment. *Marine Ecology Progress Series* 340: 139–153.
Huettel M and Webster IT (2001) Pore water flow in permeable sediments. In: Boudreau BP and Jorgensen BB (eds.) *The Benthic Boundary Layer*, pp. 144–179. New York: Oxford University Press.
Huettel M, Ziebis W, and Forster S (1996) Flow-induced uptake of particulate matter in permeable sediments. *Limnology and Oceanography* 41: 309–322.
Huettel M, Ziebis W, Forster S, et al. (1998) Advective transport affecting metal and nutrient distributions and interfacial fluxes in permeable sediments. *Geochimica et Cosmochimica Acta* 62: 613–631.
Huh C-A, Lin H-L, Lin S, et al. (2009) Modern accumulation rates and a budget of sediment off the Gaoping (Kaoping) River, SW Taiwan: A tidal and flood dominated depositional environment around a submarine canyon. *Journal of Marine Systems* 76: 405–416.
Hulthe G, H. S, and H.P.O. J (1998) Effect of oxygen on degradation rate of refractory and labile organic matter in continental margin sediments. *Geochimica et Cosmochimica Acta* 62: 1319–1328.
Humphrey AE (1972) The kinetics of biosystems: A review. In: Gould RF (ed.) *Chemical Reactor Engineering Advances in Chemistry*, vol. 109, pp. 630–671. Washington, DC: American Chemical Society.
Hurd DC (1973) Interactions of biogenic opal, sediment and seawater in the Central Equatorial Pacific. *Geochimica et Cosmochimica Acta* 37: 2257–2282.
Hurd DC and Theyer F (1975) Changes in the physical and chemical properties of biogenic silica from the Central Equatorial Pacific. I. Solubility, specific surface area, and solution rate constants of acid-cleaned samples. In: Gibbs TRPJ (ed.) *Analytical Methods in Oceanography*. *Advances in Chemistry Series,* pp. 211–230. Washington, DC: American Chemical Society.
Jahnke RA (1985) A model of microenvironments in deep-sea sediments-formation and effects on porewater profiles. *Limnology and Oceanography* 30: 956–965.
Jahnke RA (1996) The global ocean flux of particulate organic carbon: Areal distribution and magnitude. *Global Biogeochemical Cycles* 10: 71–88.
Jahnke RA (2004) Transport processes and organic matter cycling in coastal sediments. In: Robinson AR and Brink KH (eds.) *The Global Coastal Ocean Multiscale Interdisciplinary Processes*, pp. 163–191. Boston: Harvard University Press.
Jahnke RA (2010) Global synthesis. In: Liu K-K, Atkinson L, Quinones R, and Talaue-McManus L (eds.) *Carbon and Nutrient Fluxes in Continental Margins: A Global Synthesis*, pp. 597–615. Berlin: Springer.
Jahnke RA, Craven DB, and Gaillard J-F (1994) The influence of organic matter diagenesis on $CaCO_3$ dissolution at the deep-sea floor. *Geochimica et Cosmochimica Acta* 58: 2799–2809.
Jahnke RA, Craven DB, McCorkle DC, et al. (1997) $CaCO_3$ dissolution in California continental margin sediments: The influence of organic matter remineralization. *Geochimica et Cosmochimica Acta* 61: 3587–3604.
Jahnke RA and Jahnke DB (2004) Calcium carbonate dissolution in deep sea sediments: Reconciling microelectrode, pore water and benthic flux chamber results. *Geochimica et Cosmochimica Acta* 68: 47–59.
Jansen H and Ahrens MJ (2004) Carbonate dissolution in the guts of benthic deposit feeders: A numerical model. *Geochimica et Cosmochimica Acta* 68: 4077–4092.
Jensen DL, Boddum JK, Tjell JC, et al. (2002) The solubility of rhodochrosite ($MnCO_3$) and siderite ($FeCO_3$) in anaerobic aquatic environments. *Applied Geochemistry* 17: 503–511.
Johnson TC (1976) Biogenic opal preservation in pelagic sediments of a small area in the eastern tropical Pacific. *Geological Society of America Bulletin* 87: 1273–1282.
Jorgensen BB (1977) Bacterial sulfate reduction within reduced microniches of oxidized marine sediments. *Marine Biology* 41: 7–17.
Jorgensen BB (2006) Bacteria and marine biogeochemistry. In: Schulz HD and Zabel M (eds.) *Marine Geochemistry*, 2nd edn., pp. 169–206. Berlin: Springer.

Jorgensen BB and Kasten S (2006) Sulfur cycling and methane oxidation. In: Schulz HD and Zabel M (eds.) *Marine Geochemistry*, pp. 271–309. Berlin: Springer.

Kamatani A, Ejiri N, and Treguer P (1988) The dissolution kinetics of diatom ooze from the Antarctic area. *Deep Sea Research* 35: 1195–1203.

Kamatani A and Riley JP (1979) Rate of dissolution of diatom silica walls in seawater. *Marine Biology* 55: 29–35.

Kao S-J, Shiah F-K, Wang C-H, et al. (2006) Efficient trapping of organic carbon in sediments on the continental margin with high fluvial sediment input off southwestern Taiwan. *Continental Shelf Research* 26: 2520–2537.

Kastner M, Keene JB, and Gieskes JM (1977) Diagenesis of siliceous oozes. 1. Chemical controls on rate of opal-A to Opal-CT transformation-experimental study. *Geochimica et Cosmochimica Acta* 41: 1041.

Keil RG, Dickens AF, Arnarson T, et al. (2004) What is the oxygen exposure time of laterally transported organic matter along the Washington margin? *Marine Chemistry* 92: 157–165.

Keir RS (1980) Dissolution kinetics of biogenic calcium carbonates in seawater. *Geochimica et Cosmochimica Acta* 44: 241–252.

Keir RS and Michel RL (1993) Interface dissolution control of the C-14 profile in marine sediment. *Geochimica et Cosmochimica Acta* 57: 3563–3573.

Kineke GC, Sternberg RW, Trowbridge JH, et al. (1996) Fluid-mud processes on the Amazon continental shelf. *Continental Shelf Research* 16: 667–696.

King SL, Froelich PN, and Jahnke RA (2000) Early diagenesis of germanium in sediments of the Antarctic South Atlantic: In search of the missing Ge sink. *Geochimica et Cosmochimica Acta* 64: 1375–1390.

Kinsman DJJ (1969) Modes of formation, sedimentary associations, and diagnostic features of shallow-water and supratidal evaporites. *AAPG Bulletin* 53: 830–840.

Klump JV and Martens CS (1989) The seasonality of nutrient regeneration in an organic-rich coastal sediment: Kinetic modeling of changing pore-water nutrient and sulfate distributions. *Limnology and Oceanography* 34: 559–577.

Komada T, Druffel ERM, and Trumbore SE (2004) Oceanic export of relict carbon by small mountainous rivers. *Geophysical Research Letters* 31: L07504.

Köning E, Brummer G-J, Van Raaphorst W, et al. (1997) Settling, dissolution and burial of biogenic silica in the sediments off Somalia (northwestern Indian Ocean). *Deep-Sea Research Part II* 44: 1341–1360.

Koretsky CM, Meile C, and Van Cappellen P (2002) Quantifying bioirrigation using ecological parameters: A stochastic approach. *Geochemical Transactions* 3: 17–30.

Kristensen E and Holmer M (2001) Decomposition of plant materials in marine sediment exposed to different electron acceptors (O_2, NO_3^-, and SO_4^{2-}), with emphasis on substrate origin, degradation kinetics, and the role of bioturbation. *Geochimica et Cosmochimica Acta* 65: 419–433.

Kristensen E and Kostka JE (2005) Macrofaunal burrows and irrigation in marine sediment: Microbiological and biogeochemical interactions. In: Kristensen E, Kostka JE, and Haese R (eds.) *Interactions Between Macro- and Microorganisms in Marine Sediments*, p. 390. Washington, DC: American Geophysical Union.

Ku TCW and Walter LM (2003) Syndepositional formation of Fe-rich clays in tropical shelf sediments, San Blas Archipelago, Panama. *Chemical Geology* 197: 197–213.

Ku TCW, Walter LM, Coleman ML, et al. (1999) Coupling between sulfur recycling and syndepositional carbonate dissolution: Evidence from oxygen and sulfur isotope compositions of pore water sulfate, South Florida Platform, U.S.A. *Geochimica et Cosmochimica Acta* 63: 2529–2546.

Kuehl SA, DeMaster DJ, and Nittrouer CA (1986) Nature of sediment accumulation on the Amazon continental shelf. *Continental Shelf Research* 6: 209–225.

Kump LR, Brantley SL, and Arthur MA (2000) Chemical, weathering, atmospheric CO_2, and climate. *Annual Review of Earth and Planetary Sciences* 28: 611–667.

Laruelle GG, Durr HH, Slomp CP, et al. (2010) Evaluation of sinks and sources of CO_2 in the global coastal ocean using a spatially-explicit typology of estuaries and continental shelves. *Geophysical Research Letters* 37: L15607.

Lasaga AC and Holland HD (1976) Mathematical aspects of non-steady state diagenesis. *Geochimica et Cosmochimica Acta* 40: 257–266.

Lecroart P, Maire O, Schmidt S, et al. (2010) Bioturbation, short-lived radioisotopes, and the tracer-dependence of biodiffusion coefficients. *Geochimica et Cosmochimica Acta* 74: 6049–6063.

Leithold EL, Blair NE, and Perkey DW (2006) Geomorphologic controls on the age of particulate organic carbon from small mountainous and upland rivers. *Global Biogeochemical Cycles* 20: GB3022.

Lewin JC (1961) The dissolution of silica from diatom walls. *Geochimica et Cosmochimica Acta* 21: 182–198.

Liu K-K, Atkinson L, Quiñones R, et al. (2010) *Carbon and Nutrient Fluxes in Continental Margins: A Global Synthesis*. Berlin: Springer.

Loucaides S, Cappellen P, Roubeix V, et al. (2012a) Controls on the recycling and preservation of biogenic silica from biomineralization to burial. *Silicon* 4: 7–22.

Loucaides S, Koning E, and Van Cappellen P (2012b) Effect of pressure on silica solubility of diatom frustules in the oceans: Results from long-term laboratory and field incubations. *Marine Chemistry* 136–137: 1–6.

Loucaides S, Michalopoulos P, Presti M, et al. (2010) Seawater-mediated interactions between diatomaceous silica and terrigenous sediments: Results from long-term incubation experiments. *Chemical Geology* 270: 68–79.

Luther GW, Reimers CE, Nuzzio DB, and Lovalvo D (1999) In situ deployment of voltammetric, potentiometric, and amperometric microelectrodes from a ROV to determine dissolved O_2, Mn, Fe, S(-2), and pH in porewaters. *Environmental Science and Technology* 33: 4352–4356.

Lyons TW, Scott C, Reinhard C, et al. (2009) Euxinia in the Proterozoic ocean, trace metal abundances, and the potential impacts on life. *Geochimica et Cosmochimica Acta* 73: A807–A807.

Lyons TW and Severmann S (2006) A critical look at iron paleoredox proxies: New insights from modern euxinic marine basins. *Geochimica et Cosmochimica Acta* 70: 5698–5722.

Machel HG (2004) Concepts and models of dolomitization: A critical reappraisal. *Geological Society, London Special Publications* 235: 7–63.

Mackenzie FT and Garrels RM (1966) Chemical mass balance between rivers and oceans. *American Journal of Science* 264: 507–525.

Mackenzie FT, Ristvet BL, Thorstenson DC, et al. (1981) Reverse weathering and chemical mass balance in a coastal environment. In: Martin JM, Burton JD, and Eisma D (eds.) *River Inputs to the Ocean*, pp. 152–187. Switzerland: UNEP-UNESCO.

Mackin JE (1986) Control of dissolved Al distributions in marine sediments by clay reconstitution reactions: Experimental evidence leading to a unified theory. *Geochimica et Cosmochimica Acta* 50: 207–214.

Mackin JE and Aller RC (1984) Dissolved Al in sediments and waters of the East China Sea – Implication for authigenic mineral formation. *Geochimica et Cosmochimica Acta* 48: 281–297.

Mackin JE and Aller RC (1986) The effects of clay mineral reactions on dissolved Al distributions in sediments and waters of the Amazon Continental-Shelf. *Continental Shelf Research* 6: 245–262.

Mackin JE and Aller RC (1989) The nearshore marine and estuarine chemistry of dissolved Aluminium and rapid authigenic mineral precipitation. *Reviews in Aquatic Sciences* 1: 537–554.

Madison AS, M. TB, and Luther GW (2011) Simultaneous determination of soluble manganese(III), manganese(II) and total manganese in natural (pore)waters. *Talanta* 84: 374–381.

Martin WR and Banta GT (1992) The measurement of sediment irrigation rates: A comparison of the Br^- tracer and $^{222}Rn/^{226}Ra$ disequilibrium techniques. *Journal of Marine Research* 50: 125–154.

Martin WR and Bender ML (1988) The variability of benthic fluxes and sedimentary remineralization rates in response to seasonally variable organic carbon rain rates in the deep sea: A modeling study. *American Journal of Science* 288: 561–574.

Martin WR, McNichol AP, and McCorkle DC (2000) The radiocarbon age of calcite dissolving at the sea floor: Estimates from pore water data. *Geochimica et Cosmochimica Acta* 64: 1391–1404.

Martin W and Sayles F (2003) The recycling of biogenic material at the seafloor. In: Mackenzie FT and Holland HD (eds.) *Treatise on Geochemistry*, pp. 37–67. Amsterdam: Elsevier.

Mayer LM (1994a) Relationships between mineral surfaces and organic-carbon concentrations in soils and sediments. *Chemical Geology* 114: 347–363.

Mayer LM (1994b) Surface-area control of organic-carbon accumulation in continental-shelf sediments. *Geochimica et Cosmochimica Acta* 58: 1271–1284.

Mayer L, Benninger L, Bock M, et al. (2002) Mineral associations and nutritional quality of organic matter in shelf and upper slope sediments off Cape Hatteras, USA: A case of unusually high loadings. *Deep-Sea Research Part II* 49: 4587–4597.

Mayer LM, Schick LL, Self RFL, et al. (1997) Digestive environments of benthic macroinvertebrate guts: Enzymes, surfactants and dissolved organic matter. *Journal of Marine Research* 55: 785–812.

McCave IN, Chandler RC, Swift SA, et al. (2002) Contourites of the Nova Scotian continental rise and the HEBBLE area. *Memoirs of Geological Society, London* 22: 21–38.

McManus J, Hammond DE, Berelson WM, et al. (1995) Early diagenesis of biogenic opal: Dissolution rates, kinetics, and paleoceanographic implications. *Deep-Sea Research Part II* 42: 871–903.

Meile C, Koretsky C, and Van Cappellen P (2001) Quantifying bioirrigation in aquatic sediments: An inverse modeling approach. *Limnology and Oceanography* 46: 164–177.

Meysman FJR, Boudreau BP, and Middelburg JJ (2003) Relations between local, nonlocal, discrete and continuous models of bioturbation. *Journal of Marine Research* 61: 391–410.

Meysman FJR, Galaktionov OS, Gribsholt B, et al. (2006) Bioturbation in permeable sediments: Advective pore-water transport induced by burrow ventilation. *Limnology and Oceanography* 51: 142–156.
Meysman FJR, Malyuga VS, Boudreau BP, et al. (2008) Quantifying particle dispersal in aquatic sediments at short time scales: Model selection. *Aquatic Biology* 2: 239–254.
Michalopoulos P and Aller RC (1995) Rapid clay mineral formation in Amazon delta sediments – Reverse weathering and oceanic elemental cycles. *Science* 270: 614–617.
Michalopoulos P and Aller RC (2004) Early diagenesis of biogenic silica in the Amazon Delta: Alteration, authigenic clay formation, and storage. *Geochimica et Cosmochimica Acta* 68: 1061–1085.
Michalopoulos P, Aller RC, and Reeder RJ (2000) Conversion of diatoms to clays during early diagenesis in tropical, continental shelf muds. *Geology* 28: 1095–1098.
Middelburg JJ (1989) A simple rate model for organic-matter decomposition in marine-sediments. *Geochimica et Cosmochimica Acta* 53: 1577–1581.
Middelburg JJ, De Lange GJ, and Vanderweijden CH (1987) Manganese solubility control in marine pore waters. *Geochimica et Cosmochimica Acta* 51: 759–763.
Middelburg JJ and Meysman FJR (2007) Burial at sea. *Science* 316: 1294–1295.
Middelburg JJ and Soetaert K (2004) The role of sediments in shelf ecosystem dynamics. *Geochimica et Cosmochimica Acta* 68: A343–A343.
Middelburg JJ, Soetaert K, and Herman PMJ (1997) Empirical relationships for use in global diagenetic models. *Deep-Sea Research Part I* 44: 327–344.
Middelburg JJ, Soetaert K, Herman PMJ, et al. (1996) Denitrification in marine sediments: A model study. *Global Biogeochemical Cycles* 10: 661–673.
Middelburg JJ, Vlug T, and Vandernat F (1993) Organic-matter mineralization in marine systems. *Global and Planetary Change* 8: 47–58.
Milliman JD and Droxler AW (1996) Neritic and pelagic carbonate sedimentation in the marine environment: Ignorance is not bliss. *Geologische Rundschau* 85: 496–504.
Milliman JD and Farnsworth KL (2011) *River Discharge to the Coastal Ocean: A Global Synthesis*. Cambridge: Cambridge University Press.
Misra S and Froelich PN (2012) Lithium isotope history of cenozoic seawater: Changes in silicate weathering and reverse weathering. *Science* 335: 818–823.
Morse JW (1978) Dissolution kinetics of calcium-carbonate in sea-water. 6. Near-equilibrium dissolution kinetics of calcium carbonate-rich deep-sea sediments. *American Journal of Science* 278: 344–353.
Morse JW (2003) *Formation and Diagenesis of Carbonate Sediments*. *Treatise on Geochemistry*, pp. 67–85. Amsterdam: Elsevier.
Morse JW, Andersson AJ, and Mackenzie FT (2006) Initial responses of carbonate-rich shelf sediments to rising atmospheric pCO(2) and "ocean acidification": Role of high Mg-calcites. *Geochimica et Cosmochimica Acta* 70: 5814–5830.
Morse JW, Arvidson RS, and Luttge A (2007) Calcium carbonate formation and dissolution. *Chemical Reviews* 107: 342–381.
Morse JW and Mackenzie FT (1990) *Geochemistry of Sedimentary Carbonates*. Amsterdam: Elsevier.
Mucci A (1991) The solubility and free-energy of formation of natural kutnahorite. *The Canadian Mineralogist* 29: 113–121.
Müller PJ and Suess E (1979) Productivity, sedimentation rate, and sedimentary organic matter in the oceans-I. Organic carbon preservation. *Deep-Sea Research* 26: 1347–1362.
Odin GS (1988) *Green Marine Clays*. New York: Elsevier.
Odin GS and Frohlich F (1988) Glauconv from the Kerguelen plateau (Southern Indian Ocean). In: Odin GS (ed.) *Green Marine Clays*, pp. 277–294. Amsterdam: Elsevier.
Pallud C and Van Cappellen P (2006) Kinetics of microbial sulfate reduction in estuarine sediments. *Geochimica et Cosmochimica Acta* 70: 1148–1162.
Pamatmat MM (1971) Oxygen consumption by seabed. 4. Shipboard and laboratory experiments. *Limnology and Oceanography* 16: 536–550.
Pastor L, Cathalot C, Deflandre B, et al. (2011a) Modeling biogeochemical processes in sediments from the Rhone River prodelta area (NW Mediterranean Sea). *Biogeosciences* 8: 1351–1366.
Pastor L, Deflandre B, Viollier E, et al. (2011b) Influence of the organic matter composition on benthic oxygen demand in the Rhone River prodelta (NW Mediterranean Sea). *Continental Shelf Research* 31: 1008–1019.
Patterson WP and Walter LM (1994) Syndepositional diagenesis of modern platform carbonates - Evidence from isotopic and minor element data. *Geology* 22: 127–130.
Paul EA and van Veen JA (1978) The use of tracers to determine the dynamic nature of organic matter. *Transactions of 11th International Congress of Soil Science* 3: 61–89.
Pedersen TF and Price NB (1982) The geochemistry of manganese carbonate in Panama Basin sediments. *Geochimica et Cosmochimica Acta* 46: 59–68.
Pfeifer K, Hensen C, Adler M, et al. (2002) Modeling of subsurface calcite dissolution, including the respiration and reoxidation processes of marine sediments in the region of equatorial upwelling off Gabon. *Geochimica et Cosmochimica Acta* 66: 4247–4259.
Pope RH, Demaster DJ, Smith CR, et al. (1996) Rapid bioturbation in equatorial Pacific sediments: Evidence from excess Th-234 measurements. *Deep-Sea Research Part II* 43: 1339–1364.
Powell EN, Staff GM, Davies DJ, et al. (1989) Macrobenthic death assemblages in modern marine environments: Formation, interpretation, and application. *Aquatic Sciences* 1: 555–589.
Prahl FG, De Lange GJ, Lyle M, et al. (1989) Post-depositional stability of long-chain alkenones under contrasting redox conditions. *Nature* 341: 434–437.
Prahl FG, De Lange GJ, Scholten S, et al. (1997) A case of post-depositional aerobic degradation of terrestrial organic matter in turbidite deposits from the Madeira Abyssal Plain. *Organic Geochemistry* 27: 141–152.
Premuzic ET, Benkovitz CM, Gaffney JS, et al. (1982) The nature and distribution of organic matter in the surface sediments of world oceans and seas. *Organic Geochemistry* 4: 63–77.
Presti M and Michalopoulos P (2008) Estimating the contribution of the authigenic mineral component to the long-term reactive silica accumulation on the western shelf of the Mississippi River Delta. *Continental Shelf Research* 28: 823–838.
Rabouille C, Caprais JC, Lansard B, et al. (2009) Organic matter budget in the Southeast Atlantic continental margin close to the Congo Canyon: In situ measurements of sediment oxygen consumption. *Deep-Sea Research Part II* 56: 2223–2238.
Rabouille C, Gaillard JF, Treguer P, et al. (1997) Biogenic silica recycling in surficial sediments across the Polar Front of the Southern Ocean (Indian Sector). *Deep-Sea Research Part II* 44: 1151–1176.
Raiswell R, Buckley F, Berner RA, et al. (1988) Degree of pyritization of iron as a paleoenvironmental indicator of bottom-water oxygenation. *Journal of Sedimentary Petrology* 58: 812–819.
Raiswell R and Canfield DE (1998) Sources of iron for pyrite formation in marine sediments. *American Journal of Science* 298: 219–245.
Ransom B, Bennett RH, Baerwald R, et al. (1997) TEM study of in situ organic matter on continental margins: Occurrence and the "monolayer" hypothesis. *Marine Geology* 138: 1–9.
Ransom B, Dongseon K, Kastner M, et al. (1998) Organic matter preservation on continental slopes: Importance of mineralogy and surface area. *Geochimica et Cosmochimica Acta* 62: 1329–1345.
Reeburgh WS (2007) Oceanic methane biogeochemistry. *Chemical Reviews* 107: 486–513.
Reimers CE, Jahnke RA, and McCorkle DC (1992) Carbon fluxes and burial rates over the continental slope and rise off central California with implications for the global carbon cycle. *Global Biogeochemical Cycles* 6: 199–224.
Reimers CE, Oezkan-Haller HT, Berg P, et al. (2012) Benthic oxygen consumption rates during hypoxic conditions on the Oregon continental shelf: Evaluation of the eddy correlation method. *Journal of Geophysical Research-Oceans* 117: C02021.
Rickard D and Luther GW III (2007) Chemistry of iron sulfides. *Chemical Reviews* 107: 514–562.
Rickert D (2000) *Dissolution kinetics of biogenic silica in marine environments*, p. 211. Kiel: Geomar Forschungszentrum fur marine Geowissenschaften.
Rickert D, Schluter M, and Wallmann K (2002) Dissolution kinetics of biogenic silica from the water column to the sediments. *Geochimica et Cosmochimica Acta* 66: 439–455.
Risvet BL (1978) *Reverse weathering reactions within recent nearshore marine sediments, Kaneohoe Bay, Oahu*. *Test Directorate Field Command*. New Mexico: Kirkland AFB.
Rude PD and Aller RC (1991) Fluorine mobility during early diagenesis of carbonate sediment-an indicator of mineral transformations. *Geochimica et Cosmochimica Acta* 55: 2491–2509.
Rude PD and Aller RC (1994) Fluorine uptake by Amazon Continental-Shelf sediment and its impact on the global fluorine cycle. *Continental Shelf Research* 14: 883–907.
Russell KL (1970) Geochemistry and halmyrolysis of clay minerals, Rio Ameca, Mexico. *Geochimica et Cosmochimica Acta* 34: 893–907.
Savin SM and Epstein S (1970) The oxygen and hydrogen isotope geochemistry of clay minerals. *Geochimica et Cosmochimica Acta* 34: 25–42.
Sayles FL (1979) Composition and diagenesis of interstitial solutions. 1. Fluxes across the seawater-sediment interface in the Atlantic Ocean. *Geochimica et Cosmochimica Acta* 43: 527–545.
Sayles FL and Bischoff JL (1973) Ferromanganoan sediments in Equatorial East Pacific. *Earth and Planetary Science Letters* 19: 330–336.
Sayles FL, Martin WR, Chase Z, et al. (2001) Benthic remineralization and burial of biogenic SiO_2, $CaCO_3$, organic carbon, and detrital material in the Southern Ocean along a transect at 170° West. *Deep-Sea Research Part II* 48: 4323–4383.
Schink DR, Guinasso NL, and Fanning KA (1975) Processes affecting concentration of silica at sediment-water interface of Atlantic Ocean. *Journal of Geophysical Research-Oceans* 80: 3013–3031.

Schneider RR, Schulz HD, and Hensen C (2006) Marine carbonates: Their formation and destruction. In: Schulz HD and Zabel M (eds.) *Marine Geochemistry*, pp. 311–337. Berlin: Springer.

Schulz HD (2006) Quantification of early diagenesis: Dissolved constituents in marine pore water. In: Zabel HDSaM (ed.) *Marine Geochemistry*, 2nd edn., pp. 73–124. Berlin: Springer.

Seiter K, Hensen C, Schroter E, et al. (2004) Organic carbon content in surface sediments – Defining regional provinces. *Deep-Sea Research Part I* 51: 2001–2026.

Seiter K, Hensen C, and Zabel M (2010) Coupling of benthic oxygen uptake and silica release: Implications for estimating biogenic particle fluxes to the seafloor. *Geo-Marine Letters* 30: 493–509.

Severmann S, McManus J, Berelson WM, et al. (2010) The continental shelf benthic iron flux and its isotope composition. *Geochimica et Cosmochimica Acta* 74: 3984–4004.

Sholkovitz E (1973) Interstitial water chemistry of the Santa Barbara Basin sediments. *Geochimica et Cosmochimica Acta* 37: 2043–2073.

Sholkovitz ER, Shaw TJ, and Schneider DL (1992) The geochemistry of rare earth elements in the seasonally anoxic water column and porewaters of Chesapeake Bay. *Geochimica et Cosmochimica Acta* 56: 3389–3402.

Smith KL, Baldwin RJ, Karl DM, et al. (2002) Benthic community responses to pulses in pelagic food supply: North Pacific Subtropical Gyre. *Deep-Sea Research Part I* 49: 971–990.

Smith CR, Hoover DJ, Doan SE, et al. (1996) Phytodetritus at the abyssal sea floor across 10 degrees of latitude in the central equatorial Pacific. *Deep-Sea Research Part II* 43: 1309–1338.

Soetaert K, Herman PMJ, and Middelburg JJ (1996a) A model of early diagenetic processes from the shelf to abyssal depths. *Geochimica et Cosmochimica Acta* 60: 1019–1040.

Soetaert K, Herman PMJ, and Middelburg JJ (1996b) Dynamic response of deep-sea sediments to seasonal variations: A model. *Limnology and Oceanography* 41: 1651–1668.

Soetaert K, Middelburg JJ, Herman PMJ, et al. (2000) On the coupling of benthic and pelagic biogeochemical models. *Earth-Science Reviews* 51: 173–201.

Stahl H, Glud A, Schroeder CR, et al. (2006) Time-resolved pH imaging in marine sediments with a luminescent planar optode. *Limnology and Oceanography-Methods* 4: 336–345.

Stockdale A, Davison W, and Zhang H (2009) Micro-scale biogeochemical heterogeneity in sediments: A review of available technology and observed evidence. *Earth-Science Reviews* 92: 81–97.

Stumm W and Morgan JJ (1996) *Aquatic Chemistry: Chemical Equilibria and Rates in Natural Waters*, 3rd edn. New York: Wiley-Interscience.

Suess E (1979) Mineral phases formed in anoxic sediments by microbial decomposition of organic matter. *Geochimica et Cosmochimica Acta* 43: 339–352.

Sun MY, Aller RC, Lee C, et al. (2002) Effects of oxygen and redox oscillation on degradation of cell-associated lipids in surficial marine sediments. *Geochimica et Cosmochimica Acta* 66: 2003–2012.

Sundby B (2006) Transient state diagenesis in continental margin muds. *Marine Chemistry* 102: 2–12.

Swart PK, Berler D, McNeill D, et al. (1989) Interstitial water geochemistry and carbonate diagenesis in the sub-surface of a Holocene mud island in Florida Bay. *Bulletin of Marine Science* 44: 490–514.

Tarutis WJ (1993) On the equivalence of the power and reactive continuum models of organic matter diagenesis. *Geochimica et Cosmochimica Acta* 57: 1349–1350.

Tengberg A, Hall POJ, Andersson U, et al. (2005) Intercalibration of benthic flux chambers II. Hydrodynamic characterization and flux comparisons of 14 different designs. *Marine Chemistry* 94: 147–173.

Tengberg A, Stahl H, Gust G, et al. (2004) Intercalibration of benthic flux chambers I. Accuracy of flux measurements and influence of chamber hydrodynamics. *Progress in Oceanography* 60: 1–28.

Thamdrup B, Fossing H, and Jorgensen BB (1994) Manganese, iron, and sulfur cycling in a coastal marine sediment, Aarhus Bay, Denmark. *Geochimica et Cosmochimica Acta* 58: 5115–5129.

Thompson CE (2009) *Tracking Organic Matter from Source to Sink in the Waiapu River Watershed: A Geochemical Perspective, Department of Marine, Earth, and Atmospheric Sciences*, p. 335. Raleigh, NC: NC State University Press.

Thomson J, Jarvis I, Green DRH, et al. (1998) Mobility and immobility of redox-sensitive elements in deep-sea turbidites during shallow burial. *Geochimica et Cosmochimica Acta* 62: 643–656.

Trask PD (1939) Organic content of recent marine sediments. In: Trask PD (ed.) *Recent Marine Sediments*, pp. 428–453. Tulsa, OK: AAPG.

Tromp TK, Van Cappellen P, and Key RM (1995) A global-model for the early diagenesis of organic-carbon and organic phosphorus in marine sediments. *Geochimica et Cosmochimica Acta* 59: 1259–1284.

Ullman WJ and Aller RC (1985) The geochemistry of iodine in near-shore carbonate sediments. *Geochimica et Cosmochimica Acta* 49: 967–978.

Van Bennekom AJ, Buma AGJ, and Nolting RF (1991) Dissolved aluminium in the Weddellcotia Confluence and effect of Al on the dissolution kinetics of biogenic silica. *Marine Chemistry* 35: 423–434.

Van Bennekom AJ, Jansen JHF, Vandergaast SJ, et al. (1989) Aluminium-rich opal: An intermediate in the preservation of biogenic silica in the Zaire (Congo) deep-sea fan. *Deep Sea Research* 36: 173–190.

Van Bennekom AJ and Van der Gast SJ (1976) Possible clay structures in frustules of living diatoms. *Geochimica et Cosmochimica Acta* 40: 1149–1152.

Van Beusekom JEE, Van Bennekom AJ, Treguer P, et al. (1997) Aluminium and silicic acid in water and sediments of the Enderby and Crozet Basins. *Deep-Sea Research Part II* 44: 987–1003.

Van Cappellen P, Dixit S, and Van Beusekom J (2002) Biogenic silica dissolution in the oceans: Reconciling experimental and field-based dissolution rates. *Global Biogeochemical Cycles* 16: 1075.

Van Cappellen P and Gaillard JF (1996) Biogeochemical dynamics in aquatic sediments. In: Lichtner PC, Steefel CI, and Oelkers EH (eds.) *Reactive Transport in Porous Media*, pp. 335–376. Washington, DC: Mineralogical Society of America.

Van Cappellen P, Gaillard J-F, and Rabouille C (1993) Biogeochemical transormations in sediments: Kinetic models of early diagenesis. In: Wollast R, Mackenzie FT, and Chou L (eds.) *Interactions of C, N, P and S Biogeochemical Cycles and Global Change*, pp. 401–445. Berlin: Springer.

Van Cappellen P and Qiu L-Q (1997a) Biogenic silica dissolution in sediments of the Southern Ocean. II. Kinetics. *Deep-Sea Research Part II* 44: 1129–1149.

Van Cappellen P and Qiu LQ (1997b) Biogenic silica dissolution in sediments of the Southern Ocean. 1. Solubility. *Deep-Sea Research Part II* 44: 1109–1128.

Volkenborn N, Polerecky L, Wethey DS, et al. (2010) Oscillatory porewater bioadvection in marine sediments induced by hydraulic activities of Arenicola marina. *Limnology and Oceanography* 55: 1231–1247.

Volkenborn N, Polerecky L, Wethey DS, et al. (2012) Hydraulic activities by ghost shrimp *Neotrypaea californiensis* induce oxic-anoxic oscillations in sediments. *Marine Ecology Progress Series* 455: 141–156.

Walsh JJ (1988) *On the Nature of Continental Shelves*. San Diego, CA: Academic Press.

Walsh JP, Nittrouer CA, Palinkas CM, et al. (2004) Clinoform mechanics in the Gulf of Papua, New Guinea. *Continental Shelf Research* 24: 2487–2510.

Walter LM, Bischof SA, Patterson WP, et al. (1993) Dissolution and recrystallization in modern shelf carbonates – Evidence from pore-water and solid-phase chemistry. *Philosophical Transactions of the Royal Society A* 344: 27–36.

Walter LM and Burton EA (1990) Dissolution of recent platform carbonate sediments in marine pore fluids. *American Journal of Science* 290: 601–643.

Walter LM and Morse JW (1985) The dissolution kinetics of shallow marine carbonates in seawater: A laboratory study. *Geochimica et Cosmochimica Acta* 49: 1503–1513.

Westrich JT and Berner RA (1984) The role of sedimentary organic matter in bacterial sulfate reduction: The G model tested. *Limnology and Oceanography* 29: 236–249.

Willey JD (1975) Silica-alumina interactions in seawater. *Marine Chemistry* 3: 241–251.

Willey JD (1978) Release and uptake of dissolved silica in seawater by marine sediments. *Marine Chemistry* 7: 53–65.

Willey JD (1980) Effects of aging on silica solubility: A laboratory study. *Geochimica et Cosmochimica Acta* 44: 573–578.

Williams LA, Parks GA, and Crerar DA (1985) Silica diagenesis. 1. Solubility controls. *Journal of Sedimentary Petrology* 55: 301–311.

Wollast R (1974) The silica problem. In: Goldberg ED (ed.) *The Sea*, pp. 359–392. New York: Wiley.

Wollast R (1998) Evaluation and comparison of the global carbon cycle in the coastal zone and in the open ocean. In: Brink KH and Robinson AR (eds.) *The Sea: The Global Coastal Ocean*, pp. 213–252. New York: Wiley.

Wollast R and Mackenzie FT (1983) Global cycle of silica. In: Aston SR (ed.) *Silicon Geochemistry and Biogeochemistry*, pp. 39–76. New York: Academic Press.

Woulds C, Middelburg JJ, and Cowie GL (2012) Alteration of organic matter during infaunal polychaete gut passage and links to sediment organic geochemistry. Part I: Amino acids. *Geochimica et Cosmochimica Acta* 77: 396–414.

Yeh HW and Eslinger EV (1986) Oxygen isotopes and the extent of diagenesis of clay minerals during sedimentation and burial in the sea. *Clays and Clay Minerals* 34: 403–406.

Zhu QZ, Aller RC, and Fan YZ (2006) Two-dimensional pH distributions and dynamics in bioturbated marine sediments. *Geochimica et Cosmochimica Acta* 70: 4933–4949.

Zhu ZB, Aller RC, and Mak J (2002) Stable carbon isotope cycling in mobile coastal muds of Amapa, Brazil. *Continental Shelf Research* 22: 2065–2079.